Advancing T cell-based immunotherapies through targeted engineering with CRISPR-Cas9

by

Gillian Carleton
B.Sc. University of Victoria, 2018

A Dissertation Submitted in Partial Fulfillment of
the Requirements for the Degree of

DOCTOR OF PHILOSOPHY

in the Department of Biochemistry and Microbiology

University of Victoria

We acknowledge and respect the Lək^{w}əŋən (Songhees and Esquimalt) Peoples on whose territory the university stands, and the Lək^{w}əŋən and W̱SÁNEĆ Peoples whose historical relationships with the land continue to this day.

Supervisory Committee

Advancing T cell-based immunotherapies through targeted engineering with CRISPR-Cas9

by

Gillian Carleton
B.Sc. University of Victoria, 2018

Supervisory Committee

Dr. Julian J. Lum (Department of Biochemistry and Microbiology, University of Victoria)
Supervisor

Dr. Perry Howard (Department of Biochemistry and Microbiology, University of Victoria)
Departmental member

Dr. Francis Nano (Department of Biochemistry and Microbiology, University of Victoria)
Departmental member

Dr. Stephanie Willerth (Department of Mechanical Engineering, University of Victoria)
Non-departmental member

Abstract

T cell-based immunotherapies such as chimeric antigen receptor T (CAR-T) cell therapy have undoubtably revolutionized the treatment of cancer. However, the broad effectiveness of CAR-T cell therapy is hindered by several unresolved problems, most notably a lack of therapeutic efficacy in treating solid tumor cancers. A second challenge stems from the widespread use of viral vectors in CAR-T manufacturing, which poses safety risks to patients receiving treatment. Here, we showed that genome editing with CRISPR-Cas9 can be used to overcome both of these issues.

As the solid tumor microenvironment (TME) is known to be metabolically suppressive, we devised a single-step editing method to enhance the metabolism and effector function of CAR-T cells. This approach combined CRISPR-mediated homology-directed repair with a gene-trap approach to link CAR integration with simultaneous deletion of a metabolic gene of interest. For proof-of-concept, we targeted the folate receptor alpha (aFR) CAR to the locus of the essential autophagy gene *ATG5*, and showed that editing at *ATG5* could be achieved with a high level of on-target specificity. Functionally, deletion of *ATG5* led to alterations in glucose and glutamine metabolism and enhanced CAR-T cell efficacy under nutrient-restricted conditions *in vitro* and *in vivo*.

To address the safety concerns associated with viral transduction, we developed a process for nonviral manufacturing of clinical-grade CAR-T cells for B-cell malignancies. This approach used electroporation of a Cas9 ribonucleoprotein complexed with a linear double-stranded DNA template to facilitate site-specific insertion of a CD22 CAR at the T cell receptor alpha chain (*TRAC*) locus. *In vitro,* nonviral CD22 CAR-T cells exhibited comparable antitumor activity to lentiviral CD22 CAR-T cells. thereby establishing feasibility of our nonviral manufacturing process.

Taken together, the results of these studies highlight the broad applicability of CRISPR-Cas9 as a tool for engineering safer, more effective T cell-based immunotherapies for patients with cancer.

Table of Contents

List of Tables

List of Figures

List of Abbreviations

1-MNA – 1-methylnicotinamide

2-DG – 2-deoxy-D-glucose

2HG – (R)-2-hydroxyglutarate

αFR – folate receptor alpha

AAV – adeno-associated virus

AAVS1 – adeno-associated virus integration site 1

ASCT2 – alanine serine cysteine transporter 2

AHR – aryl hydrocarbon receptor

AMBRA1 – activating molecule in Beclin 1-regulated autophagy protein 1

AML – acute myeloid leukemia

AMPK – adenosine monophosphate activated protein kinase

ATG – autophagy-related gene

BCMA – B-cell maturation antigen

CAF – cancer-associated fibroblast

CAR-T – chimeric antigen receptor T

CRISPR – clustered regularly interspaced short palindromic repeats

crRNA – CRISPR RNA

DNA-PK – DNA-dependent protein kinase

DSB – double-strand break

dsDNA – double-stranded DNA

E:T – effector-to-target

EBF2 – early B cell factor 2

ECM – extracellular matrix

EF1α – elongation factor 1 alpha

FACS – fluorescence-activated cell sorting

FAO – fatty acid oxidation

FBXW7 – F-box and WD repeat domain containing 7

FDA – Food and Drug Administration

FIP200 – FAK family-interacting protein of 200 kDa

GABARAP – gamma-aminobutyric acid receptor-associated protein

GAPDH – glyceraldehyde phosphate dehydrogenase

gDNA – genomic DNA

GLUT – glucose transporter

GMP – good manufacturing practices

GUIDE-seq – genome-wide unbiased identification of double-strand breaks enabled by sequencing

GVHD – graft-vs-host disease

gRNA – guide RNA

HDAC – histone deacetylase

HDR – homology-directed repair

HGSOC – high grade serous ovarian carcinoma

HIF-1α – hypoxia inducible factor 1 alpha

HiFiCas9 – high fidelity Cas9

IFN-γ – interferon gamma

IL-2 – interleukin 2

IL-10 – interleukin 10

Indels – insertions and deletions

ITAM – immunoreceptor tyrosine-based activation motif

LAT1 – large amino acid transporter 1

LC3 – microtubule-associated protein light chain 3

LC-MS – liquid chromatography-mass spectrometry

LIR – LC3-interacting region

LNP – lipid nanoparticle

MDSC – myeloid derived suppressor cell

MFI – median fluorescence intensity

MHC – major histocompatibility complex

MOI – multiplicity of infection

mTORC1 – mammalian target of rapamycin complex 1

NGS – Next Generation Sequencing

NHEJ – non-homologous end joining

NSG – NOD/SCID/IL-2Rγ-null

OXPHOS – oxidative phosphorylation

PARP - poly ADP-ribose polymerase

p115 – general vesicular transport factor

PAM – protospacer adjacent motif

PBMC – peripheral blood mononuclear cell

PD1 – programmed cell death protein 1

PGA – poly-l-glutamic acid

PI3KC3 – class III phosphatidylinositol-3-kinase

PI3P – phosphatidylinositol-3-phosphate

RNP – ribonucleoprotein

scFv – single chain variable fragment

sgRNA – single guide RNA

SpCas9 - *S. pyogenes* Cas9

ssDNA – single-stranded DNA

SQSTM1 – sequestosome-1

TALEN – transcription activator-like effector nuclease

TAM – tumor-associated macrophage

T_{cm} – central memory T cell

TCR – T cell receptor

tCTS – truncated Cas targeting sequence

T_{eff} – effector T cell

TGF-β – transforming growth factor beta

TIL – tumor infiltrating lymphocytes

T_m – memory T cell

TME – tumor microenvironment

TNF-α – tumor necrosis factor alpha

TRAC – T cell receptor alpha chain

tracrRNA – trans-activating CRISPR RNA

T_{reg} – regulatory T cell

T_{rm} – tissue-resident memory T cell

ULK1 – Unc-51-like kinase 1

VEGF - vascular endothelial growth factor

VHH – variable heavy domain of heavy chain

VPS34 – vacuolar protein sorting 34

ZFN – zinc-finger nuclease

Acknowledgements

Thank you to my supervisor Julian Lum, who over the past six years has become a mentor, a friend, and an ally in the fight for equitable and inclusive research practices.

Thank you to Yannick Doyon and Sébastien Levesque, the other half of our gene-editing team without whom I'd still be trying to figure out what an indel is.

Thank you to the past Lum lab members who welcomed me with open arms as an undergraduate, especially Marisa Kilgour, who quite literally taught me how to pipette. Thank you to the current Lum lab members, who have created such a positive research environment that it's now impossible for me to leave.

Thank you to our animal care team, Tracey Sutcliffe, Ahmed Olodo, Alison Bohnet, and Laura Giguere, and to all the mice sacrificed for our *in vivo* experiments.

Thank you to our collaborators who made these studies feasible, and to everyone at the Deeley Research Centre who provided technical guidance, career advice, or commiserated with me in silence when my experiments failed.

Thank you to my committee, for their unending patience and support through the many ups and downs of this degree.

Thank you to Sammy, who kept me fed and watered when I otherwise would have wasted away while writing my dissertation, and to Jeff, who has already been calling me Dr. Badger for years.

Thank you to Atlas, for teaching me that all problems can be solved by taking a break to nap in the sun.

Lastly, thank you to my family. I couldn't have done this without you.

Preamble

This dissertation is a compilation of two distinct projects. The first project covers metabolic engineering of CAR-T cells for solid tumor immunotherapy, and the second covers nonviral manufacturing of CAR-T cells for implementation in the Canadian cell therapy field.

Chapter 1 provides a broad overview of CAR-T cell therapy, introduces concepts related to genome editing, and presents two genome editing strategies to improve CAR-T efficacy and safety. This chapter also includes hypotheses and aims, and contains sections adapted from *Metabolic engineering for optimized CAR-T cell therapy* (McPhedran, Carleton, and Lum, 2024). Chapter 2 covers the development and validation of a single-step gene-editing process for CAR-T cell metabolic engineering, while Chapter 3 presents a comprehensive efficacy analysis of our metabolically-enhanced CAR-T therapy for ovarian cancer. Material from this section forms the basis of a manuscript entitled *Targeted CAR integration at ATG5 improves therapeutic efficacy of αFR CAR-T cells for ovarian cancer* (Carleton *et al.*, in preparation), and a patent entitled *Compositions and methods for enhanced lymphocyte-mediated immunotherapy* (Carleton, DeVorkin, Doyon, and Lum, WO2020163953). Chapter 4 contains preliminary feasibility data for a made-in-Canada, nonviral CAR-T cell therapy for B-cell malignancies, and Chapter 5 explores future directions related to the field of CAR-T cell genome editing.

These studies involved the use of human specimens and live animals. We have Research Ethics Board (REB) approval through the University of Victoria (18-1275) and the University of British Columbia (H18-01783), a University of Victoria Biosafety Protocol (19-0067), a University of British Columbia Biosafety Protocol (B23-0067), and a University of Victoria Animal Use Protocol (2022-011).

Chapter 1: Harnessing the power of genome editing to improve efficacy and safety of Canadian-made CAR-T cell therapies

Authors:

Gillian A. Carleton[1,2], Sarah J. McPhedran[1,2], and Julian J. Lum[1,2].

Affiliations:

1. Department of Biochemistry and Microbiology, University of Victoria, Victoria, BC.
2. Trev and Joyce Deeley Research Centre, BC Cancer, Victoria, BC.

Author contributions:

G.A.C wrote the text.
S.J.M contributed to sections 1.4.1 and 1.5.3.
G.A.C. created both figures (using Biorender.com).
G.A.C. and J.J.L. edited the text.

1.1 Prologue

In the past decade, immunotherapies such as immune checkpoint blockade, cancer vaccines, and adoptive cellular therapies have become powerful tools for treating cancer. The success of these therapeutics depends largely on endogenous T lymphocytes (T cells), cells in the adaptive immune system with the capacity to directly kill tumor cells through the release of cytotoxic molecules. Chimeric antigen receptor T (CAR-T) cell therapy has emerged as a particularly successful type of adoptive T cell therapy, with unprecedented response rates observed in patients with hematological malignancies. However, there are several challenges that still need to be addressed in order for this therapy to reach its full potential. First, CAR-T cells show limited efficacy against solid tumor cancers. This can be attributed in part to the metabolically demanding solid tumor microenvironment, which constrains T cell function through multiple mechanisms. Second, clinical CAR-T cell products are manufactured using randomly-integrating viral vectors, and this practice poses safety risks due to the potential for oncogenic transformation. Accordingly, recent efforts have centered around using genome editing technologies to improve both efficacy and safety of CAR-T cell therapies for clinical use.

1.2 What is CAR-T cell therapy?

CAR-T cell therapy is a type of adoptive cell therapy wherein a patient's T cells are redirected towards a tumor antigen through *ex vivo* engineering with a chimeric antigen receptor, or CAR. The antigen recognition domain of a CAR is derived from a monoclonal antibody, specifically the variable regions of the heavy and light chains (V_H and V_L, respectively), which are joined by a flexible linker into a single chain variable fragment (scFv). The scFv is fused to a costimulatory domain (often CD28 or 4-1BB), and finally to the CD3ζ signaling domain from the endogenous T cell receptor (TCR)[1]. The combination of a costimulatory domain with the CD3ζ signaling domain provides the two signals traditionally required for T cell activation[2]. Upon antigen binding, CAR-T cells form an immune synapse with the target cell to facilitate direct cytolysis through the release of perforin and granzymes[3].

CAR-T cells differ from endogenous T cells in two key ways. First, CAR-antigen engagement occurs in a non-major histocompatibility complex (MHC)-restricted manner, meaning that CAR-T cells can recognize a wide variety of surface antigens instead of being limited to MHC-presented peptides[4] (Figure 1). Second, while endogenous T cells expressing the co-receptor CD4 have no intrinsic cytolytic capacity and act through indirect, cytokine-mediated mechanisms, CD4-positive CAR-T cells can directly lyse target cells, albeit at a slower rate than cytotoxic CD8-positive CAR-T cells[5].

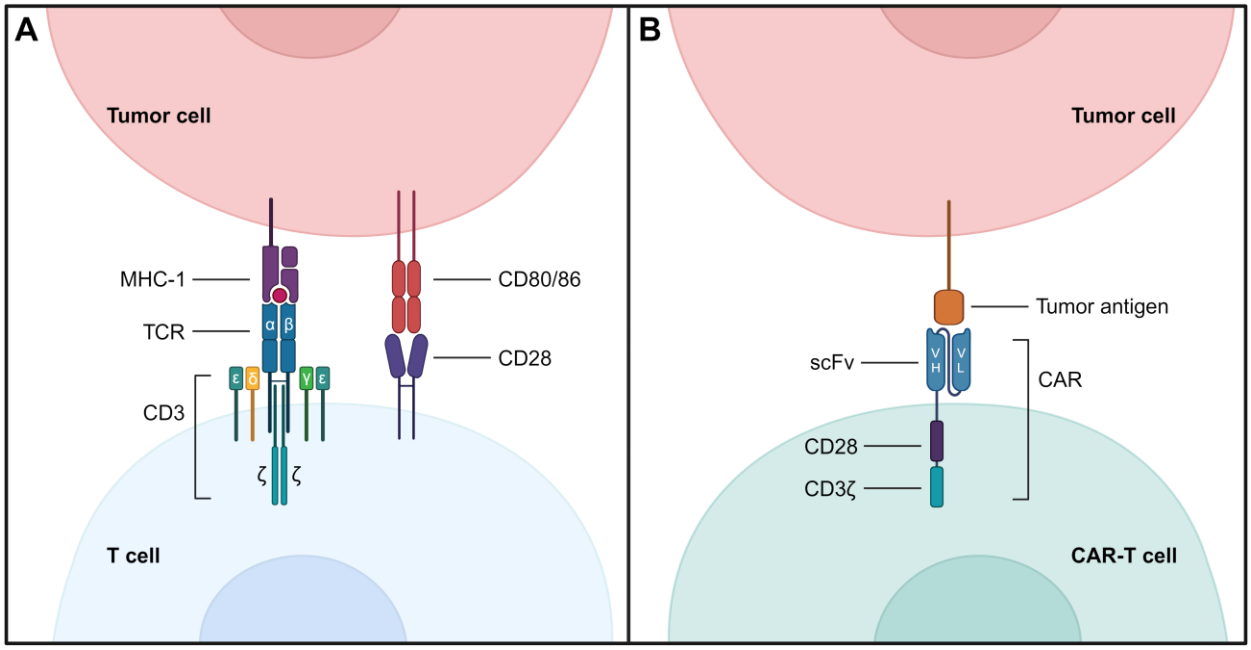

Figure 1. Differences in antigen recognition between T cells and CAR-T cells.
(A) Schematic showing MHC-restricted antigen engagement between a T cell and a tumor cell. Here, the TCR α:β heterodimer binds a specific peptide:MHC ligand, and signaling is mediated by phosphorylation of four CD3 molecules: CD3γ, CD3δ, CD3ε, and CD3ζ. A second signal is provided through the binding of CD80/86 to the costimulatory receptor CD28[6]. **(B)** Schematic showing antigen engagement between a CAR-T cell and a tumor cell. Here, the CAR scFv binds directly to a surface antigen, and signaling is mediated by a CD28 costimulatory domain and a CD3ζ signaling domain[2]. Image created with Biorender.com.

CAR-T cell therapy has demonstrated exceptional success in treating hematological malignancies, with CAR-T cells targeting the B cell antigen CD19 achieving up to 90% response rates in patients with relapsed/refractory B-cell lymphoma and chronic lymphocytic leukemia[7]. Since 2017, four CD19 CAR-T cell therapies have been approved by the US Food and Drug Administration (FDA) and the list of disease indications has widened to include adult and pediatric B-cell acute lymphoblastic leukemia. Two CAR-T therapies targeting B-cell maturation antigen (BCMA) have also been recently approved for the treatment of multiple myeloma[2]. Outside of the cancer space, CD19 CAR-T cells have shown great promise in treating patients with systemic lupus erythematosus, highlighting the broad applicability of this therapy[8].

1.3 Genome editing of CAR-T cells with CRISPR-Cas9

Over the last two decades, advances in gene-editing technology have enabled efficient *ex vivo* engineering of the T cell genome. These technologies include transposons, transcription activator-like effector nucleases (TALENs), zinc-finger nucleases (ZFNs), and RNA-guided clustered regularly interspaced short palindromic repeats (CRISPR) systems. CRISPR-Cas9 is a Type 2 CRISPR system derived from *Streptococcus pyogenes* that uses the RNA-guided nuclease Cas9 to cleave target DNA sequences. While CRISPR-Cas9 evolved as a microbial adaptive immune system, it can be easily harnessed to facilitate genome editing in eukaryotic cells and has already been employed in numerous clinical trials for cancer immunotherapy[9]. In 2020, the results of a first-in-human clinical trial were published in which the genes encoding programmed cell death protein 1 (*PD1*) and T cell receptor alpha chain (*TRAC*) were deleted in TCR-transgenic T cells targeted towards the cancer-testis antigen NY-ESO-1[10]. More recently, a CD19 CAR sequence was directly inserted into the *PD1* locus, thereby generating PD1-knockout CAR-T cells in a single editing step[11]. These reports and others demonstrate the feasibility of generating CRISPR-engineered CAR-T cells for clinical use.

The CRISPR-Cas9 genome editing system consists of the nuclease Cas9, and two RNA components: the CRISPR RNA (crRNA), which contains a 20-nucleotide guide RNA (gRNA) sequence, and the trans-activating CRISPR RNA (tracrRNA) which contains a binding region for Cas9. Together, the crRNA and tracrRNA make up a single guide RNA (sgRNA) molecule. The

sgRNA uses Watson-Crick base pairing to direct Cas9 to the target genomic region, a matching 20-base pair sequence immediately followed by a 5'-NGG protospacer adjacent motif (PAM), where Cas9 induces a double-strand break (DSB) three base pairs upstream of the PAM[12]. The DSB is repaired by one of two endogenous DNA repair pathways: non-homologous end joining (NHEJ), or homology-directed repair (HDR). Each of these pathways can be leveraged to facilitate precision genome editing. In the absence of a repair template, the DSB is repaired by NHEJ, which creates small insertions and deletions (indels) and may lead to gene knockout if Cas9 is targeted to a coding exon. Conversely, an exogenous repair template can be delivered alongside the gene-editing components to promote integration of a new DNA sequence by HDR (Figure 2).

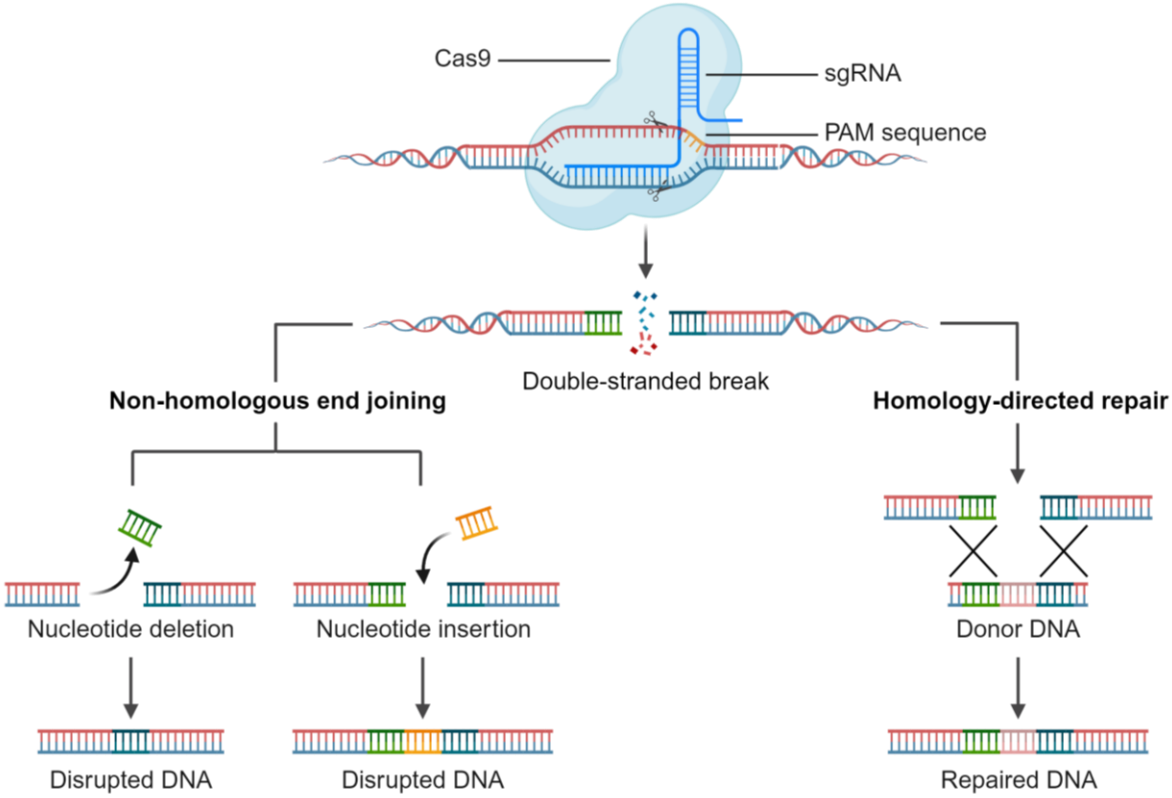

Figure 2. Genome editing with CRISPR-Cas9.

A 20-nucleotide sequence on the sgRNA guides Cas9 to a precise location in the genome, where it cleaves both strands of DNA. The resulting double-stranded break is repaired by non-

homologous end joining or homology-directed repair. sgRNA, single guide RNA; PAM, protospacer-adjacent motif. Image created with Biorender.com.

1.4 Technological considerations for CAR-T cell genome editing in the clinical setting

1.4.1 Choice of donor template

In T cells, components of the CRISPR-Cas9 system are delivered via electroporation, a process in which an electrical pulse is applied to create temporary pores in the cell membrane and facilitate transport of nucleic acids. Human codon-optimized Cas9 can be supplied as mRNA, or more commonly as recombinant protein with a nuclear localization signal, which is complexed before electroporation with sgRNA to create a ribonucleoprotein (RNP). For HDR experiments, a donor template can be delivered immediately after electroporation by adeno-associated viral vector (AAV), or by co-electroporation with double-stranded or single-stranded DNA. One of the primary challenges for genome editing of T cells is achieving high levels of transgene integration while mitigating the cellular toxicity that accompanies the introduction of large amounts of exogenous DNA. A second issue concerns the integration of the gene-editing components into a standardized clinical manufacturing workflow, which requires adherence to Good Manufacturing Practices (GMP). Given these considerations, the choice of donor template is of particular importance when designing a strategy for genome editing in the clinical setting. A brief description of three most common delivery methods for edited T cell therapies and their associated advantages and disadvantages are presented here.

Adeno-associated virus (AAV). While AAV is most commonly used for *in vivo* gene therapy[13], AAV vectors are also well-suited for genome editing with CRISPR-Cas9. In particular, AAV vectors have a large transgene capacity and have been shown to edit T cells with high efficiency and minimal toxicity[14]. This was demonstrated in a recent clinical trial where a CD19 CAR was targeted to the *TRAC* locus by AAV-mediated HDR[15]. However, AAV delivery comes with several technical challenges, such as high costs and specialized facilities for producing GMP-grade AAV.

Double-stranded (ds) DNA or RNA templates. Exogenous dsDNA or RNA templates are easily manufactured without specialized equipment, and can be incorporated into most clinical processes without additional technical challenges. However, editing efficiency is often much lower than AAV delivery (and further decreases with increasing template size), and the introduction of naked DNA can trigger immune activation through nucleic acid sensors[16,17]. For RNA delivery via carriers, such as lipid nanoparticles (LNPs), transient expression and efficiency are yet to be functionally validated. Toxicity is also much higher than AAV delivery, but RNA modifications and transient dsDNA-sensor inhibition in combination with HDR enhancers have been shown to improve viability, and have already been integrated into clinical manufacturing workflow making their implementation straightforward[18].

Single-stranded (ss) DNA templates. The use of ssDNA templates is also gaining traction as an alternative method to overcome dsDNA toxicity and improve knock-in efficiencies. A recent preclinical study used an ssDNA repair template to integrate a CAR at the *TRAC* locus in a GMP-compatible process, highlighting this method's amenability for clinical application[19].

1.4.2 Off-target risk assessment

Another important consideration for clinical genome editing with CRISPR-Cas9 is the potential for off-target editing, where Cas9 induces a DSB despite mismatches between the gRNA sequence and the off-target DNA region. This is enabled by a mechanism called mismatch tolerance[20]. In general, mismatches change the structural conformation of the gRNA-DNA duplex to prevent binding of the Cas9 nuclease domains to a non-target strand. However, mismatches in the PAM-distal region can escape detection and lead to the formation of an alternative conformation that facilitates nuclease activation and off-target cleavage[21]. Therefore, special attention to gRNA design is crucial for limiting potential off-target effects. This can be achieved through the use of bioinformatics tools like CRISPOR, which identifies potential mismatches and uses an algorithm for *in silico* prediction of off-target cleavage events[22]. Off-target effects can also be mitigated through the use of HiFiCas9, a high-fidelity Cas9 variant that is GMP-certified for clinical use[23].

While Health Canada is yet to release guidance on gene-edited cell therapy products, the FDA recommends that a comprehensive safety assessment be performed on all therapies that use human genome editing[24]. A key component of this safety assessment is the identification and verification of off-target sites. This can be accomplished through molecular methods like genome-wide unbiased identification of double-strand breaks enabled by sequencing (GUIDE-Seq), which uses integration of an oligodeoxynucleotide tag to enable sequencing-based identification of all potential DSBs associated with a given gRNA sequence. GUIDE-Seq has a high level of specificity and is widely-accepted as a tool for off-target risk assessment during clinical manufacturing of gene-edited CAR-T cells[25].

1.4.3 Closed system manufacturing of gene-edited CAR-T cells for clinical use

CAR-T cell manufacturing in Canada uses the Miltenyi CliniMACS Prodigy, an instrument that facilitates semi-automated, closed-system cell processing. The Prodigy uses a library of pre-installed protocols to orchestrate each step of the manufacturing process, beginning with CD4- and CD8-positive T cell isolation from patient apheresis product all the way to formulation of the final CAR-T therapy. Recently, Miltenyi released an electroporator module for the Prodigy that offers full customization of voltage parameters to support manufacturing of gene-edited CAR-T cells. With the first electroporator module now at operational readiness, the cell therapy field is primed for the implementation of genome editing strategies that enhance efficacy, safety, and accessibility of Canadian-made CAR-T cell therapies.

1.5 Engineering CAR-T cell metabolic pathways to improve therapeutic efficacy for solid tumors

1.5.1 CAR-T cell therapy is ineffective at treating solid tumors

In contrast to the impressive response rates achieved in hematological malignancies, the development of effective CAR-T therapies for solid tumor cancers has proven to be challenging for numerous reasons. First, there is significant antigen heterogeneity in solid tumors, both between patients and between different tumor sites within the same patient. This is further compounded by the fact that tumor cells downregulate antigen in response to therapy, so patients

who experience a recurrence may present with untreatable, antigen-negative disease[26]. Second, the tumor stroma limits T cell infiltration through physical and biochemical mechanisms, such as increased extracellular matrix (ECM) deposition and vascular remodelling[27]. Lastly, the solid tumor microenvironment (TME) is metabolically suppressive due to nutrient insufficiencies, hypoxia, and the presence of immune-inhibitory metabolites[28,29]. As CAR-T cell function is profoundly regulated by metabolic activity, metabolic suppression in the TME represents a significant challenge to the development of effective CAR-T therapies for solid tumors[30].

1.5.2 Metabolism is indispensable for CAR-T cell function

T cells require precise coordination of metabolic pathways to meet biosynthetic and energetic demands, and CAR-T cells are no exception to this rule. In the endogenous setting, effector T cells (T_{eff}) activated via the TCR undergo a rapid metabolic shift from oxidative phosphorylation (OXPHOS) to aerobic glycolysis[31]. Aerobic glycolysis enables regulation of effector genes by glycolytic enzymes such as glyceraldehyde phosphate dehydrogenase (GAPDH), which directly binds to interferon gamma (IFN-γ) transcripts under glucose-deprived conditions[32,33]. In addition to increased glucose requirements, T_{eff} cells also rely on extracellular glutamine for proliferation and effector function, and upregulate amino acid transporters in response to antigen stimulation[34,35]. After antigen clearance, a small population of T_{eff} cells persist to form long-lived memory T cells (T_m). In general, T_m cells return to a more quiescent state characterized by mitochondrial metabolism, although different subsets may use fatty acid oxidation (FAO) and glycolysis in addition to OXPHOS[36,37].

In CAR-T cells, the glycolytic switch is mediated by phosphorylation of immunoreceptor tyrosine-based activation motifs (ITAMs) on the cytoplasmic tails of CD3 molecules, meaning that CAR-T cells with a CD3ζ signaling domain retain the capacity to rapidly activate glycolysis in response to antigen stimulation[38]. Likewise, sustained glycolytic metabolism is supported by signaling through CD28, while mitochondrial metabolism is promoted by 4-1BB, and both are common costimulatory molecules in modern CAR architecture[39,40]. Therefore, it is clear that perturbations in any of the metabolic pathways described above can severely limit therapeutic efficacy of CAR-T cells *in vivo*.

1.5.3 The solid tumor microenvironment is metabolically suppressive

The solid tumor microenvironment encompasses two distinct compartments: the tumor parenchyma, which contains neoplastic cells that form the solid tumor mass, and the stroma, which is composed primarily of connective tissue and separates the parenchyma and normal host tissues[41]. The stroma contains mesenchymal cells, endothelial cells, and cancer-associated fibroblasts (CAFs), in addition to a wide variety of immune cell types that are recruited by chemokines and other signaling factors[42]. While tumor cells are often considered the major players in the metabolic ecosystem, local metabolite availability is also influenced by cross-talk and competition between different stromal cell subsets[43]. Therefore, both tumor and stroma contribute to the development of a metabolically-suppressive TME.

The solid TME metabolically limits T cell function through two primary mechanisms. The first is *metabolic restriction*, in which nutrient and oxygen delivery to the TME is insufficient due to poor vascularization and hypoxia. Under these conditions, T cells upregulate hypoxia inducible factor 1 alpha (HIF-1α) which facilitates increased expression of glucose transporters (e.g. GLUT1, GLUT3)[44,45]. However, tumor cells, CAFs, myeloid-derived suppressor cells (MDSCs), and tumor-associated macrophages (TAMs) also heavily consume glucose, leaving T cells without an adequate supply to fuel glycolytic metabolism[46–48]. This results in decreased production of IFN-γ, reduced proliferative capacity, and impaired cytolytic function[49]. Tumor cells and cancer-associated fibroblasts also deplete amino acids such as arginine, which is required for T cell proliferation and to prevent acquisition of an exhausted phenotype[50–52]. Glutamine is another amino acid that is heavily consumed by tumor cells, and glutamine deficiency has been shown to promote CD4 T cell differentiation into anti-inflammatory regulatory T cells (T_{regs}), which suppress effector T cell function[53]. Of note, MDSCs and TAMs also heavily consume arginine and glutamine, and therefore contribute to depletion of these key metabolites in the TME[54–57].

The second mechanism is *metabolic suppression*, in which metabolic by-products are secreted into the TME and exert immunomodulatory functions on T cells. Several prominent immune modulatory metabolites include adenosine and kynurenine (produced by tumor cells, CAFs, MDSCs, and TAMs), and lactate, which is primarily secreted by tumor cells and CAFs. Other

examples include methylglyoxal, (R)-2-hydroxyglutarate (2HG), and 1-methylnicotinaminde (1-MNA)[58–62], all of which have been shown to be abundant in the TME across multiple cancer types. These immunosuppressive metabolites act in a multitude of ways to constrain T cell function. Adenosine binds to the A_2A receptor on T cells, which is a negative regulator of TCR signaling and IFN-γ production[63,64], while kynurenine reduces proliferation and IFN-γ production by activating the transcription factor aryl hydrocarbon receptor (AHR)[65]. Lactate limits T cell function by lowering the pH of the TME, resulting in decreased cytokine production and cytotoxic activity in T cells, and increased accumulation of suppressive immune cells[66,67]. Methylglyoxal, which is produced by tumor cells and MDSCs, suppresses T cell function by depleting the essential amino acid L-arginine[68], and 2HG, which is primarily secreted by IDH-mutated tumors, inhibits TCR signaling and impairs T cell activation and antitumor immunity[61]. Lastly, recent work from our lab shows that the production of 1-MNA by tumor cells and CAFs enhances expression of the cancer-promoting cytokine tumor necrosis factor alpha (TNF-α) while at the same time inhibiting expression of IFN-γ in CAR-T cells[62].

1.5.4 CAR-T cell metabolic pathways can be modified using genome editing

While pharmacological efforts to constrain tumor metabolism have yielded some encouraging preclinical results, corresponding success has yet to be attained in the clinical setting[69]. This may be attributed to the fact that tumor cells and effector T cells share many of the same metabolic features, creating a narrow therapeutic window of opportunity in which to deliver metabolically-targeted pharmacological agents. However, it has recently been demonstrated in murine models that the suppressive effects of tumor metabolism can be mitigated by targeting T cells directly, for example by overexpressing glucose transporters or constitutively activating transcription factors involved in mitochondrial biogenesis[70,71]. These results suggest that genetic modification of T cell metabolic pathways could be a strategy to enhance antitumor immunity.

Indeed, CRISPR-Cas9 has already been used to rewire metabolic pathways in CAR-T cells through direct editing of metabolic genes. One such example is Regnase-1, which regulates mTORC1 signaling and purine metabolism during inflammation[72] and was recently identified in an *in vivo* CRISPR-Cas9 knockout screen as critical for T cell persistence[73]. In a follow-on study, deletion of Regnase-1 in CAR-T cells was shown to increase production of IFN-γ and

granzyme B, reduce T cell exhaustion, and improve antitumor activity[74]. A second example is the A_2A receptor, which is activated by the well-known immune-suppressive metabolite adenosine. Deletion of the A_2A receptor in CAR-T cells was recently shown to enhance IFN-γ and TNF-α production and improve tumor rejection *in vivo*, with no compromise to overall CAR-T persistence[75]. These studies demonstrate that genome editing with CRISPR-Cas9 can be used to successfully overcome both metabolic restriction and metabolic suppression.

1.5.5 Targeting the autophagy pathway to enhance CAR-T cell efficacy

Autophagy is a cytoplasmic salvage pathway in which intracellular components are sequestered and degraded by lysosomes (Figure 3). At basal levels, autophagy acts as a housekeeping process to maintain the integrity of the cell through selective and non-selective degradation of misfolded proteins and damaged organelles. However, under conditions of stress such as nutrient deprivation, autophagy is highly activated and functions to prolong survival by catabolizing cellular components for energy generation and biosynthetic substrates[76]. Autophagy is regulated by the opposing actions of mammalian target of rapamycin complex 1 (mTORC1) and adenosine monophosphate activated protein kinase (AMPK). Under nutrient-replete conditions, mTORC1 inhibits autophagy to enable cell growth and metabolic activity. Conversely, stress signals such as starvation and decreased cellular energy activate AMPK, which in turn promotes initiation of autophagy[76]. Autophagy is also directly induced by hypoxia (through HIF signaling) and high levels of ammonia derived from glutamine catabolism[77]. Given these factors and others, it is clear that the solid TME provides numerous stimuli for autophagy activation.

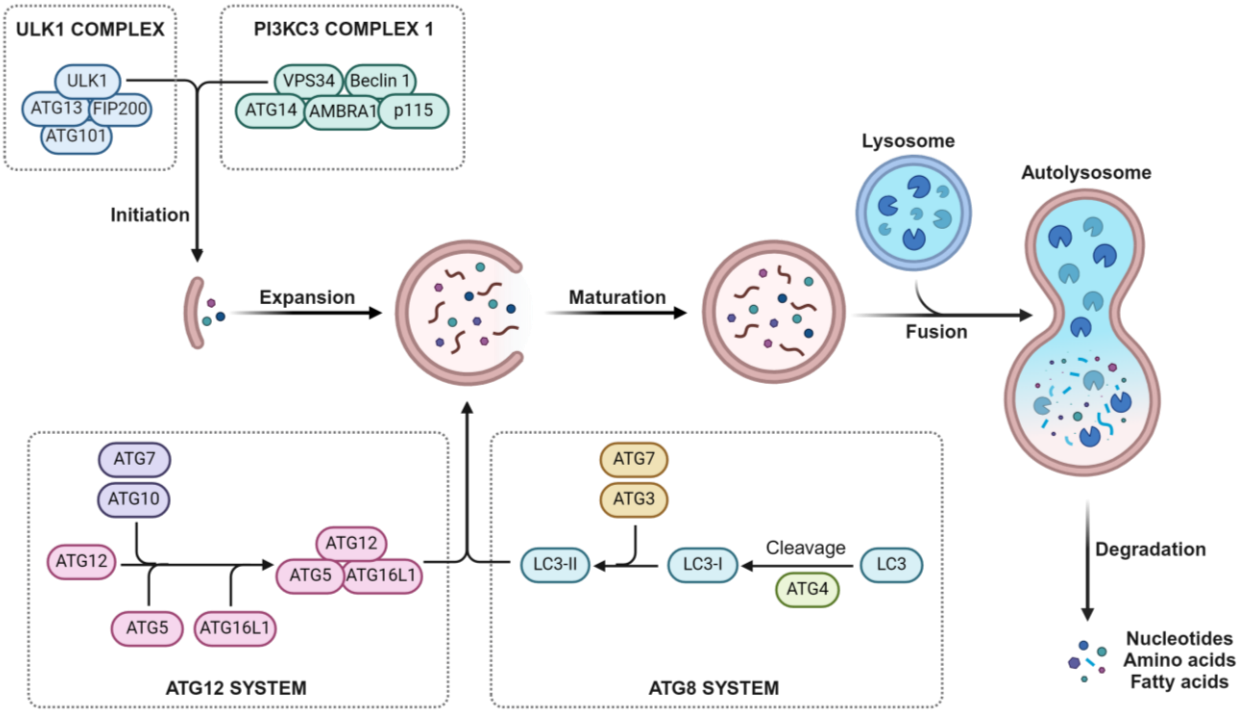

Figure 3. An overview of the mammalian autophagy pathway.

Autophagy is induced by activation of the ULK1 complex, containing ULK1, ATG13, FIP200, and ATG101. The ULK1 complex phosphorylates PI3KC3 complex 1 (consisting of VPS34, Beclin 1, ATG14, AMBRA1, and p115), which in turn facilitates the biogenesis of an isolation membrane through production of the signaling lipid phosphatidylinositol-3-phosphate (PI3P)[78]. Expansion of the isolation membrane is accomplished by two ubiquitin-like conjugation systems, the ATG12 system and the ATG8 system. In the ATG12 system, ATG12 is activated by the E1-like enzyme ATG7 and transferred to the E2-like enzyme ATG10, before ultimately becoming conjugated to ATG5. The ATG12-ATG5 conjugate forms a complex with ATG16L1 to enable binding to the membrane. In the ATG8 system, LC3 is cleaved by ATG4, activated by ATG7, transferred to ATG3, and conjugated to the membrane lipid phosphatidylethanolamine (PE) to form LC3-II. This lipidation reaction is promoted by the ATG12-ATG5-ATG16L1 complex which acts as an E3-like enzyme[79]. In addition to expansion and closure of the membrane, LC3-II is also involved in sequestration of cargo labelled with receptors containing an LC3-interacting region (LIR)[80]. Once the membrane is sealed, the ATG proteins are stripped from the membrane in a process called maturation. Finally, the mature autophagosome fuses with a lysosome, and acid hydrolases degrade the autophagic cargo into amino acids, fatty acids, and nucleotides to be

released back into the cytosol. ULK1, Unc-51-like kinase 1; ATG, autophagy-related; FIP200, FAK family-interacting protein of 200 kDa; PI3KC3, class III phosphatidylinositol-3-kinase; VPS34, vacuolar protein sorting 34; AMBRA1, activating molecule in Beclin 1-regulated autophagy protein 1; p115, general vesicular transport factor; LC3, microtubule-associated protein light chain 3. Image created with Biorender.com.

The role of autophagy in tumor cells has been well-described, with the general consensus being that autophagy activation in the later stages of tumor progression supports tumor growth and survival[81–83]. Less is known about how autophagy regulates immune cell function in the context of cancer, although there is a growing body of evidence to support autophagy inhibition as a mechanism for promoting T cell activation. For example, it was recently demonstrated that genetic deletion of the essential autophagy gene *FIP200* correlates with increased T cell infiltration in a mouse model of breast cancer[84]. Similarly, mice lacking the Atg8/LC3 family member gamma-aminobutyric acid type A receptor-associated protein (GABARAP) show inhibited tumor growth and increased production of the pro-inflammatory cytokines interleukin 2 (IL-2) and IFN-γ[85]. Our lab has demonstrated that genetic deletion of *Atg5* in murine T cells allows tumor-infiltrating lymphocytes (TIL) to retain an immunologically- and metabolically-polarized phenotype characterized by elevated glycolysis, increased production of effector cytokines, and epigenetic reprogramming of immune response genes[86]. These results support genome editing of the autophagy pathway as a strategy to enhance CAR-T cell efficacy in solid tumors.

1.6 Improving safety and accessibility of Canadian CAR-T therapies through nonviral manufacturing

1.6.1 CAR-T cell therapy and the Canadian health system

In 2018, Health Canada approved the first CD19 CAR-T therapy for Canadian patients with relapsed or refractory large B-cell lymphoma, follicular lymphoma, and primary mediastinal B-

cell lymphoma. Since then, the list of approved CAR-T therapies in Canada has expanded rapidly, with six products available to Canadian patients as of 2024. However, these therapies are extremely costly. Reimbursement of the first two CD19 CAR-T cells, tisagenlecleucel and axicabtagene ciloleucel, was estimated to reach $840 million in the first three years alone[87]. In an attempt to make CAR-T therapy more sustainable in the context of a publicly-funded healthcare system, the first Canadian CAR-T trial (CLIC-01) was launched in December of 2019 through a collaborative pan-Canadian effort[88]. In addition to treating over 60 patients to date, CLIC-01 demonstrated feasibility of a non-commercial CAR-T cell manufacturing platform and laid the groundwork for future made-in-Canada CAR-T products.

1.6.2 Challenges associated with current CAR-T manufacturing practices

A significant challenge in the Canadian cell therapy field is the reliance on viral vectors for CAR-T cell manufacturing, specifically lentivirus. At present, the Ottawa Biotherapeutics Manufacturing Centre is the only Canadian site with capacity to produce viral particles at scale for a CAR-T trial, which could create a bottleneck as demand increases. Viral vector production also requires extensive quality control and assurances[89], which adds another layer of operational complexity. Furthermore, the use of viral vectors in cell therapies introduces issues related to safety, such as the risk of insertional mutagenesis and potential oncogenic transformation due to random transgene integration[90,91]. While the risk of developing a T-cell malignancy after CAR-T treatment is low, the FDA recently issued a boxed warning for all approved CAR-T therapies[92].

A second limitation of the current manufacturing process is the personalized nature of autologous CAR-T cells. First, the quality of the final product can be significantly impacted by the characteristics of the starting material. For example, a higher proportion of naïve, stem cell, and central memory T cells in the apheresis product is linked to improved CAR-T cell expansion *ex vivo*, as well as more durable responses *in vivo*[93–95]. However, these favourable T cell lineages are depleted by repeated cycles of chemotherapy[96,97]. As CAR-T cells are yet to be approved for first-line therapy, this means that eligible patients will already be at an immunological disadvantage due to previous treatment regimens. Second, there is large patient-to-patient variability in both CAR transduction efficiency and CAR-T expansion[88], which can increase the risk of a manufacturing failure. Lastly, using autologous cells adds a time delay of 10-12 days

while the CAR-T therapy is produced, which may prove detrimental to patients with a high disease burden. Given these challenges, there is growing interest in advancing allogeneic cell therapies to improve efficacy and accessibility for patients. As the field moves towards this "off-the-shelf" model, there is a pressing need to develop alternative manufacturing processes that support production of allogeneic CAR-T cells at Canadian point-of-care sites.

1.6.3 Nonviral CAR-T cell manufacturing with CRISPR-Cas9

Nonviral genome editing with CRISPR-Cas9 can be used to improve safety and accessibility of Canadian-made CAR-T therapies. First, the CAR transgene can be delivered using double-stranded DNA (dsDNA) or single-stranded (ssDNA) donor templates, which eliminates the need for viral vectors and reduces safety risks associated with random integration. Second, the editing ability of Cas9 can be leveraged to delete genes associated with alloreactivity, thereby facilitating creation of allogeneic CAR-T therapies. In addition to an improved safety profile, dsDNA and ssDNA donor templates are also cheaper and easier to produce than the lentivirus or retrovirus used for most CAR-T studies. In particular, dsDNA donors can be rapidly produced at the bench using large-volume PCR with a high-fidelity polymerase, making them an ideal choice for preclinical efficacy experiments. However, in comparison to viral donor templates such as AAV6, completely nonviral methods have historically been hindered by low knock-in efficiency and high toxicity[98]. Therefore, successful implementation of a nonviral CAR-T manufacturing system will require new strategies to improve efficiency and viability, and these strategies must seamlessly integrate into the current clinical pipeline.

1.7 Conclusion

CAR-T cell therapy has undoubtably revolutionized the treatment of hematological malignancies. However, the broad effectiveness of this therapy is hindered by several unresolved issues, most notably a lack of therapeutic efficacy in treating solid tumor cancers. A second issue stems from the widespread use of viral vectors in CAR-T manufacturing, which poses safety risks due to the potential for oncogenic transformation. Genome editing with CRISPR-Cas9 can

be used to overcome both of these challenges and improve the efficacy, safety, and accessibility of CAR-T cell therapy for patients with cancer.

1.8 Hypotheses and aims

1.8.1 Hypotheses

1. CRISPR-mediated deletion of the autophagy pathway enhances CAR-T cell cytotoxicity.
2. Nonviral engineering of CAR-T cells is feasible and can be implemented within the current Canadian cell therapy infrastructure.

1.8.2 Aims

1. Develop a CRISPR-Cas9 genome editing strategy for all-in-one editing at the *ATG5* locus.
2. Optimize editing parameters to maximize HDR efficiency.
3. Determine specificity of editing at *ATG5* using GUIDE-Seq.
4. Metabolically and immunologically characterize *ATG5*-knockout CAR-T cells.
5. Assess *in vitro* cytotoxicity of *ATG5*-knockout CAR-T cells under standard and immunosuppressive conditions.
6. Assess therapeutic efficacy of *ATG5*-knockout CAR-T cells against ovarian tumors *in vivo*.
7. Develop a genome editing method for nonviral production of CD22 CAR-T cells.
8. Validate *in vitro* cytotoxicity of nonviral CD22 CAR-T cells.
9. Test clinically-relevant methods to improve efficiency of nonviral manufacturing.

Chapter 2: Method development for single-step metabolic engineering of CAR-T cells with CRISPR-Cas9

Authors:

Gillian A. Carleton[1,2], Sébastien Levesque[3,4,5,6,7], Yannick Doyon[8,9], and Julian J. Lum[1,2]

Affiliations:

1. Department of Biochemistry and Microbiology, University of Victoria, Victoria, BC.
2. Trev and Joyce Deeley Research Centre, BC Cancer, Victoria, BC.
3. Division of Hematology/Oncology, Boston Children's Hospital, Boston, MA.
4. Department of Pediatric Oncology, Dana-Farber Cancer Institute, Boston, MA.
5. Harvard Stem Cell Institute, Cambridge, MA.
6. Broad Institute, Cambridge, MA.
7. Department of Pediatrics, Harvard Medical School, Boston, MA.
8. Centre Hospitalier Universitaire de Québec Research Center – Université Laval, Québec, QC.
9. Université Laval Cancer Research Centre, Québec, QC.

Author contributions:

G.A.C designed and performed experiments, analyzed the data, and wrote the text. G.A.C, S.L., and Y.D. designed the CAR donor templates. S.L. designed the fluorescent donor construct and generated *ATG5*-edited K562 clones. S.L. and Y.D. performed the GUIDE-Seq experiment and analyzed the sequencing data.

Author contributions to tables and figures:

G.A.C. created Table 1 and Table 2.
G.A.C. created Figure 4A and S.L. created Figure 4B.
S.L. created Figure 5A, B, and C, and G.A.C. created Figure 5D and E.
G.A.C. created Figures 6 and 7.
S.L. created Figure 8A and B, and G.A.C. created Figure. 8C.
G.A.C. and J.J.L edited the text.

2.1 Abstract

CAR-T cell therapy has revolutionized the treatment of hematological malignancies. However, similar responses have yet to be attained in solid tumors, due in part to suppressive mechanisms in the tumor microenvironment that limit CAR-T cell efficacy. To overcome these barriers, engineering strategies must facilitate additional modifications beyond mere introduction of a CAR construct. Here, we combined CRISPR-mediated homology-directed repair with a gene-trap approach to facilitate single-step metabolic engineering of CAR-T cells. Using an AAV6 donor template, we integrated a CAR at the locus of the essential autophagy gene *ATG5* to generate CAR-T cells with simultaneous deletion of the autophagy pathway. We uncovered a novel role for AAV6 dose in regulating CAR-T cytotoxicity, and showed that *ATG5*-knockout CAR-T cells made with increased AAV6 exhibited superior cytotoxicity when compared to CAR-T cells made with lower doses. Lastly, we used GUIDE-Seq to identify potential off-target editing events, and showed that specificity of our *ATG5* editing system could be improved by a high-fidelity Cas9 mutant. Our results demonstrate the feasibility of generating CRISPR-engineered CAR-T cells in a single-step editing process, and more broadly, provide a technical framework for the development of future gene-edited CAR-T therapies.

2.2 Introduction

The effectiveness of CAR-T cells in treating solid tumors is impeded by several factors, including antigen heterogeneity, physical barriers to CAR-T cell infiltration, and metabolic suppression by the tumor microenvironment[26–29]. Given these challenges, there is a growing consensus that successful tumor clearance will require functional enhancement beyond mere introduction of a CAR construct. However, clinical CAR-T therapies rely on viral production methods, specifically randomly-integrating retrovirus or lentivirus, which offer few opportunities to make additional modifications to the genome[99]. While efforts have been made to facilitate co-expression of a CAR and a second transgene, these approaches have their own drawbacks. For example, dual transduction with two separate vectors increases the risk of insertional mutagenesis and potential oncogenic transformation[100]. Similarly, encoding both genes on the

same vector is challenging due to limited packaging capacity[101]. Larger inserts are also packaged with less efficiency, which negatively impacts viral titer and transduction rate[102].

In comparison to retroviral and lentiviral transduction, genome editing offers a high level of precision and customization to support advanced CAR-T cell engineering. Indeed, CRISPR-Cas9 has already shown potential in addressing some of the concerns associated with treating solid tumors. Examples of this include improved antigen sensitivity[103], decreased CAR-T cell exhaustion[104], and resistance to adenosine-mediated suppression in the TME[75]. CRISPR-Cas9 gene-editing can be used in combination with viral transduction, as was demonstrated by Stadtmauer *et al*. in the landmark clinical trial where TCR-transgenic T cells were produced using lentivirus and subsequent editing of three genomic loci was carried out by RNP electroporation[10]. However, the targetable nature of CRISPR-Cas9 can also be exploited to achieve CAR delivery coupled with *simultaneous* functional enhancement, namely, by inserting the CAR directly into the locus of the gene to be deleted.

Here, we develop a gene-editing method to engineer CAR-T cells deficient for the essential autophagy gene *ATG5*. By using a gene-trapping approach to combine targeted CAR integration with concomitant silencing at *ATG5*, our method generates *ATG5*-knockout CAR-T cells in a single editing step, thereby eliminating the need for viral CAR transduction and circumventing the challenges associated with randomly-integrating vectors.

2.3 Materials and Methods

2.3.1 Cell line culture

K562 human leukemia cells (CCL-243, ATCC) were grown in RPMI 1640 (Gibco) supplemented with 10% heat-inactivated fetal bovine serum (FBS; Sigma), 2 mM L-glutamine (ThermoFisher), and 1% penicillin-streptomycin (ThermoFisher). Luciferase-expressing SKOV3 human ovarian cancer cells (SKOV3-Luc, a gift from Dr. Julian Smazynski) were grown in McCoy's 5A (Gibco) supplemented with 10% heat inactivated FBS, 1% penicillin-streptomycin, and 2 μg/ml puromycin (Gibco).

2.3.2 Guide RNA screening in K562 cells

ATG5-targeting gRNA sequences were designed using the online tool CRISPOR[22] and cloned into pSpCas9(BB)-2A-GFP (Addgene #48138, a gift from Feng Zhang). For gRNA screening, 200,000 K562 cells were electroporated with SpCas9-sgRNA vector (500 ng or 750 ng, as indicated) on the 4D-Nucleofector X Unit (Lonza) using the SF nucleofection kit and pulse code FF-120. Genomic DNA (gDNA) was extracted from electroporated cells 3 days post-electroporation using QuickExtract (Lucigen) as per the manufacturer's protocol. The percentage of edited alleles was quantified using the Surveyor mutation detection kit (Transgenomics) as previously described[105]. Samples were run on 10% PAGE gels, imaged with a ChemicDoc MP system (Bio-Rad), and image quantifications performed using Image Lab software (Bio-Rad). All gRNA sequences can be found in Supplementary Table 6.

2.3.3 Selection of *ATG5*-knockout K562 clones

Single cell-derived K562 clones expressing the fluorescent mScarlet-I reporter from the *ATG5* locus were generated as previously described[106]. In brief, the ATG5-I2A-824 gRNA sequence was cloned into eSpCas9(1.1)_No_FLAG_*ATP1A1*_G3_Dual_sgRNA (Addgene #86613) to generate a Cas9-expressing vector targeting both *ATG5* and *ATP1A1*. K562 cells were electroporated with 350 ng of eSpCas9 vector, 700 ng of *ATG5*-mScarlet-I_NLS donor, and 5 pmol of *ATP1A1*-Q118R-N129D ssODN donor. Cells were treated with the Na/K-ATPase inhibitor ouabain octahydrate (0.5 μM; Sigma) for 3 days post-transfection to enrich for editing at *ATP1A1*, then single-cell sorted on mScarlet-I expression using a FACSAria cytometer (BD Biosciences) and cultured in 96-well plates.

2.3.4 *ATG5* complementation assay

K562 cells constitutively expressing ATG5 from the *AAVS1* safe-harbour locus were generated as previously described[107]. In brief, the *ATG5* cDNA cassette (GenScript) was cloned into *AAVS1*_Puro_PGK1_3xFLAG_Twin_Strep (Addgene #68375) to generate an *ATG5* donor template with homology arms for *AAVS1*. K562 *ATG5*-knockout clone 5 was electroporated with 350 ng of eSpCas9 vector targeting *AAVS1* and 700 ng of *AAVS1*_Puro_PGK1_ATG5-cDNA

donor and single-cell clones were picked and expanded for 10 days in methylcellulose-based semi-solid RPMI medium (Gibco) supplemented with 0.5 μg/ml puromycin (Gibco).

Wild-type, *ATG5*-knockout, and *ATG5*-complemented K562 cells were assessed for autophagy function using a standard flux assay. Cells were cultured for 20 hours at 37°C in medium supplemented with 30 μM hydroxychloroquine and/or 200 nM rapamycin (both Cayman Chemicals), as indicated. After culture, cells were pelleted and resuspended in RIPA buffer (50 mM Tris-HCl pH 7.4, 1% NP-40, 0.25% Na-deoxycholate, 150 mM NaCl, 1 mM EDTA) supplemented 1:100 with protease and phosphatase inhibitor cocktail (ThermoFisher). Cells were lysed for 30 minutes on ice, then centrifuged for 10 minutes at 13000 rpm and 4°C. Lysates were mixed 1:10 with sample reducing agent and 1:4 with LDS buffer (both Invitrogen) and heated for 10 minutes at 70°C before loading onto 4-12% gradient Bis-Tris gels (Invitrogen). Protein was transferred onto nitrocellulose membranes, blocked for 60 minutes in blocking buffer (LI-COR Biosciences) diluted 1:1 with phosphate-buffered saline (PBS; Gibco), and stained overnight at 4°C with anti-ATG5 (1/500; Sigma, #A0731), anti-LC3 (1/500; Novus Biologicals, #NB100-2220), anti-Tubulin (1:1000; Santa Cruz Biotechnology, #SC-32293), or anti-GAPDH (1:1000; Novus Biologicals, #NB300-221) as indicated. After washing, membranes were incubated for 1 hour at room temperature with anti-mouse (1/10,000; Cell Signaling, #7076S) or anti-rabbit (1/5000; Invitrogen, #A21109) secondary antibodies. All staining was performed in blocking buffer diluted 1:1 with PBS.

2.3.5 Design and synthesis of components for T cell editing

The *ATG5*-targeting gRNA (ATG5-I2A-824; originally designed using CRISPOR) was selected for T cell editing experiments after screening in K562 cells as described in section 2.3.2. The *AAVS1*-targeting guide RNA (AAVS1-I1)[108] was previously described in the literature. Guide RNAs were synthesized by IDT (Alt-R sgRNA), resuspended in nuclease-free water to 100 μM, and stored at -80°C. All gRNA sequences can be found in Supplementary Table 6.

CAR donor sequences (ATG5-αFR and AAVS1-αFR) were designed around a published αFR-CAR construct[109]. The CAR comprised a CD8 leader sequence, an scFv targeting human αFR, a CD8 hinge and transmembrane domain, a CD28 costimulatory domain, and a CD3ζ intracellular

domain. Each donor included a splice acceptor (SA) and 2A self-cleaving peptide (2A) sequence immediately upstream of the CAR, and a bovine growth hormone polyadenylation (pA) sequence immediately downstream of the CAR. Full donor sequences were synthesized as gBlocks (IDT) and cloned into adeno-associated virus serotype 6 (AAV6) vectors using Gibson assembly. Recombinant CAR-AAV6 was produced by the viral vector core at the Canadian Neurophotonics Platform, and the virus was resuspended in PBS 320 mM NaCl + 5% D-sorbitol + 0.001% pluronic acid and stored at -80ºC until use. All donor sequences can be found in Supplementary Table 7.

2.3.6 T cell isolation and culture

Peripheral blood mononuclear cells (PBMCs) were isolated from healthy donor leukapheresis products (STEMCELL) by Ficoll gradient density centrifugation. CD3+ T cells were isolated from PBMCs using positive selection CD3 microbeads (Miltenyi) as per the manufacturer's protocol. T cells were stimulated with 25 μl Immunocult CD3/CD28 T cell activators (STEMCELL) per 1 million cells and cultured in Immunocult-XF medium (STEMCELL) supplemented with 1% penicillin-streptomycin (ThermoFisher), 2 mM L-glutamine (ThermoFisher), and 300 U/ml IL-2 (Peprotech). Activated T cells were expanded for 3 days prior to electroporation.

2.3.7 T cell electroporation and CAR-AAV6 transduction

ATG5- and *AAVS1*-targeting RNPs were prepared as previously described[110]. In brief, sgRNA (100 μM, IDT) was mixed in a 2:1:1 molar ratio with poly-l-glutamic acid (PGA; 100 mg/ml, Sigma) and SpCas9 or HiFiCas9 nuclease as indicated (10 mg/ml, both IDT), and incubated for 15 minutes at 37ºC. T cells were resuspended in electroporation buffer P3 (Lonza), mixed with RNPs at a ratio of $1x10^6$ cells/50 pmol RNP (on a Cas9 basis), and electroporated in 16-well nucleocuvette strips on the 4D-Nucleofector X Unit (Lonza) using pulse code EO115 or EH115 as indicated. For RNP-only experiments, 80 μl of pre-warmed T cell medium (no IL-2) was added to each well immediately post-electroporation, and the nucleocuvette strip was returned to the incubator for 15 minutes at 37ºC. After 15 minutes, T cells were transferred to a 48-well plate at a density of $1x10^6$ cells/ml in complete T cell medium.

For AAV6 experiments, 80 μl of pre-warmed medium was added to each well and then T cells were gently transferred from the nucleocuvette strip to a 96-well round-bottom plate containing CAR-AAV6 (Neurophotonics) diluted in T cell medium at the indicated MOI. The plate was returned to the incubator for 6-8 hours incubation with AAV6 at a high cell density. After this incubation period, T cells were transferred to a 48-well plate at a density of $1x10^6$ cells/ml in complete T cell medium.

2.3.8 Indel quantification

Genomic DNA was extracted from edited cells for quantification of indels by Surveyor nuclease assay, Sanger sequencing, or amplicon sequencing (Illumina). Genomic DNA was also extracted from wild-type cells to use as a negative control. In brief, 500,000 to 1 million cells were collected, centrifuged for 5 minutes at 1200 rpm, aspirated, and resuspended in 30-50 μl QuickExtract solution (Lucigen). Samples were mixed by vigorous pipetting and incubated in a thermocycler at the following settings: 15 min at 65°C, 15 min at 68°C, 10 min at 98°C. Genomic DNA was quantified by NanoDrop (ThermoFisher) and normalized to 100 ng/μl with nuclease-free water.

For Surveyor nuclease assay, genomic DNA was PCR-amplified using Phusion polymerase (New England BioLabs). Indels were detected using the Surveyor Mutation Detection kit (IDT) as per the manufacturer's recommendations. In brief, edited and wild-type amplicons were hybridized using a thermocycler, digested with Surveyor nuclease, and the cleavage products visualised by gel electrophoresis.

For Sanger sequencing, genomic DNA was PCR-amplified using KAPA-HiFi polymerase (Roche). PCR products were purified and sequenced on an ABI 3730xl Data Analyzer (Applied Biosystems). Edited and wild-type sequences were compared and indel quantification performed using the online TIDE algorithm[111] as per the recommended guidelines.

For amplicon sequencing, primers containing Illumina forward and reverse adapters were used for a first round of PCR, and the products were purified using AMPure XP magnetic beads (Beckman-Coulter) and evaluated for quality by electrophoresis. A second round of PCR and

bead purification was performed for indexing, and amplicons were sequenced on an Illumina MiSeq. Alignment of amplicon sequences to the reference *ATG5* sequence was performed using CRISPResso2[112] with the default parameters, and indels were quantified as the percentage of modified reads. All primer sequences can be found in Supplementary Table 8.

2.3.9 Flow cytometry analysis

Percentage of CAR-positive cells after electroporation and CAR-AAV6 transduction was determined by multicolor flow cytometry. T cells were collected ($1x10^6$ cells per condition), stained with fixable viability dye eF506 (1/2000; Invitrogen #65-0866-14) for 15 minutes at 4ºC, then washed and resuspended in Human TruStain FcX blocking solution (Biolegend) and Brilliant Stain Buffer Plus (BD Biosciences) for 10 minutes at room temperature. After blocking, cells were stained for 20 minutes at room temperature with the following antibody cocktail diluted in flow cytometry staining buffer: CD3-BV750 (1/100; Biolegend #344845) and CAR-AF647 (1/50; Cell Signaling #69782S). Cells were resuspended in flow cytometry staining buffer prior to acquisition on a Cytek Aurora spectral flow cytometer. Cytometry data were analyzed using SpectroFlo (Cytek) and FlowJo v10.10 (BD Life Sciences). A detailed list of all antibodies can be found in Supplementary Table 9.

2.3.10 Magnetic bead enrichment

CAR-T cells were collected, centrifuged for 5 minutes at 1500 rpm and 4°C, and washed once prior to staining for 30 minutes at room temperature with AF647-conjugated anti-G4S linker antibody (Cell Signaling, #69782S) diluted 1:50 in PBS. After staining, cells were washed twice, then incubated for 15 minutes at 4°C with anti-AF647 microbeads (Miltenyi) at a ratio of 10 µl beads per 5 million cells in cell-enrichment buffer (PBS supplemented with 0.5% heat-inactivated human serum (Sigma)). Cells were washed once with cell-enrichment buffer, then passed through an MS column (Miltenyi) for positive enrichment of labelled cells.

2.3.11 Quantitative PCR analysis

RNA was isolated from enriched CAR-T cells using the RNeasy Plus Mini Kit (QIAGEN) as per the manufacturer's protocol. cDNA was synthesized using the qScript cDNA Synthesis Kit

(Quanta Bioscience). Primers were designed to target the CAR sequence or the housekeeping gene *ACTB*, and cDNA was PCR-amplified using PowerUp SYBR Green Master Mix (ThermoFisher). Samples were run in triplicate on the StepOnePlus Real-Time PCR system (Applied Biosystems) using Microamp Fast Optical 96-Well Reaction Plates (Applied Biosystems). Mean CT values for each triplicate sample were normalized against mean CT values for *ACTB*, and relative fold change in CAR gene expression was calculated as 2^(-ΔCT). All primer sequences can be found in Supplementary Table 8.

2.3.12 GUIDE-Seq

GUIDE-Seq was performed as previously described[113,25]. In brief, GUIDE-Seq oligos modified with 5' phosphorylation and two phosphorothioate linkages between the last two nucleotides at the 3' end were synthesized by IDT. Oligos were resuspended in 50 mM NaCl, 10 mM Tris-HCl (pH 8.0), and 1 mM EDTA, and annealed by heating to 95^{o}C for 10 minutes, followed by gradual cooling on a thermocycler. For K562 cells, 2x10^{5} cells were electroporated with 750 ng SpCas9-sgRNA vector and 100 pmol of annealed GUIDE-Seq oligos as per section 2.3.1. For T cells, 1x10^{6} cells were electroporated with 50 pmol SpCas9 RNP and 100 pmol annealed GUIDE-Seq oligos as per section 2.3.7. Genomic DNA was harvested using the QIAmp UCP DNA Micro Kit (QIAGEN) and sequenced by Sanger sequencing, and GUIDE-Seq oligo tag integration was confirmed using TIDE[111] and DECODR[114].

The Next Generation Sequencing (NGS) library preparation procedure was modified from the original GUIDE-Seq procedure. After mechanical fragmentation, end-repair and A-tailing were directly performed using the NEBNext UltraII DNA kit (New England Biolabs). A new custom universal Y-adapter based on Illumina TruSeq sequences was designed to include a Unique Molecular Index (UMI) in the sequencing read instead of the index read. This adapter was ligated as described in the NEBNext Ultra II procedure using a final concentration of 133 nM. Ligated DNA was purified using AMPure XP beads (Beckman-Coulter) at a 0.9X volumetric ratio, then PCR-amplified with either Minus or Plus primers using Q5 DNA polymerase (New England Biolabs) with the following cycling conditions: 30 sec at 98^{o}C; 10 cycles of 10 sec at 98^{o}C, 30 sec at 55^{o}C, 30 sec at 72^{o}C; 15 cycles of 10 sec at 98^{o}C, 30 sec at 65^{o}C, 30 sec at 72^{o}C; 2 min at 72^{o}C; 4^{o}C hold. PCR products were purified with 0.9X AMPure XP beads and

quantified by Qubit dsDNA HS assay (Invitrogen). A second PCR amplification was performed using 10 ng of purified DNA from PCR1 and Illumina TruSeq dual-indexing primers (30 sec at 98°C; 8 cycles of 10 sec at 98°C, 30 sec at 55°C, 30 sec at 72°C; 2 min at 72°C; 4°C hold). PCR products were purified using 0.85X AMPure XP beads, quantified by Qubit dsDNA HS assay, and run on a Bioanalyzer High Sensitivity DNA chip (Agilent). Samples were pooled in equimolar amounts and sequenced on a 1.4% (35M read block) of a NovaSeq S4 PE150 lane (Illumina) at the Centre d'Expertise et de Services Génome Québec (Montréal, QC). All GUIDE-Seq primer and adapter sequences can be found in Supplementary Table 10.

2.3.13 Analysis of GUIDE-Seq sequencing data

Sequencing data from the GUIDE-Seq procedure was analyzed using the guideseq_ibis pipeline (https://github.com/enormandeau/guideseq_ibis). Raw reads were trimmed for quality using trimmomatic (v0.36, min_length 100, crop_length 200), and only reads containing the expected alien sequence (maximum hamming distance of 1) and only one copy of the GUIDE-Seq ODN sequence (maximum hamming distance of 6) were retained. For these reads, the Unique Read Identifiers (UMIs) and first eight nucleotides were used to rename the sequence, and these tagged reads were then mapped onto the latest GRCh38 human genome assembly with bwa (v0.7.17-r1188, -T 10) and samtools (v1.12, -S -q 1 -F 4 -F 256 -F 2048). The alignment sam files were then sorted by chromosome name and position. The UMI and first eight nucleotides of the reads and the starting positions of their alignments were used to detect duplicated reads. To identify double stranded breaks (DSBs), alignment sites were scanned for peaks of coverage in decreasing order of depth of coverage, and pairs of ODN+ and ODN- were reported until the pairs did not meet the minimum coverage threshold (min_length 100, min_coverage 50, window_size 10, position_error 5, bin_size 10000). To account for small errors in sequencing and mapping, read counts were collected within "window_size" nucleotides around each peak, and pairs of ODN sequences were only kept if they fell within "position_error" nucleotides of their relative expected positions. Identified sequences on-target and off-target were reported for each sample with their chromosome and position localisation, the identifier and name of any gene they overlapped, and metrics about the counts of ODN+ and ODN- reads. Chromosomal positions and targeted genes of all identified off-targets can be found in Table 1. Complete GUIDE-Seq results can be found in Table 2.

2.3.14 *In vitro* cytotoxicity assay

A luciferase-based assay was used to measure CAR-T cell cytotoxicity. In brief, CAR-T cells were co-cultured in a 96-well plate with luciferase-expressing SKOV3 human ovarian cancer cells (SKOV3-Luc) at the indicated effector-to-target (E:T) cell ratios. SKOV3-Luc cells were also cultured alone to determine the maximum luciferase expression (RLU_{max}), while medium-only wells were used to account for background luminescence ($RLU_{background}$). After 24 hours, D-Luciferin (1/20; Revvity Health Sciences) was added to each well, mixed by pipetting, and the plate was incubated in the dark for 5 minutes. Luminescence was measured on a Varioskan Lux plate reader (Thermo Scientific), and specific tumor cell lysis calculated as (RLU_{sample}/((RLU_{max}-$RLU_{background}$)) x 100.

2.4 Figures and Tables

Table 1. List of GUIDE-Seq genomic targets.

Guide	Genomic target	Sequence	PAM	Mismatches
On-target	*ATG5* intron 2	GCACCGAGTAGTACCACTTG	AGG	-
Off-target 1	*LOC105374445* ncRNA	GC**C**CCGAGTAGT**G**CCACTTG	TGG	2
Off-target 2	*EBF2* intron 1	**A**CACC**C**AG**C**AGTACCAC**C**TG	AGG	4

Table 2. GUIDE-Seq results.

K562 cells

Target ID	Chromosome/Gene	Site 1	Site 2	Count 1	Count 2	Total reads
On-target	Chr6 – *ATG5*	106314933	106315033	1020	1951	2971
Off-target 1	Chr4 – N/A	48270100	48270200	373	789	1162
Off-target 2	Chr8 – *EBF2*	26042535	26042635	97	95	192

T cells – Donor 1 (Day 3)

Target ID	Chromosome/Gene	Site 1	Site 2	Count 1	Count 2	Total reads
On-target	Chr6 – *ATG5*	106314933	106315033	525	784	1309
Off-target 1	Chr4 – N/A	48270100	48270200	291	851	1142
Off-target 2	Chr8 – *EBF2*	26042535	26042635	-	-	-

T cells – Donor 2 (Day 3)

Target ID	Chromosome/Gene	Site 1	Site 2	Count 1	Count 2	Total reads
On-target	Chr6 – *ATG5*	106314933	106315033	343	594	937
Off-target 1	Chr4 – N/A	48270100	48270200	195	665	860
Off-target 2	Chr8 – *EBF2*	26042535	26042635	-	-	-

T cells – Donor 2 (Day 11)

Target ID	Chromosome/Gene	Site 1	Site 2	Count 1	Count 2	Total reads
On-target	Chr6 – *ATG5*	106314933	106315033	2966	4505	7471
Off-target 1	Chr4 – N/A	48270100	48270200	1940	5046	6986
Off-target 2	Chr8 – *EBF2*	26042535	26042635	188	255	443

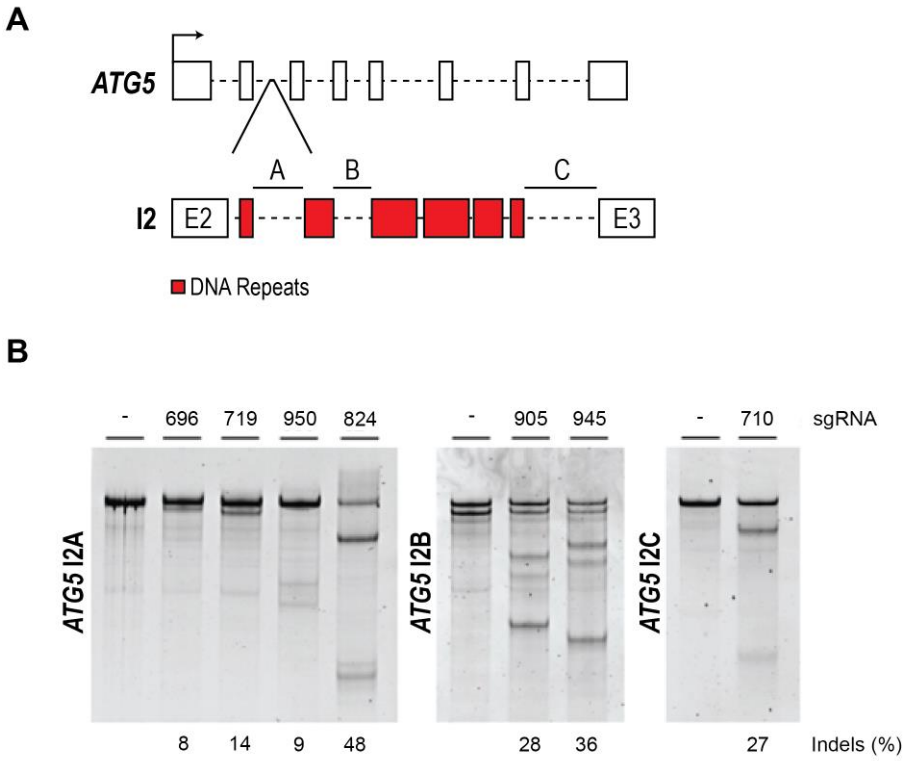

Figure 4. Guide RNA screening identifies a highly active gRNA at intron 2 of *ATG5*.
(A) Genomic structure and target regions within intron 2 (I2) of *ATG5*. A, B, and C denote non-repetitive target DNA sequences used to design gRNAs using the online tool CRISPOR[22]. **(B)** Surveyor nuclease assay showing percentage of insertions and deletions (indels) in K562 cells three days post-electroporation with SpCas9-sgRNA plasmid. Lanes labelled with "-" represent the control amplicon for that region. Cleavage products smaller than the control amplicon represent mutations induced by editing with each sgRNA.

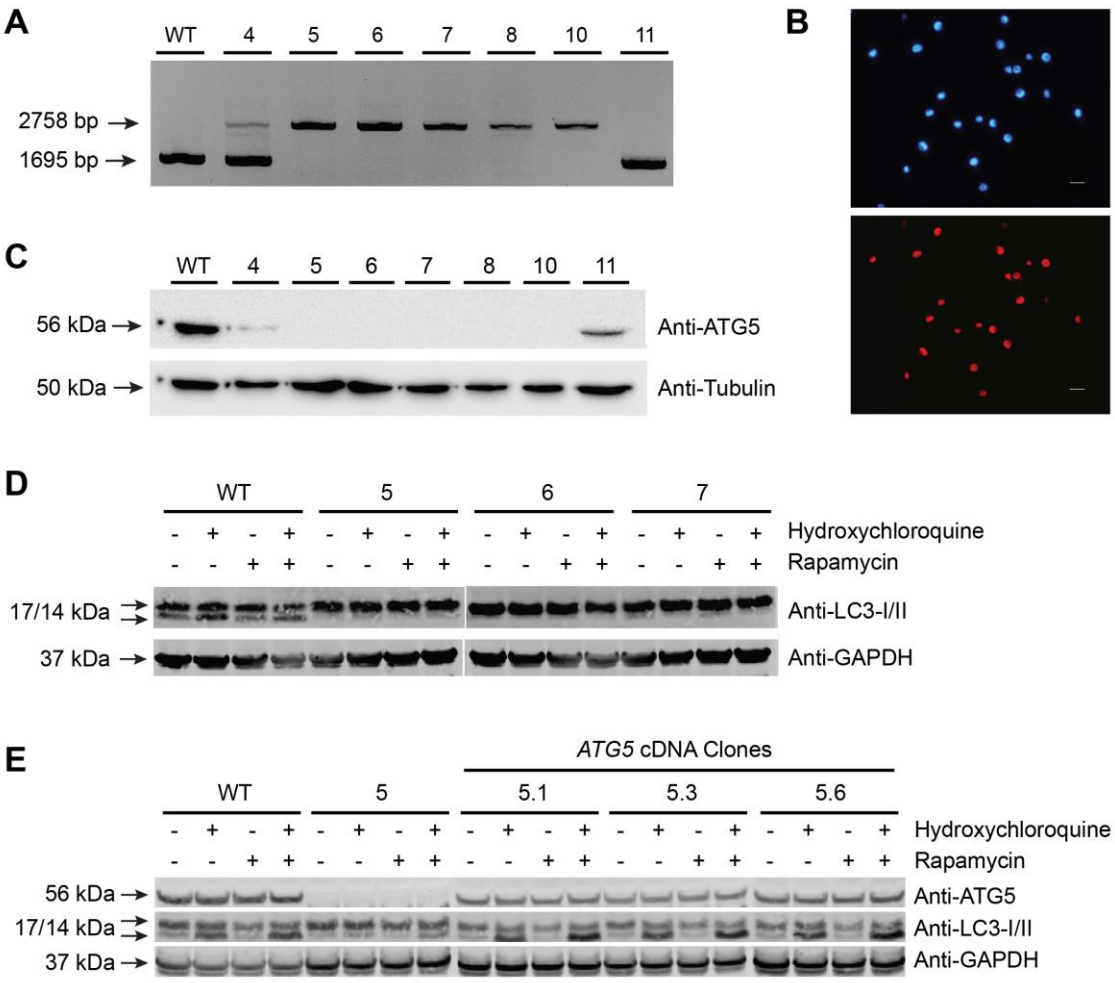

Figure 5. Integration of a donor construct at *ATG5* eliminates functional autophagy. **(A)** Out-out PCR showing donor integration at intron 2 of *ATG5*. **(B)** Fluorescent images of *ATG5*-knockout K562 cells showing Hoechst nuclear staining (top) and mScarlet fluorescence (bottom). **(C)** Western blot showing loss of ATG5 in mScarlet-integrated K562 clones. **(D-E)** Western blots showing response to treatment with hydroxychloroquine and/or rapamycin in *ATG5*-knockout clones (D) and *ATG5* cDNA clones (E). Loss of LC3-II indicating impaired autophagic flux is observed in clones 5,6,7. Restoration of autophagy function is observed in clones 5.1, 5.3, 5.6.

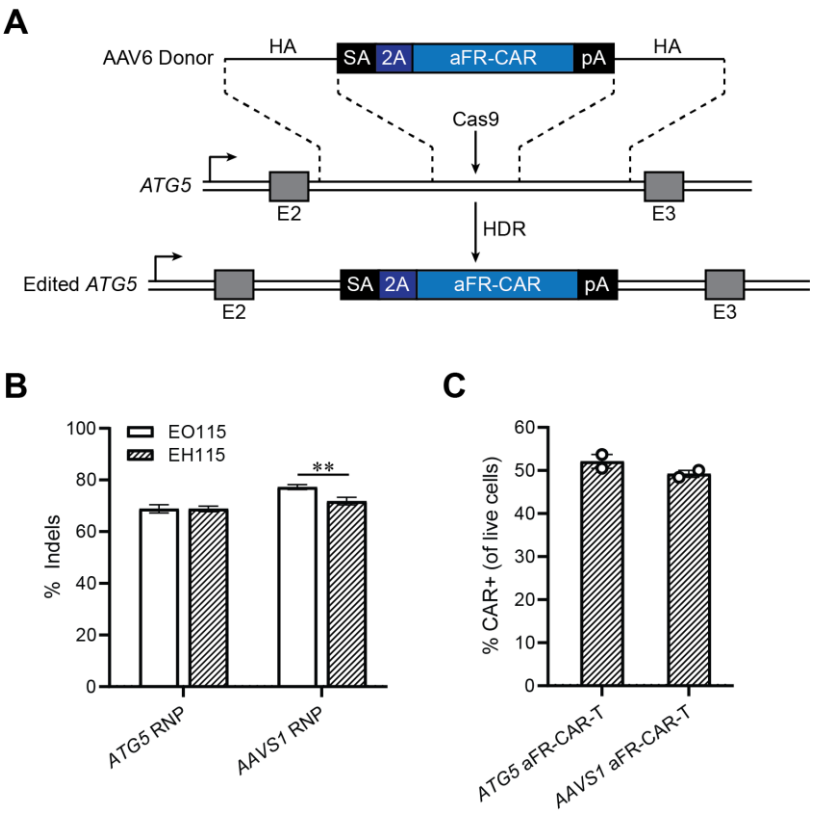

Figure 6. RNP electroporation and CAR-AAV6 transduction generates *ATG5*-knockout CAR-T cells.

(A) Schematic of the AAV6 donor template and *ATG5* locus after CAR integration. Exons (E) 2 and 3 of *ATG5* are shown as grey boxes. Also annotated are the splice acceptor site (SA), 2A self-cleaving peptide sequence (2A), polyadenylation sequence (pA), and homology arms (HA). **(B)** Indel quantification as determined by TIDE analysis from Sanger sequencing. CD3+ T cells were electroporated on the Lonza 4D using pulse codes EO115 (open bars) or EH115 (shaded bars) with RNPs targeting *ATG5* or *AAVS1*, and genomic DNA was harvested three days post-electroporation. Results are from three different healthy donors, n = 3 technical replicates per donor. **(C)** Bar graph showing percent CAR+ cells ten days after RNP electroporation and CAR-AAV6 transduction at an MOI of $1x10^4$. Results are from two different healthy donors, n = 1 replicate per donor. All error bars represent +/- SEM. P values were determined by Welch's *t* test (**p<0.01).

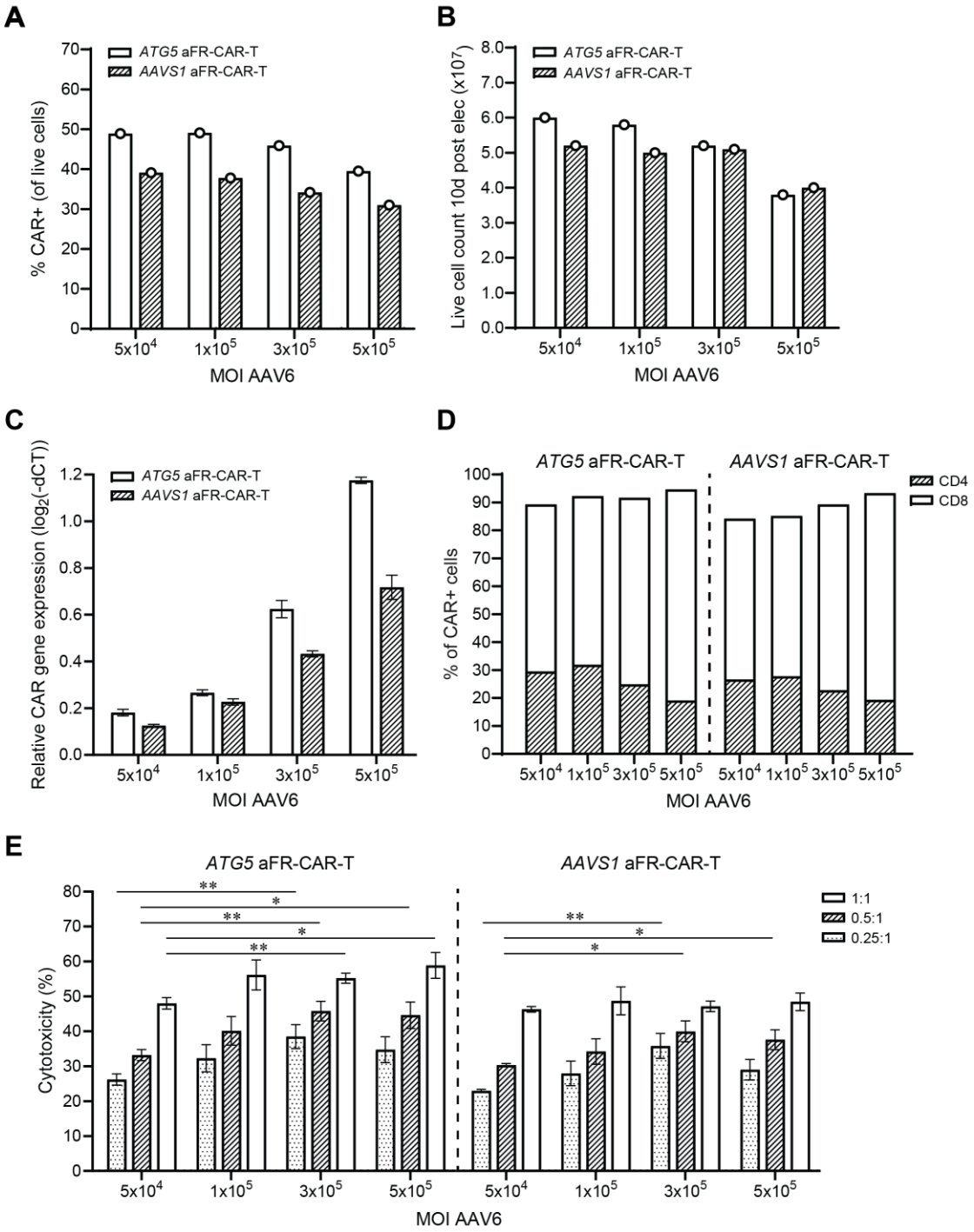

Figure 7. AAV6 dosage regulates CAR-T cell cytotoxicity.

(A-B) Bar graphs showing percent CAR+ cells (A) and number of live cells (B) ten days after RNP electroporation and CAR-AAV6 transduction at the indicated MOIs. Results are from one healthy donor. **(C)** Bar graph showing CAR gene expression after RNP electroporation and

CAR-AAV6 transduction at the indicated MOIs. CAR gene expression (relative to the housekeeping gene *ACTB*) was determined by qPCR. Results are from one healthy donor, n = 3 technical replicates. **(D)** Bar graph showing percentage of CD4+ and CD8+ CAR-T cells after RNP electroporation and CAR-AAV6 transduction at the indicated MOIs. Results are from one healthy donor. **(E)** Bar graph showing percent cytotoxicity of luciferase-expressing SKOV3 ovarian tumor cells after 24h co-culture with *ATG5* αFR-CAR-T cells (left) or *AAVS1* αFR-CAR-T cells (right) at effector-to-target cell ratios of 1:1, 0.5:1, or 0.25:1. Results are from 2 experiments performed with CAR-T cells from the same healthy donor, n = 4 technical replicates per experiment. All error bars represent +/- SEM. P values for each E:T ratio were determined by one-way ANOVA (*$p < 0.05$, **$p<0.01$).

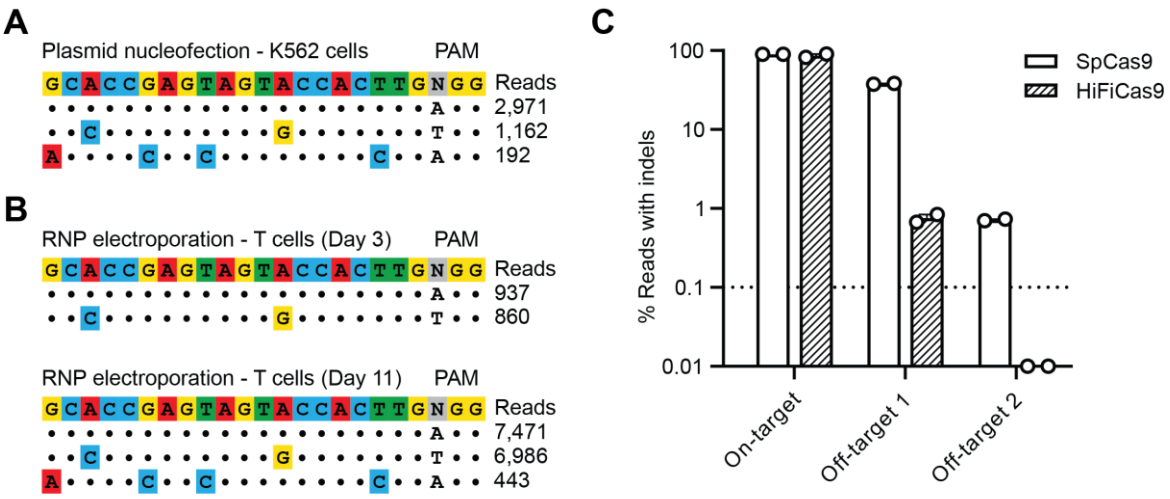

Figure 8. Off-target editing with *ATG5* sgRNA is mitigated by HiFiCas9.

(A) Allele plot showing off-target sites identified using GUIDE-Seq. K562 cells were electroporated with SpCas9-sgRNA plasmid targeting intron 2 of *ATG5* and GUIDE-Seq dsDNA tag. Genomic DNA was harvested three days post-electroporation. Dots represent matches with the intended target sequences, while mismatches are colored. **(B)** Same as **(A)** but with CD3+ T cells electroporated with SpCas9 RNPs targeting *ATG5* intron 2 and GUIDE-Seq dsDNA. Genomic DNA was harvested on Day 3 (top) or Day 11 (bottom) post-electroporation. Day 3 GUIDE-Seq read counts are from one of two different healthy donors. Day 11 read counts are from one healthy donor. **(C)** Indel quantification as determined by CRISPResso2 analysis from targeted amplicon sequencing. CD3+ T cells were electroporated with SpCas9 or HiFiCas9 RNPs targeting *ATG5* intron 2, and genomic DNA was harvested three days post-electroporation. The dotted line indicates a 0.1% limit of detection. Results are from n = 2 independent experiments performed with T cells from two different healthy donors.

2.5 Results

2.5.1 Design and validation of a gene-trap approach for integration at *ATG5* with concomitant loss of autophagy function

To design a gene-trap approach for donor integration at *ATG5*, we used the UCSC Genome Browser[115] to determine the first intron shared by all *ATG5* variants. This corresponded to intron 2 of the canonical *ATG5* sequence (transcript variant 1). We examined the sequence for intron 2, and selected three regions free of repetitive DNA elements that would be suitable for editing (Fig. 4A). We used the bioinformatics tool CRISPOR[22] to identify all possible gRNA sequences in each region of intron 2, and selected seven gRNAs with the highest predicted level of editing efficiency and a minimum MIT specificity score of 90. Each gRNA was transfected into K562 cells and the editing efficiency was quantified by Surveyor nuclease assay, which detects and cleaves mismatches between wild-type and edited DNA sequences (Fig. 4B). The gRNA with the most cleavage products and therefore the most indels (*ATG5*-824) was chosen for all future experiments.

Next, we built a donor construct containing an mScarlet fluorescent reporter gene preceded by a splice acceptor. The construct contained a polyadenylation sequence at the 3' end to terminate downstream transcription, and was designed without an exogenous promoter to determine whether the endogenous *ATG5* promoter could be used to drive transgene expression. We transfected K562 cells and confirmed that integration of the donor sequence correlated with a loss of ATG5 protein (Fig. 5A, C). Using fluorescence microscopy, we observed a strong fluorescent signal in our population of edited cells (Fig. 4B), which validated our proposed strategy of using the endogenous promoter. Functionally, mScarlet-integrated K562 cells showed complete ablation of autophagy as determined by a standard autophagy flux assay, wherein treatment with hydroxychloroquine failed to induce lipidation of LC3-I to LC3-II (Fig. 5D). Re-integration of an *ATG5* cDNA cassette into the intergenic locus *AAVS1* restored production of LC3-II (Fig. 5E), thereby confirming that autophagy-deficient phenotype we observed in mScarlet-integrated cells was specifically due to on-target editing at *ATG5*.

2.5.2 Homology-directed repair using AAV6 facilitates efficient CAR integration at *ATG5*

After establishing the feasibility of our gene-trap approach, we developed and optimized a method for high-efficiency CAR-T cell editing in CD3+ T cells. As our CAR target, we chose the ovarian cancer antigen folate receptor alpha (αFR), which has demonstrated an acceptable safety and toxicity profile in two clinical trials[109,116–118]. We designed two AAV6 donor templates containing a second-generation αFR-CAR construct with homology arms for integration at *ATG5* (Fig. 6A) or *AAVS1*. We screened T cell-specific electroporation parameters on the Lonza 4D nucleofector and identified EO115 as the pulse code with the highest production of indels after RNP electroporation (Fig. 6B). Immediately post-electroporation, we incubated cells with concentrated CAR-AAV6 for eight hours at a high cell density (4-5x10^6 cells/ml). This method generated greater than 45% CAR-positive cells in both CAR-T groups using T cells from two different healthy donors and an AAV6 multiplicity of infection (MOI) of 1x10^4 vector genomes per cell (vg/cell; Fig. 6C).

2.5.3 High-dose AAV6 generates a CAR-T product with increased functionality

Although a CAR knock-in percentage of 45% is reasonable for an edited cell therapy product, we sought to determine whether a higher MOI could potentially improve CAR knock-in rates. We tested four higher doses of CAR-AAV6 (ranging from 5x10^4 to 5x10^5 vg/cell), but unexpectedly, failed to see any increase in CAR+ cells by flow cytometry (Fig. 7A). A loss of viability was also observed at the highest dose (Fig. 7B), an effect that has been previously reported[119]. However, analysis by qPCR revealed MOI-dependent increases in CAR gene expression (Fig. 7C), which could indicate a higher proportion of bi-allelic editing events that would not necessarily be detected by flow cytometry. Higher doses of AAV6 also seemed to favor a shift towards more CD8+ T cells in the final CAR-T product (Fig. 7D). When we compared cytotoxicity between CAR-T cells made using different doses of AAV6, we observed a significant enhancement in cytotoxicity at high MOIs (Fig. 7E). Notably, this effect was more pronounced for *ATG5*-knockout CAR-T cells than for *AAVS1* CAR-T cells, with significantly improved cytotoxicity across all effector-to-target ratios when CAR-T cells were made with an MOI of 3x10^5 as compared to 5x10^4 (Fig. 7E, left panel). After weighing the benefits of

increased function against a loss in viability and proliferative capacity due to AAV6 toxicity, we selected an MOI of $3x10^5$ vg/cell as the optimal dose for generating *ATG5*-knockout CAR-T cells.

2.5.4 HiFiCas9 enables robust and specific editing at *ATG5*

Lastly, we performed off-target analysis to determine the specificity profile of our *ATG5*-824 gRNA. To screen for off-target edits, we used GUIDE-Seq, a method in which DSBs associated with a specific gRNA are tagged with oligodeoxynucleotides to enable identification by sequencing. We began by mapping all DSBs induced by plasmid electroporation in K562 cells, and detected GUIDE-Seq oligo tag integration at two additional sites outside of the on-target region at *ATG5* intron 2 (Fig. 8A; Table 1). The first off-target site ("OT1", located on chromosome 4 in a non-coding RNA sequence) accounted for the majority of the off-target reads, with 1162 reads vs. 2971 reads for the *ATG5* on-target site (Table 2). Editing at the second site ("OT2", located on chromosome 8 in the gene encoding the transcription factor *EBF2*) was much lower in comparison, with only 192 reads.

Next, we repeated the GUIDE-Seq process in CD3+ T cells from two healthy donors. In the first experiment (donor 1), we saw tag integration at OT1 three days after RNP electroporation with *ATG5*-824 and SpCas9, but were unable to detect any editing at OT2 (Fig. 8B, top panel). Given the low frequency of cleavage events at this site observed in K562 cells, we performed sequencing on Day 3 and Day 11 for the second experiment (donor 2), and were able to identify edits at both off-target sites in T cells by Day 11 (Fig. 8B, bottom panel). The majority of off-target editing occurred at OT1, with comparably few edits at OT2 (Table 2). We then tested whether a high-fidelity Cas9 mutant ('HiFiCas9") could be used to improve the specificity of our *ATG5*-824 gRNA. We repeated electroporations in both healthy donors using HiFiCas9 RNPs, and measured indels at each off-target site using amplicon sequencing. In comparison to wild-type Cas9 ("SpCas9"), HiFiCas9 completely abrogated editing at OT2 (below the 0.1% limit of detection) and reduced editing at OT1 to below 1% in both donors, while maintaining high on-target activity at *ATG5* (Fig. 8C). These results demonstrate that HiFiCas9 can be used to improve the specificity of editing at *ATG5*, an important safety consideration in the context of designing gene-edited cell therapy products for clinical application.

2.6 Discussion

Translating the success of CAR-T cells to solid cancer immunotherapy requires strategies to facilitate additional genetic modifications during the manufacturing process. In this chapter, we developed a method for CAR-T cell engineering that combines CRISPR-mediated homology-directed repair and gene-trapping into a single-step editing process. We established feasibility of this approach by targeting an αFR CAR to the locus of the autophagy gene *ATG5* to generate autophagy-deficient CAR-T cells for ovarian cancer immunotherapy.

ATG5 is an essential component of the ATG12-ATG5-ATG16L1 complex that facilitates lipidation of LC3-I to LC3-II, and is therefore considered indispensable for autophagy[79,120]. However, a key feature of metabolic networks is redundancy, wherein duplicate genes or alternative pathways ensure homeostasis is maintained in spite of perturbations to the system[121]. Therefore, after we confirmed donor integration and loss of ATG5 through DNA- and protein-based methods, we used functional assays to demonstrate inhibition of the LC3-I to LC3-II lipidation reaction. The results from these studies confirmed that CAR integration at *ATG5* would lead to complete ablation of the autophagy pathway, and that this effect would be stable even when an autophagy-inducing stimulus was applied.

Given the large size of the αFR CAR, we used AAV vectors to deliver the donor template during the editing process. AAV is a non-pathogenic DNA virus with serotypes that exhibit distinct cellular tropism, of which serotype 6 is widely used to facilitate HDR in immune-cell genome editing experiments[122,123]. A wide range of AAV6 doses have been reported in the literature, with MOIs as low as $2.5x10^3$ vg/cell and as high as $1x10^6$ vg/cell demonstrating efficient editing in human stem and progenitor cells (HSPCs) and T cells, respectively[104,119]. Therefore, we conducted a dose-escalation experiment to determine the optimal MOI for high-efficiency editing at *ATG5*. To our surprise, we saw no real difference in CAR expression across the four MOIs tested, and in fact, we saw a trend towards decreasing CAR integration with increasing MOI of AAV6. This result was in direct contrast to previous reports suggesting that high-dose AAV6 improves editing efficiency[124,125], although it should be noted that we only performed this experiment once due to the large amount of AAV6 required.

Interestingly, despite seeing no differences in CAR surface expression, we did detect MOI-dependent increases in CAR gene expression. One potential explanation for this result could be an increase in random integration, as AAV vectors have been shown to randomly integrate into the host genome, albeit at low frequencies[126]. However, the unique design of our donor template makes this explanation unlikely, as CAR expression requires precise insertion downstream of an endogenous promoter and in-frame with a coding gene sequence. A second explanation could be a dose-dependent increase in biallelic integration events, an effect which has been previously demonstrated in the literature[125]. This would result in higher CAR expression on a per-cell basis without changing the overall percentage of CAR-positive cells detected by flow cytometry. In support of this explanation, we saw increased *in vitro* cytotoxicity by CAR-T cells made with higher doses of AAV6. This effect was more pronounced for *ATG5*-integrated as opposed to *AAVS1*-integrated CAR-T cells, which aligned with our previous work showing differences in antitumor function between murine T cells with a homozygous versus a heterozygous knockout of *Atg5*[86]. These results suggest that AAV6 exerts a dose-dependent role on the cytotoxic function of gene-edited CAR-T cells, and this effect is likely mediated by increased biallelic CAR integration. Therefore, using a high-dose AAV6 transduction protocol could be a strategy to bias biallelic editing events for engineering approaches that require homozygous knockout of the target gene.

As the manufacturing of cell therapy products requires modification of a large number of cells, even low frequency off-target events can have significant consequences. However, the potential for off-target editing can be mitigated through careful gRNA design. Here, we used the bioinformatics tool CRISPOR to identify all gRNA sequences in intron 2 of *ATG5*. CRISPOR provides a specificity score for each gRNA (the "MIT specificity score") that summarizes all potential off-targets off a guide and can be used as an indicator of gRNA quality[127,128]. While we set a minimum MIT specificity score of 90 when identifying potential gRNAs for this study, it is important to note that high-specificity guides can still facilitate off-target cleavage. Accordingly, we used GUIDE-Seq to map DSBs associated with our *ATG5* gRNA, and uncovered two sites with measurable off-target editing. While any off-target editing is undesirable from a safety perspective, we were especially concerned by the potential for DSBs at the second off-target site. In comparison to OT1, which was found in a non-coding sequence, OT2 was found in the first

intron of the transcription factor *EBF2.* Although small indels induced by DSB repair at this location would be spliced out, CRISPR-Cas9 has been shown to induce formation of other DSB repair products such as large chromatin deletions[129]. In this scenario, unintended DSBs at OT2 could cause mutations in the coding sequence of *EBF2*. However, we were able to completely abrogate off-target editing at this site (and reduce editing at OT1 to below 1%) by using a high-fidelity Cas9 mutant (HiFiCas9). Importantly, there was no concomitant decrease in on-target editing when using HiFiCas9, which has been demonstrated with other engineered Cas9 mutants[23].

In conclusion, this study establishes feasibility for single-step CRISPR engineering of CAR-T cells for cancer immunotherapy, and uncovers a novel role for MOI-dependent regulation of edited CAR-T cell cytotoxicity. Furthermore, our results demonstrate the importance of combining both *in silico* and *in vitro* approaches to improve guide specificity and mitigate unintended off-target events in gene-edited cells intended for human cell therapy use.

Chapter 3: CRISPR-Cas9 engineering of the autophagy pathway improves therapeutic efficacy of CAR-T cells for ovarian cancer

Authors:

Gillian A. Carleton[1,2], Sébastien Levesque[3,4,5,6,7], Lauren G. Zacharias[8,] Tracey Sutcliffe[9], Peter H. Watson[2,10], Ralph J. DeBerardinis[8,11], Yannick Doyon[12,13], and Julian J. Lum[1,2]

Affiliations:

1. Department of Biochemistry and Microbiology, University of Victoria, Victoria, BC.
2. Trev and Joyce Deeley Research Centre, BC Cancer, Victoria, BC.
3. Division of Hematology/Oncology, Boston Children's Hospital, Boston, MA.
4. Department of Pediatric Oncology, Dana-Farber Cancer Institute, Boston, MA.
5. Harvard Stem Cell Institute, Cambridge, MA.
6. Broad Institute, Cambridge, MA.
7. Department of Pediatrics, Harvard Medical School, Boston, MA.
8. Children's Research Institute, UT Southwestern, Dallas, TX.
9. Animal Care Services, University of Victoria, Victoria, BC.
10. Biobanking and Biospecimen Research Services, Deeley Research Centre, BC Cancer, Victoria, BC.
11. Howard Hughes Medical Institute, UT Southwestern Medical Center, Dallas, TX.
12. Centre Hospitalier Universitaire de Québec Research Center – Université Laval, Québec, QC.
13. Université Laval Cancer Research Centre, Québec, QC.

Author contributions:

G.A.C designed and performed experiments, analyzed the data, and wrote the text. G.A.C created all figures. G.A.C, S.L., and Y.D. designed the CAR donor templates. L.G.Z. and R.J.D generated the metabolite profiling data. T.S. performed tumor injections and CAR-T cell infusions for animal experiments. P.H.W. oversaw biospecimen collection through the IROC-TTR. G.A.C and J.J.L edited the text.

3.1 Abstract

T-cell based immunotherapies such as CAR-T cell therapy face substantial hurdles when confronting solid tumors. This is particularly apparent in the case of ovarian cancer, where an inhospitable tumor microenvironment limits CAR-T cell infiltration and function through metabolic suppression. However, engineering of CAR-T cell metabolic pathways can be used to circumvent immune suppression and improve therapeutic efficacy. Here, we used CRISPR-Cas9 to delete the essential autophagy gene *ATG5* in CAR-T cells targeted against the ovarian cancer antigen folate receptor alpha (αFR). Using liquid chromatography mass spectrometry, we demonstrated that deletion of *ATG5* increased amino acid uptake and induced a shift from mitochondrial to glycolytic metabolism in *ex vivo*-expanded CAR-T cells. Functional assays revealed enhanced production of the effector cytokine interferon gamma (IFN-γ) by *ATG5*-knockout CAR-T cells, which translated to superior *in vitro* cytotoxicity as compared to unedited CAR-T cells. Overall, *ATG5*-knockout CAR-T cells effectively controlled growth of OVCAR3 ovarian tumors *in vivo*. These results provide conclusive evidence that autophagy deletion enhances CAR-T metabolism and antitumor function, and more broadly, support metabolic engineering as a strategy to improve CAR-T efficacy in solid tumors such as ovarian cancer.

3.2 Introduction

Immunotherapy has undoubtedly revolutionized the management of cancer. However, the effectiveness of certain immunotherapies, such as CAR-T cell therapy, has been largely restricted to certain subsets of patients and/or disease indications. For example, while CD19 CAR-T cell therapy has demonstrated unprecedented success in the treatment of leukemias and lymphomas[7], similar results have yet to be achieved in the context of non-liquid cancers such as ovarian cancer[130]. Ovarian cancer is a heterogeneous disease with multiple histological subtypes including endometrioid, clear-cell, mucinous, and the most common subtype, high-grade serous ovarian carcinoma (HGSOC). While survival varies across histotype and stage, prognosis is poor for patients diagnosed with advanced HGSOC, with five-year survival rates of 41% and 20% for stage III and stage IV, respectively[131]. The current standard of care for patients with HGSOC is platinum/taxane-based chemotherapy, along with front-line or maintenance therapy with the

inhibitors bevacizumab (targeting VEGF, vascular endothelial growth factor) and olaparib (targeting PARP, poly ADP-ribose polymerase)[132]. However, despite the recent success of immunotherapeutic agents for other cancer indications, the promise of immunotherapy has yet to be realized for ovarian cancer. This is especially apparent in the case of CAR-T therapy where multiple Phase 1 trials completed in recent years have failed to achieve a single clinical response[117,118,133–135]. Similarly, immune checkpoint blockade with the anti-PD1 antibodies nivolumab and pembrolizumab have yielded disappointing response rates of less than 15% in patients with HGSOC[132]. While the precise reasons for the resistance of ovarian cancer to immunotherapy are still being elucidated, the suppressive nature of the ovarian TME plays a significant role in hindering antitumor immune responses.

The ovarian cancer ecosystem is unique in that it encompasses two distinct environments: the primary solid TME, and a liquid microenvironment termed malignant ascites[136]. Malignant ascites is an inflammatory fluid that accumulates in the abdominal cavity of patients with peritoneal and pelvic metastases, and is a classic feature of advanced disease[137]. Like the solid TME, malignant ascites contains multiple cell types such as disseminated tumor cells, stromal cells, and innate and adaptive immune cells, and soluble factors such as cytokines and metabolites[138,139]. Importantly, T cell function is metabolically constrained in both the solid and the ascitic environments. For example, highly-glycolytic tumor cells deplete the solid TME of glucose and produce elevated levels of the immune-inhibitory metabolite lactate, which has been shown to impair cytokine production by T cells[29,140,141]. Similarly, arginase-expressing CAFs deplete the solid TME of L-arginine, a crucial metabolite for T cell survival and function[51,52]. CAFs also produce high levels of 1-methylnicotinamide, an immune-regulatory metabolite that has been shown to suppress CAR-T cell cytotoxicity *in vitro*[62]. In the ascites, tryptophan metabolism by disseminated tumor cells leads to accumulation of the downstream metabolite kynurenine, which has well-known inhibitory effects on T cells[65,142]. Ascites exposure has also been shown to inhibit expression of the transporter GLUT1 and reduce glycolytic capacity in T cells[143]. Lastly, hypoxia is present in both environments, although to a lesser extent in the ascitic TME[144–146]. In T cells, sustained exposure to hypoxia induces a transcriptional program that accelerates exhaustion, limits cytolytic activity, and upregulates autophagy[147,148].

Autophagy is an evolutionarily-conserved catabolic process that recycles intracellular components through lysosomal degradation. At homeostasis, a basal level of autophagy eliminates damaged organelles and misfolded proteins. However, under conditions of stress, such as nutrient deprivation and hypoxia, autophagy mediates bulk degradation of cytoplasmic components to supply the cell with metabolic substrates and promote survival[149]. While the role of autophagy in immune cell function is multifaceted and complex, there is growing evidence suggesting that autophagy attenuates immune effector responses[84–86].

In Chapter 2, we developed a gene-editing method for engineering αFR CAR-T cells with concomitant deletion of the essential autophagy gene *ATG5*. Here, we show that *ATG5*-knockout CAR-T cells acquire a distinct metabolic phenotype characterized by alterations in glucose and amino acid metabolism. Functionally, deletion of *ATG5* enhances antigen-dependent cytokine production and improves CAR-T cell antitumor efficacy against human ovarian tumors *in vitro* and *in vivo*.

3.3 Materials and Methods

3.3.1 Cell line culture

HEK293T cells (CRL-3216, ATCC) were grown in DMEM (Gibco) supplemented with 10% heat-inactivated fetal bovine serum (FBS; Sigma) and 1% penicillin-streptomycin (ThermoFisher). Luciferase-expressing SKOV3 human ovarian cancer cells (SKOV3-Luc, a gift from Dr. Julian Smazynski) were grown in McCoy's 5A (Gibco) supplemented with 10% heat inactivated FBS, 1% penicillin-streptomycin, and 2 μg/ml puromycin (Gibco). OVCAR3 human ovarian cancer cells (HTB-161, ATCC) were grown in ATCC-formulated RPMI 1640 (Gibco) supplemented with 20% heat inactivated FBS, 0.01 mg/mL bovine insulin (Sigma), and 1% penicillin-streptomycin.

3.3.2 Design and synthesis of genome editing components

ATG5-targeting gRNAs (ATG5-I2A-824 and ATG5-E4-56) were designed using the online tool CRISPOR[22]. The *AAVS1*-targeting gRNA (AAVS1-I1) was previously described in the

literature[108]. Guide RNAs were synthesized by IDT (Alt-R sgRNA), resuspended in nuclease-free water to 100 μM, and stored at -80°C. All gRNA sequences can be found in Supplementary Table 6.

CAR donor sequences (ATG5-αFR, ATG5-EF1α-αFR, and AAVS1-EF1α-αFR) were designed around a published αFR-CAR construct[109]. The CAR comprised a CD8 leader sequence, a single-chain variable fragment targeting human αFR, a CD8 hinge and transmembrane domain, a CD28 costimulatory domain, and a CD3ζ intracellular domain. Each donor included a splice acceptor (SA) and 2A self-cleaving peptide (2A) sequence immediately upstream of the CAR, and a bovine growth hormone polyadenylation (pA) sequence immediately downstream of the CAR. Donors with an exogenous promoter contained a full-length elongation factor 1 alpha (EF1α) promoter sequence between the 2A and CAR. All donor sequences can be found in Supplementary Table 7.

Full donor sequences were synthesized as gBlocks (IDT) and cloned into adeno-associated virus serotype 6 (AAV6) vectors using Gibson assembly. Recombinant CAR-AAV6 was produced by the viral vector core at the Canadian Neurophotonics Platform. Virus was resuspended in PBS 320 mM NaCl + 5% D-sorbitol + 0.001% pluronic acid and stored at -80°C until use.

3.3.3 Lentivirus production

The αFR-CAR sequence was synthesized by GenScript and cloned into a second-generation lentiviral expression vector. The CAR was inserted between an EF1α core promoter sequence and a 2A-EGFP sequence used to measure transduction efficiency.

To generate lentivirus, HEK293T cells were co-transfected with αFR-CAR vector, packaging plasmid, and envelope plasmid (psPAX2, Addgene #12260, and pMD2.G, Addgene #12259; both gifts from Dr. Didier Trono) at a 1:1:1 ratio using Lipofectamine 3000 (Invitrogen) as per the manufacturer's protocol. Virus-containing supernatant was collected, filtered, and concentrated by ultra-centrifugation at 25,000 rpm for 90 minutes at 4°C. Viral pellets were resuspended in Opti-MEM (Gibco) and stored at -80°C.

3.3.4 T cell isolation, activation, and culture

Peripheral blood mononuclear cells (PBMCs) were isolated from healthy donor leukapheresis products (STEMCELL) by Ficoll gradient density centrifugation. CD3+ T cells were isolated from PBMCs using positive selection CD3 microbeads (Miltenyi). T cells were activated with 25 μl Immunocult CD3/CD28 T cell activators (STEMCELL) per 1 million cells and cultured in Immunocult-XF medium (STEMCELL) supplemented with 1% penicillin-streptomycin, 2 mM L-glutamine (ThermoFisher), and 300 U/ml IL-2 (Peprotech).

3.3.5 T cell electroporation and CAR-AAV6 transduction

RNPs were prepared as previously described[110]. In brief, sgRNA (100 μM, IDT) was mixed in a 2:1:1 molar ratio with poly-l-glutamic acid (PGA; 100 mg/ml, Sigma) and SpCas9 or HiFiCas9 nuclease as indicated (10 mg/ml, both IDT), and incubated for 15 minutes at 37ºC. T cells were resuspended in electroporation buffer P3 (Lonza), mixed with RNPs at a ratio of $1x10^6$ cells/50 pmol RNP (on a Cas9 basis), and electroporated in 16-well nucleocuvette strips on the 4D-Nucleofector X Unit (Lonza) using pulse code EO115. For RNP-only conditions, 80 μl of pre-warmed T cell medium (no IL-2) was added to each well immediately post-electroporation, and the nucleocuvette strip was returned to the incubator for 15 minutes at 37ºC. After 15 minutes, T cells were transferred to a 48-well plate at a density of $1x10^6$ cells/ml in complete T cell medium.

For AAV6 experiments, 80 μl of pre-warmed medium was added to each well and then T cells were gently transferred from the nucleocuvette strip to a 96-well round-bottom plate containing CAR-AAV6 (Neurophotonics) diluted in T cell medium at the indicated MOI. The plate was returned to the incubator for 6-8 hours incubation with AAV6 at a high cell density. After this incubation period, T cells were transferred to a 48-well plate at a density of $1x10^6$ cells/ml in complete T cell medium.

3.3.6 Indel quantification

Genomic DNA was extracted from RNP-only cells for quantification of insertions and deletions (indels) by Sanger sequencing. Genomic DNA was also extracted from wild-type cells to use as a negative control. In brief, 500,000 to 1 million cells were collected, centrifuged for 5 minutes at

1200 rpm, aspirated, and resuspended in 30-50 μl QuickExtract solution (Lucigen). Samples were mixed by vigorous pipetting and incubated in a thermocycler at the following settings: 15 min at 65ºC, 15 min at 68ºC, 10 min at 98ºC. Genomic DNA was quantified by NanoDrop (ThermoFisher) and normalized to 100 ng/μl with nuclease-free water.

Primers were designed for each sgRNA sequence to generate amplicons of approximately 400-700 bp surrounding the predicted Cas9 cut site, and PCR amplification was performed using KAPA-HiFi polymerase (Roche). PCR products were purified and sequenced on an ABI 3730xl Data Analyzer (Applied Biosystems). Edited and wild-type sequences were compared and indel quantification performed using the online TIDE algorithm[111] as per the recommended guidelines. All PCR primer sequences can be found in Supplementary Table 8.

3.3.7 Magnetic bead enrichment

Cells were collected, centrifuged for 5 minutes at 1500 rpm and 4°C, and washed once prior to staining for 30 minutes at room temperature with AF647-conjugated anti-G4S linker antibody (1/50; Cell Signaling #69782S) diluted 1:50 in PBS. After staining, cells were washed twice, then incubated for 15 minutes at 4°C with anti-AF647 microbeads (Miltenyi) at a ratio of 10 μl beads per 5 million cells in cell-enrichment buffer (PBS supplemented with 0.5% heat-inactivated human serum (Sigma)). Cells were washed once with cell-enrichment buffer, then passed through an MS column (Miltenyi) for positive enrichment of labelled cells.

3.3.8 CAR-T cell restimulation

CAR-positive cells were plated at 500,000 to 800,000 cells/ml in fresh medium containing 20 μL/ml Immunocult CD3/CD28/CD2 T cell activators (STEMCELL). T cell activators were diluted by addition of fresh medium after 2 days of re-stimulation. For the remaining culture period, CAR-T cells were maintained at 500,000 to 1 million cells/ml and transferred to larger culture vessels as needed.

3.3.9 CAR-T cell production - Lentiviral and LentiRNP CAR-T cells

T cells were isolated and activated on Day 0 as per section 3.3.4, transduced on Day 1 with concentrated αFR-CAR lentivirus at an MOI of 1, and enriched on Day 4 by magnetic bead enrichment as per section 3.3.7. Enriched CAR-T cells were electroporated on Day 6 as per section 3.3.5. In brief, *ATG5*-knockout CAR-T cells ("*ATG5* LentiRNP CAR-T"; experimental condition) were generated by RNP-electroporation with sgRNA ATG5-E4-56, targeting exon 4 of *ATG5*. Unedited lentiviral CAR-T cells ("WT Lentiviral CAR-T"; control condition) were mock-electroporated with PBS. All CAR-T cells were restimulated on Day 8 as per section 3.3.8, and expanded for an additional 8-10 days.

3.3.10 CAR-T cell production – HDR CAR-T cells

T cells were isolated and activated on Day 0 as per section 3.3.4, and electroporated on Day 3 as per section 3.3.5. In brief, *ATG5*-integrated CAR-T cells were generated by RNP electroporation with sgRNA ATG5-I2A-824 targeting intron 2 of *ATG5*, and CAR-AAV6 transduction with either ATG5-EF1α-αFR donor ("*ATG5* EF1α HDR CAR-T"; experimental condition) or ATG5-αFR donor ("*ATG5* Endo HDR CAR-T"; experimental condition without exogenous promoter). *AAVS1*-integrated CAR-T cells were generated by RNP electroporation with sgRNA AAVS1-I1 targeting intron 1 of the safe-harbor locus *AAVS1*, and CAR-AAV6 transduction with AAVS1-EF1α-αFR donor ("*AAVS1* EF1α CAR-T"; control condition). On Day 8, CAR-T cells were enriched by magnetic bead enrichment as per section 3.3.7, restimulated as per section 3.3.8, and expanded for an additional 8-10 days.

3.3.11 Flow cytometry analysis

For glucose uptake analysis, $1x10^6$ CAR-T cells per condition were stained for 30 minutes at 37ºC in TexMACS (Miltenyi) containing 0.1 μM Glucose-Cy5 (Sigma). Cells were washed, stained with fixable viability dye eF506 (1/2000; Invitrogen #65-0844-14) for 15 minutes at 4ºC, washed again, then stained for 20 minutes at room temperature with the following antibody cocktail diluted in flow cytometry staining buffer: CD3-BV750 (1/100; Biolegend #344845), CD4-AF700 (1/100; Biolegend #300526), and CD8-PerCP (1/100; Biolegend #301030).

For immune phenotyping, CAR-T cells were stained with viability-eF506 for 15 minutes at 4ºC, then washed and resuspended in Human TruStain FcX blocking solution (Biolegend) and Brilliant Stain Buffer Plus (BD Biosciences) for 10 minutes at room temperature. After blocking, cells were stained for 20 minutes at room temperature with the following antibody cocktail diluted in flow cytometry staining buffer: CD3-BV750, CD4-AF700, CD8-PerCP, CAR-AF647 (1/50; Cell Signaling #69782S), CD45RO-PE-Cy7 (1/50; Invitrogen #25-0457-42), CCR7-APC/Fire750 (1/50; Biolegend # 353246), CD137-BV605 (1/50; Biolegend #309822), and CD279-BV421 (1/50; Biolegend #329920).

For intracellular staining, CAR-T cells were first stimulated by co-culturing for 24 hours with SKOV3 human ovarian cancer cells at an effector-to-target cell ratio of 2:1. In the last 4 hours of co-culture, GolgiStop (BD Biosciences) was added to each well as per the manufacturer's recommended dilution. At the end of the co-culture period, cells were collected and stained with viability-eF506 for 15 minutes at 4ºC, then washed and stained for 20 minutes at room temperature with the following antibody cocktail diluted in Brilliant Stain Buffer Plus and flow cytometry staining buffer: CD3-BV750, CD4-AF700, CD8-PerCP, and CAR-AF647. After surface staining, cells were resuspended in Cytofix/Cytoperm Solution (BD Biosciences) for 20 minutes at 4ºC, washed twice with Perm/Wash Buffer (BD Biosciences), and then stained for 30 minutes at 4ºC with IFN-γ-V421 (1/50; Biolegend #502508) diluted in Perm/Wash Buffer.

All cells were resuspended in flow cytometry staining buffer prior to acquisition on a Cytek Aurora spectral flow cytometer. Cytometry data were analyzed using SpectroFlo (Cytek) and FlowJo v10.10 (BD Life Sciences). A detailed list of all antibodies can be found in Supplementary Table 9.

3.3.12 Metabolite extraction for mass spectrometry

To prepare cells for metabolite profiling, triplicate samples of 2 million cells were collected from each CAR-T group, washed once with ice-cold saline solution, and vigorously resuspended in 500 μl of 80% methanol before snap freezing in liquid nitrogen. Samples were subjected to 3 freeze-thaw cycles, and centrifuged at 14,000 rpm for 15 minutes at 4°C. The metabolite-

containing supernatants were evaporated until dry. Metabolites were reconstituted in 100 µl of acetonitrile/water 80:20, vortex-mixed, and centrifuged to remove debris.

3.3.13 LC-MS metabolite profiling

Metabolite extraction was carried out as described above. Supernatants were transferred to LC-MS vials for profiling, and each sample was processed with similar cell numbers. Metabolomics analysis was performed on the Thermo Scientific Orbitrap Exploris 480 high-resolution mass spectrometer in full scan mode as previously described ([150–152]). Chromatogram review and peak area integration were performed using TraceFinder software version 5.1 (Thermo Scientific).

3.3.14 LC-MS data processing and normalization

Within each metabolomics experiment, peak areas were normalized to the total ion count (TIC) for each sample to account for variations in sample handling and instrument performance. After TIC-normalization, multiple experiments were merged into the same dataset and corrected for batch effects using EigenMS[153]. The normalized data were filtered by interquartile range, log-transformed, and auto-scaled using MetaboAnalyst[154].

3.3.15 Characterizing metabolic differences between edited CAR-T cells

To visualize differences in metabolite abundance across CAR-T groups, heatmap dendrograms were constructed on the full dataset using Ward's method to cluster Euclidean distances among metabolites. To determine the role of autophagy deletion, linear modeling was performed on normalized metabolite abundances using the Statistical Analysis [metadata table] module in MetaboAnalyst. This module employs *limma*[155], an R package specifically designed for analyzing complex multi-factor experiments. In brief, CAR-T groups were categorized according to specific metadata: autophagy (knockout vs. wildtype), method (CRISPR HDR vs. LentiRNP/Lentiviral), and donor (donor 1 vs. donor 2). The *ATG5* Endo CAR-T group was excluded from this analysis due to lack of a matched wildtype control. Differential analysis was performed with autophagy status as the primary variable, method as a covariate for adjustment, and donor as a random effect. The output of this analysis can be found in Table 3.

3.3.16 *In vitro* cytotoxicity assays

A luciferase-based assay was used to measure CAR-T cell cytotoxicity. In brief, CAR-T cells were co-cultured in a 96-well plate with luciferase-expressing SKOV3 human ovarian cancer cells (SKOV3-Luc) at the indicated effector-to-target (E:T) cell ratios. SKOV3-Luc cells were also cultured alone to determine the maximum luciferase expression (RLU_{max}), while medium-only wells were used to account for background luminescence ($RLU_{background}$). After 24 hours of co-culture, D-Luciferin (1/20; Revvity Health Sciences) was added to each well, mixed by pipetting, and the plate was incubated in the dark for 5 minutes. Luminescence was measured on a Varioskan Lux plate reader (Thermo Scientific), and specific tumor cell lysis calculated as $(RLU_{sample}/((RLU_{max}-RLU_{background}))$ x 100.

For cytotoxicity assays performed using patient-derived ascites supernatant, ascites supernatant was collected as per section 3.3.17, filtered through a 40 μm cell strainer, and used instead of medium during the co-culture period. Wells containing supernatant-only were used to determine $RLU_{background}$.

3.3.17 Collection and processing of ascites supernatant for cytotoxicity assays

Ascites was collected from an ovarian cancer patient undergoing treatment at BC Cancer. In brief, ascites was drained via paracentesis, centrifuged at 1500 rpm for 10 minutes at 4^{o}C, and the supernatant removed by pipetting before cryopreservation at -80^{o}C. The ascites supernatant used in this study was previously determined to contain 4.083 +/- 0.136 mM glucose and 0.923 +/- 0.003 mM glutamine[156]. All patient samples were obtained through the BC Cancer Tumor Tissue Repository under University of British Columbia Biosafety (B23-0067) and REB (H18-01783) protocols.

3.3.18 *In vivo* efficacy studies

All animal studies were approved by the University of Victoria's Animal Care Committee (AUP 2022-011) and performed in accordance with the Canadian Council for Animal Care guidelines. 6-8 weeks old female NOD/SCID/IL-2Rγ-null (NSG; stock #005557) mice were acquired from Jackson Laboratory. After a two-week acclimation period, each mouse was subcutaneously

injected on the left flank with $5.0x10^6$ OVCAR3 tumor cells. Once tumors reached an average area of 50-60mm^2 (approximately 35-40 days post-injection), mice were treated with $5.0x10^6$ CAR-positive cells ($5.2– 5.5x10^6$ total cells per mouse) or $5.0x10^6$ non-transduced T cells, administered via tail vein injection. An equal volume of PBS was administered as a vehicle control. Tumors were measured twice per week using digital calipers, and area (length x width) was used to quantify tumor burden. Mice were euthanized upon reaching humane endpoint (tumor area greater than 180mm^2) and overall survival was assessed by Kaplan-Meier analysis.

CAR-T cells were generated as per sections 3.3.9 and 3.3.10. All CRISPR-edited CAR-T cells (*ATG5* EF1α HDR CAR-T, *ATG5* Endo HDR CAR-T, *AAVS1* EF1α HDR CAR-T, *ATG5* LentiRNP CAR-T) were electroporated with HiFiCas9 RNPs. Lentiviral CAR-T cells (WT Lentiviral CAR-T) and non-transduced T cells (NT T cells) were electroporated with PBS.

3.4 Figures and Tables

Table 3. Statistical analysis of metabolite profiling data.

Output of limma analysis for differential metabolite abundance. Analysis was performed on normalized metabolite abundances obtained in technical triplicate from n = 2 independent healthy donors (FC = knockout – wildtype). Significance was reported as $P_{adj}<0.05$.

Metabolite	logFC	AveExpr	t	P.Value	adj.P.Val
Glucose	1.5399	2.57E-16	-4.3307	1.57E-05	0.00077
Glutamine	1.5285	-6.38E-16	-4.2986	1.81E-05	0.00077
Methionine	1.4264	9.93E-16	-4.0115	6.28E-05	0.001222
Leucine	1.4197	1.20E-15	-3.9924	6.80E-05	0.001222
Phenylalanine	1.415	-9.43E-16	-3.9793	7.19E-05	0.001222
Octanoic Acid	1.353	8.18E-17	-3.805	0.000147	0.001875
Tyrosine	1.3466	4.78E-16	-3.7869	0.000158	0.001875
Tryptophan	1.3365	-2.76E-15	-3.7585	0.000176	0.001875
Indole-3-acrylate	1.3217	3.84E-16	-3.717	0.000208	0.00191
Lysine	1.3146	-1.90E-16	-3.697	0.000225	0.00191
Asparagine	1.2998	-5.35E-15	-3.6553	0.000264	0.002043
Indoxyl sulfate	1.1942	1.88E-18	-3.3584	0.0008	0.00567
4-/5-Oxoproline	1.1787	1.44E-15	-3.3147	0.000936	0.00611
Glycerol 3-phosphate	-1.1714	1.26E-15	3.2942	0.001006	0.00611
Serine	1.1614	3.89E-15	-3.2662	0.001111	0.006293
Cytidine diphosphate	-1.0971	1.21E-17	3.0853	0.002065	0.010968
NAD+	-1.0301	-2.78E-16	2.8968	0.003816	0.018502
N-Acetylserine	-1.0271	5.87E-16	2.8885	0.003918	0.018502
Adenosine diphosphate	-1.0187	-1.92E-15	2.8648	0.004222	0.018546
Platelet-activating factor	1.0147	-3.50E-16	-2.8535	0.004374	0.018546
Uridine diphosphate	-1.0094	6.48E-16	2.8386	0.004582	0.018546
Sedoheptulose 7-phosphate	-0.99976	1.39E-16	2.8116	0.004984	0.019255
N-Acetylaspartate	-0.99372	-4.47E-16	2.7946	0.005252	0.019409
Adenosine triphosphate	-0.9826	2.15E-16	2.7633	0.00578	0.019946
Glycerophosphocholine	-0.98087	-4.07E-17	2.7585	0.005866	0.019946
Guanosine diphosphate	-0.96302	6.01E-16	2.7083	0.006828	0.022322
1-Aminocyclopropanecarboxylate	0.92148	5.42E-16	-2.5914	0.009635	0.028989
UDP-glucose	-0.91951	-6.54E-16	2.5859	0.009791	0.028989
Pyruvate	0.91827	-1.44E-15	-2.5824	0.00989	0.028989
Acetylaminoadipate	-0.88401	-3.74E-15	2.4861	0.013007	0.036237
Citrate	-0.88198	1.82E-16	2.4804	0.013216	0.036237
Malate	-0.86151	1.10E-15	2.4228	0.0155	0.041172
Fumarate	-0.85358	1.64E-15	2.4005	0.016474	0.042433
Pyridoxal	0.83502	7.78E-16	-2.3483	0.018968	0.045841

Table 3 continued.

Ala-Leu	0.83433	7.25E-16	-2.3464	0.019067	0.045841
Guanosine diphosphate mannose	-0.83192	-3.79E-16	2.3396	0.019415	0.045841
Gly-Leu	0.81984	4.65E-16	-2.3056	0.021246	0.048809
Cyclic ADP-ribose	-0.78523	-2.75E-16	2.2083	0.027353	0.061183
Allothreonine/Homoserine/Threonine	0.76764	-2.46E-15	-2.1588	0.030999	0.067561
Uridine monophosphate	0.74845	1.05E-16	-2.1048	0.035445	0.075322
NADP+	-0.72732	-1.85E-15	2.0454	0.040959	0.084916
Betaine	0.70601	4.39E-16	-1.9855	0.047243	0.095245
UDP-N-acetylglucosamine	-0.70303	5.03E-16	1.9771	0.048183	0.095245
Glycerophosphoethanolamine	-0.67704	3.01E-16	1.904	0.057069	0.11025
Aspartate	0.66083	1.69E-15	-1.8584	0.063272	0.11951
Ser-Arg	0.64519	-2.34E-16	-1.8144	0.069779	0.1272
Fructose 6-phosphate/Galactose 1-phosphate/Glucose 6-phosphate/ Mannose 6-phosphate	-0.6439	6.38E-17	1.8108	0.070336	0.1272
Threonate	-0.63765	1.28E-15	1.7932	0.073104	0.12945
N-Acetylhexosamine phosphate	-0.63171	8.91E-16	1.7766	0.075813	0.13151
alpha-Ketoglutarate	-0.55626	1.41E-15	1.5644	0.11791	0.20045
Glycerophosphoinositol	-0.54889	1.86E-15	1.5436	0.12286	0.20476
Aspartylglycosamine	-0.52885	-1.06E-15	1.4873	0.13712	0.22414
Glu-Gln	0.52513	1.89E-15	-1.4768	0.1399	0.22437
CDP-ethanolamine	-0.52071	2.02E-15	1.4644	0.14327	0.22551
Glutamate	-0.49488	-1.94E-16	1.3917	0.16418	0.25373
N-Formylmethionine	-0.45817	5.47E-16	1.2885	0.19774	0.30014
Suberate	0.4209	-7.47E-15	-1.1837	0.2367	0.35297
Adenosine diphosphate ribose	-0.40621	-4.09E-16	1.1424	0.25345	0.3697
Alanine/beta-Alanine	-0.40097	1.04E-17	1.1276	0.25962	0.3697
Thr-Arg	0.39984	4.12E-16	-1.1245	0.26097	0.3697
Hexitols	-0.39231	-8.29E-16	1.1033	0.27006	0.37631
Guanosine monophosphate	0.36397	-1.12E-15	-1.0236	0.30618	0.41766
Cellobiose/Lactose/Maltose/Melibiose/ Sucrose/Trehalose/Palatinose	0.36143	1.14E-17	-1.0164	0.30956	0.41766
Creatine	-0.35338	4.27E-15	0.99379	0.32046	0.41943
Phosphorylcholine	-0.35317	8.50E-16	0.99322	0.32074	0.41943
Succinate	-0.3478	-1.75E-15	0.97811	0.32815	0.42262
Myoinositol	-0.3053	5.03E-16	0.85859	0.39068	0.49564
Cys-Gly	-0.2927	1.38E-16	0.82315	0.41053	0.50956
Carnitine	0.29076	-3.85E-15	-0.8177	0.41364	0.50956
4-Guanidinobutanoate	-0.26909	1.77E-15	0.75676	0.44929	0.54557
Cytidine monophosphate	0.24237	-4.60E-16	-0.6816	0.49558	0.58515
Glutathione	-0.24232	3.54E-16	0.68148	0.49566	0.58515
3-Hydroxymethylglutarate	-0.18957	2.12E-16	0.53312	0.59402	0.69166
Citrulline	-0.18112	1.85E-16	0.50935	0.61057	0.69793
Proline	0.17846	1.25E-16	-0.50187	0.61582	0.69793
Adenosine monophosphate	0.16414	2.50E-15	-0.46161	0.64442	0.72073

Table 3 continued.

Adenosine	0.14936	7.20E-16	-0.42005	0.6745	0.74457
6-Oxo-NAM	-0.13695	-4.45E-17	0.38513	0.70019	0.76012
Glutathione disulfide	0.13394	-1.03E-15	-0.37667	0.70646	0.76012
Lactate	-0.12465	1.30E-15	0.35055	0.72597	0.76264
Glu-Pro	-0.12231	-1.08E-15	0.34397	0.73091	0.76264
Azelate	0.12004	-8.93E-16	-0.33758	0.73572	0.76264
2-Hydroxyglutarate	0.07461	-6.17E-16	-0.20983	0.83383	0.85392
ADP-ribose	-0.063822	-2.48E-16	0.17949	0.85758	0.86779
Taurine	-0.025978	1.08E-15	0.073058	0.94177	0.94177

Table 4. Pre-infusion staining for *in vivo* experiment 1.

CAR-T Group	CAR+ (%)	CAR+CD4+ (%)	CAR+CD8+ (%)	sgRNA	Indels (%)
ATG5 LentiRNP CAR-T	87.5	47.3	31.8	ATG5_E4	83.7
WT Lentiviral CAR-T	90.8	54.2	32.9	-	-

Table 5. Pre-infusion staining for *in vivo* experiment 2.

CAR-T Group	CAR+ (%)	CAR+CD4+ (%)	CAR+CD8+ (%)	sgRNA	Indels (%)
ATG5 EF1α HDR CAR-T	92.9	39.6	57.2	ATG5_I2	-
AAVS1 EF1α HDR CAR-T	91.0	39.7	56.7	AAVS1_I1	-
ATG5 LentiRNP CAR-T	86.8	42.2	54.7	ATG5_E4	69.0
WT Lentiviral CAR-T	89.6	28.5	66.2	-	-
ATG5 Endo HDR CAR-T	87.7	5.6	87.5	ATG5_I2	-

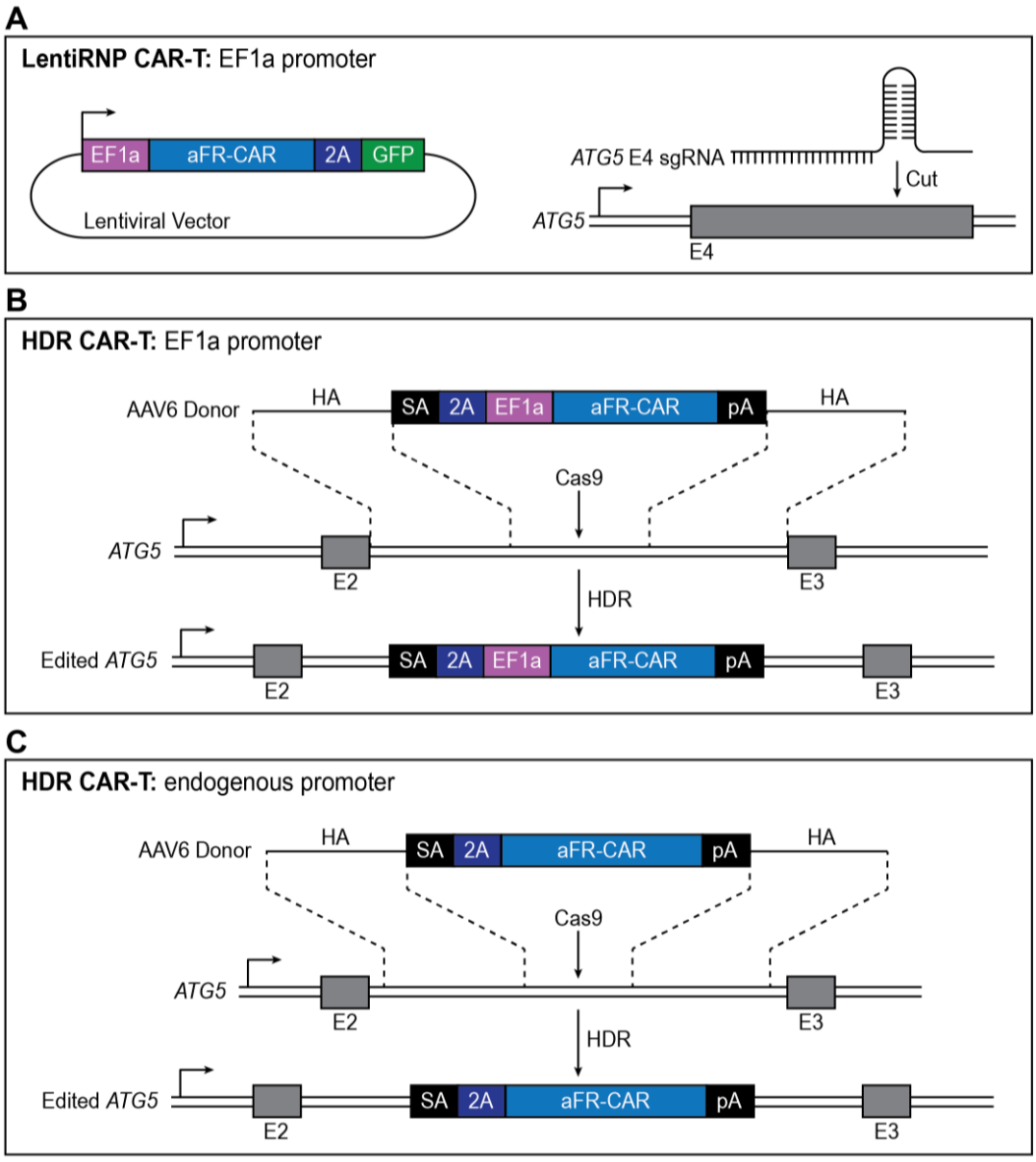

Figure 9. Generating *ATG5*-knockout CAR-T cells using three distinct CRISPR-Cas9 genome editing approaches.

(A) Schematic of the CAR lentiviral vector and sgRNA targeting exon (E) 4 of *ATG5*. The vector contains an elongation factor 1 alpha (EF1α) core promoter, the αFR-CAR cassette, a 2A self-cleaving peptide (2A), and a GFP reporter. **(B)** Schematic of the AAV6 donor template and *ATG5* intron 2 after CAR integration. The donor template contains a splice acceptor site (SA), 2A sequence, full-length EF1α promoter, αFR-CAR cassette, polyadenylation sequence (pA), and homology arms (HA). **(C)** Same as **(B)** but without an exogenous promoter.

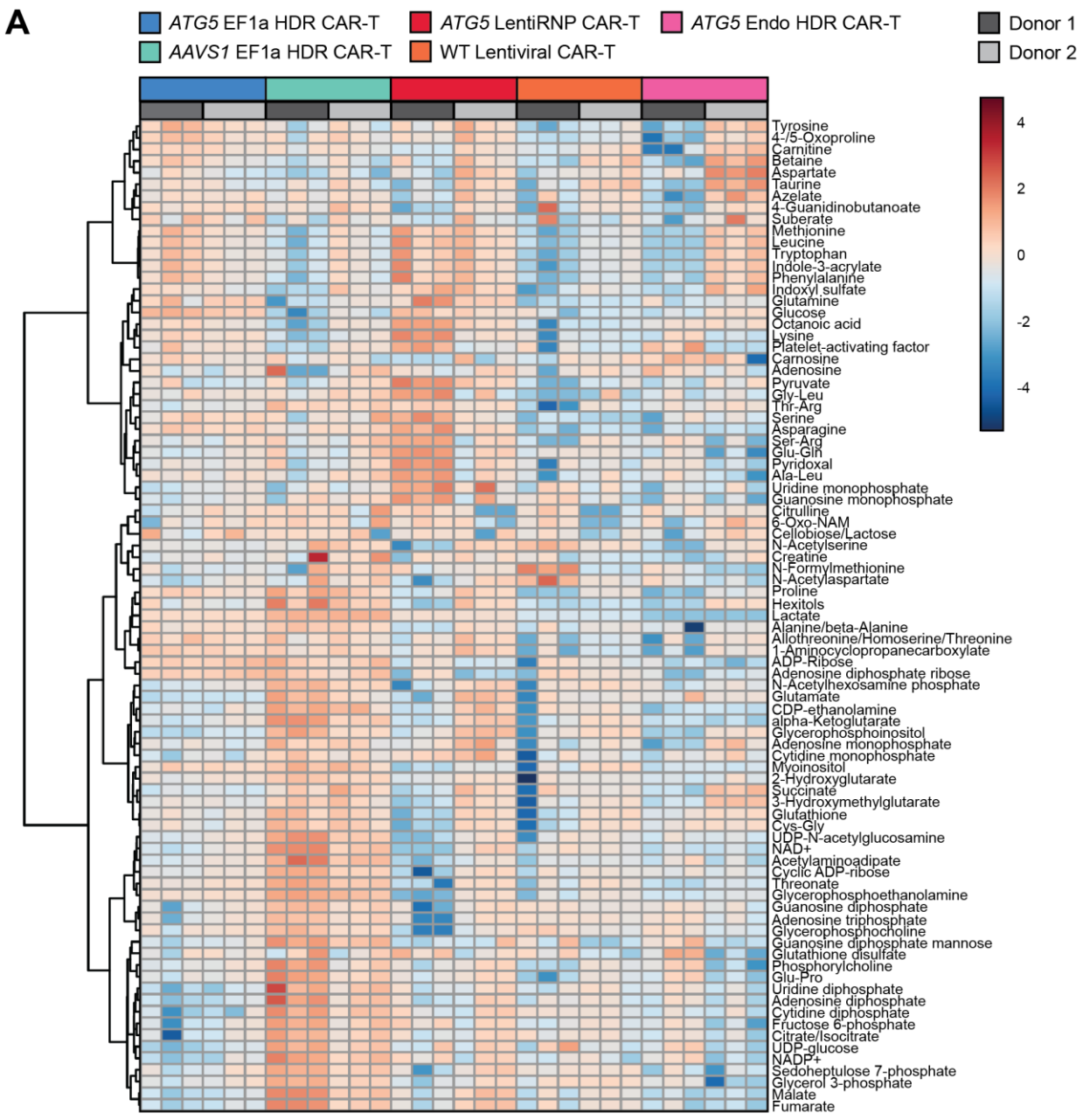

Figure 10. CAR-T cell metabolite profiling.

(A) Heatmap of normalized metabolite abundances, with dendrograms showing Ward's clustering of Euclidean distances among features. Metabolites were identified by liquid chromatography mass spectrometry analysis of enriched CAR-positive cells from five different CAR-T groups. Results are from n = 2 healthy donors, 3 technical replicates per donor.

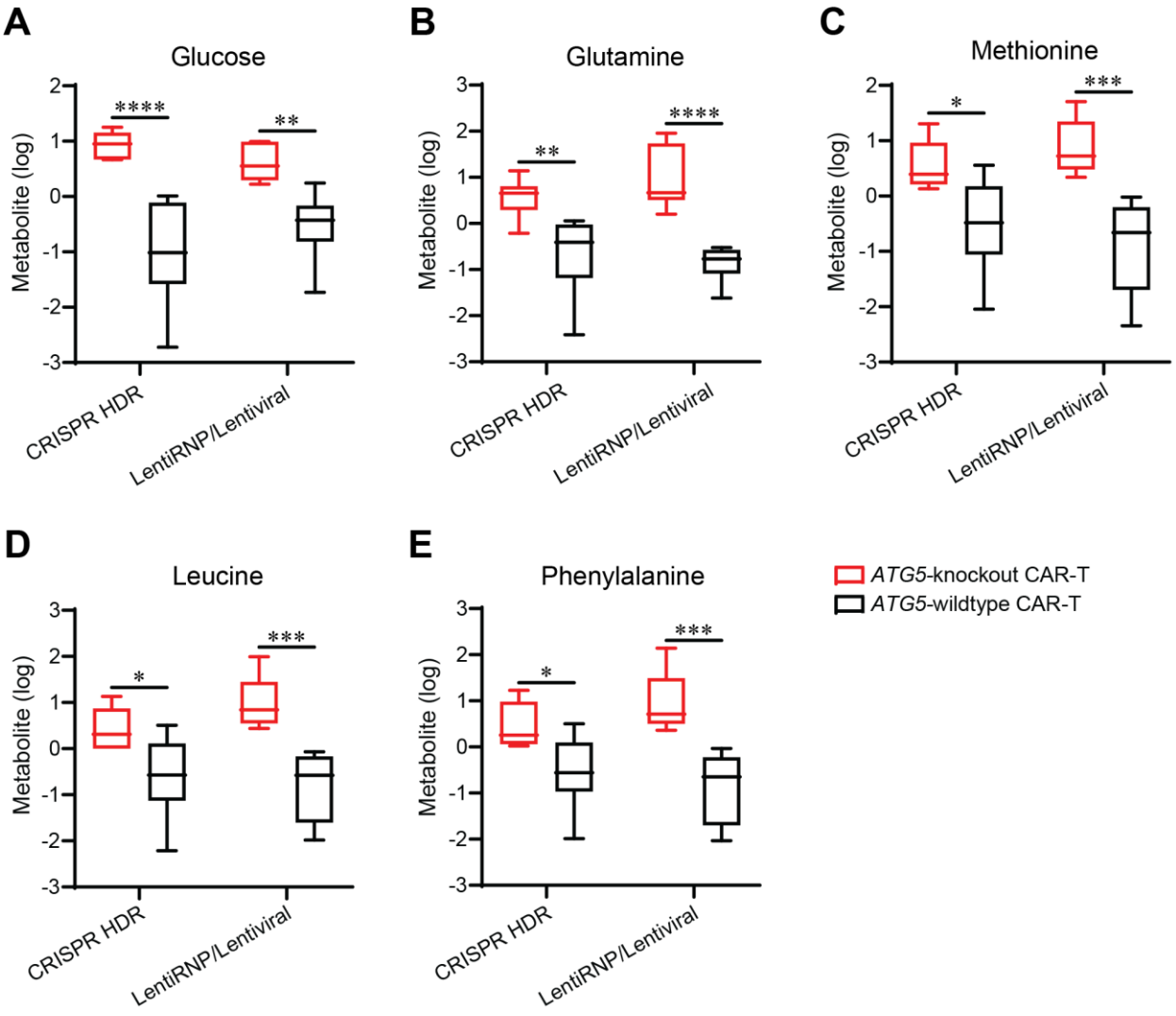

Figure 11. Metabolomic analysis reveals key differences between autophagy-knockout and autophagy-competent CAR-T cells.

(A-E) Normalized abundance of the top five differentially abundant metabolites: glucose (A), glutamine (B), methionine (C), leucine (D), and phenylalanine (E) in *ATG5*-knockout (red) or *ATG5*-wildtype (black) CAR-T cells. Boxplots show medians (lines), interquartile range (hinges), and range of data up to 1.5X interquartile range (whiskers). P values were determined by two-way ANOVA (*p<0.05, **p<0.01, ***p<0.001, ****p<0.0001).

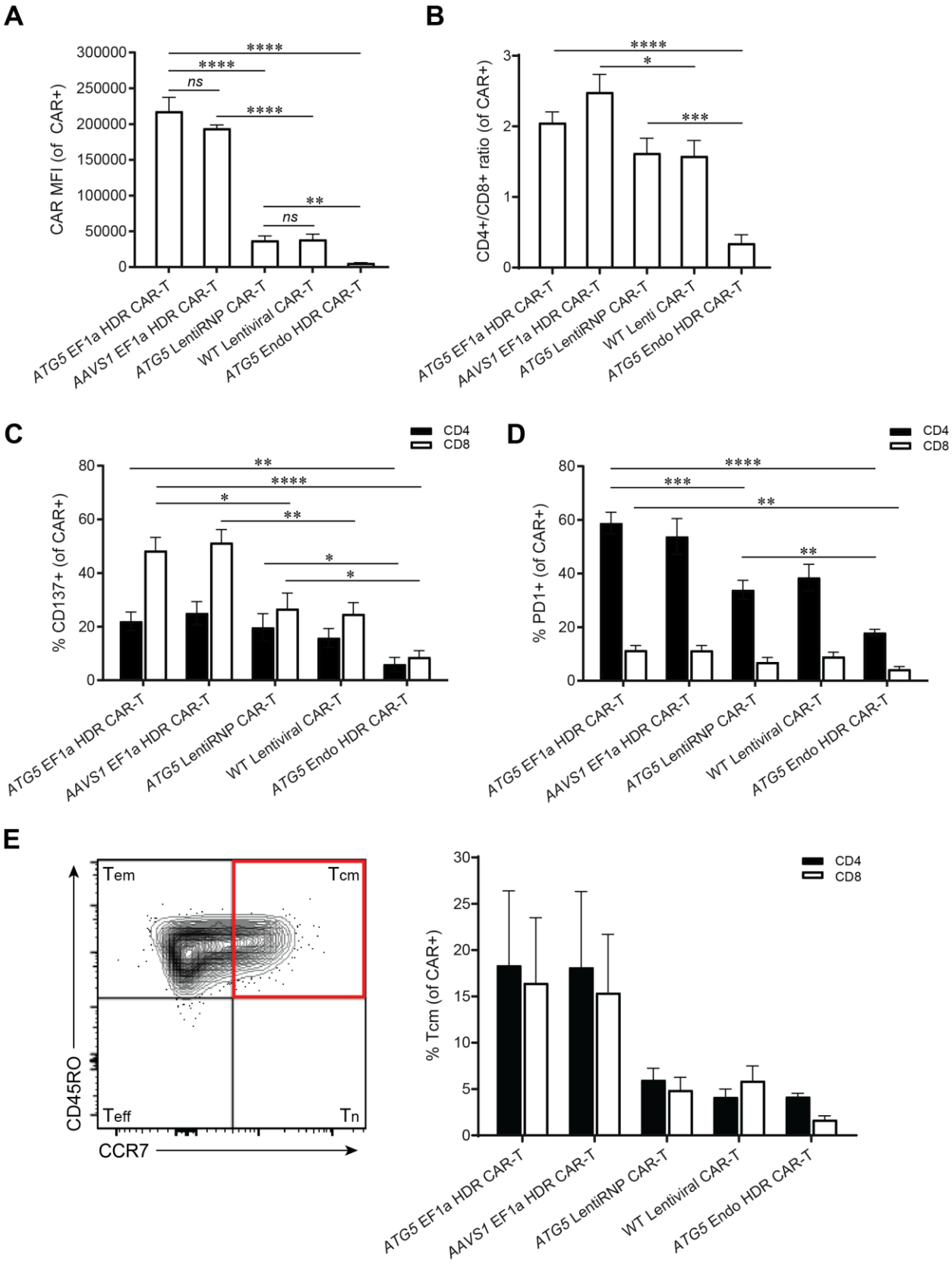
A
CAR MFI (of CAR+)
300000
250000
200000
150000
100000
50000
0
****
****
ns
****
**
ns
ATG5 EF1a HDR CAR-T
AAVS1 EF1a HDR CAR-T
ATG5 LentiRNP CAR-T
WT Lentiviral CAR-T
ATG5 Endo HDR CAR-T
B
CD4+/CD8+ ratio (of CAR+)
3
2
1
0
****
*
***
ATG5 EF1a HDR CAR-T
AAVS1 EF1a HDR CAR-T
ATG5 LentiRNP CAR-T
WT Lenti CAR-T
ATG5 Endo HDR CAR-T
C
CD4
CD8
% CD137+ (of CAR+)
80
60
40
20
0
**
****
*
**
*
*
ATG5 EF1a HDR CAR-T
AAVS1 EF1a HDR CAR-T
ATG5 LentiRNP CAR-T
WT Lentiviral CAR-T
ATG5 Endo HDR CAR-T
D
CD4
CD8
% PD1+ (of CAR+)
80
60
40
20
0
****
***
**
**
ATG5 EF1a HDR CAR-T
AAVS1 EF1a HDR CAR-T
ATG5 LentiRNP CAR-T
WT Lentiviral CAR-T
ATG5 Endo HDR CAR-T
E
Tem
Tcm
Teff
Tn
CD45RO
CCR7
CD4
CD8
% Tcm (of CAR+)
30
25
20
15
10
5
0
ATG5 EF1a HDR CAR-T
AAVS1 EF1a HDR CAR-T
ATG5 LentiRNP CAR-T
WT Lentiviral CAR-T
ATG5 Endo HDR CAR-T

Figure 12. Flow cytometry profiling identifies differences in immune phenotype between CAR-T cells made using different gene-editing methods.

(A) Bar graph showing CAR median fluorescence intensity (MFI) across each CAR-T condition. **(B)** Bar graph showing ratio of CD4+ to CD8+ CAR-T cells. **(C-D)** Bar graphs showing percent of CAR-T cells positive for the activation marker CD137 (C) and the exhaustion marker PD1 (D). **(E)** Left, representative flow cytometry plot highlighting CAR-T cells exhibiting a central memory (T_{cm}) phenotype as determined by CCR7 and CD45RO co-expression (red box). Right, bar graph showing T_{cm} phenotype across all CAR-T conditions, grouped by CD4 (black bars) and CD8 (white bars). CAR-T cells were generated by CRISPR HDR (*ATG5* EF1α HDR CAR-T, *AAVS1* EF1α HDR CAR-T, *ATG5* Endo HDR CAR-T), lentiviral transduction with sequential RNP knockout (*ATG5* LentiRNP CAR-T), or lentiviral transduction alone (WT Lentiviral CAR-T), and stained in technical duplicate ten days post-enrichment. Results are from two different healthy donors, with n = 2 independent CAR-T experiments per donor. Error bars represent +SEM. P values were determined by one-way ANOVA (*p<0.05, **p<0.01, ***p<0.001, ****p<0.0001).

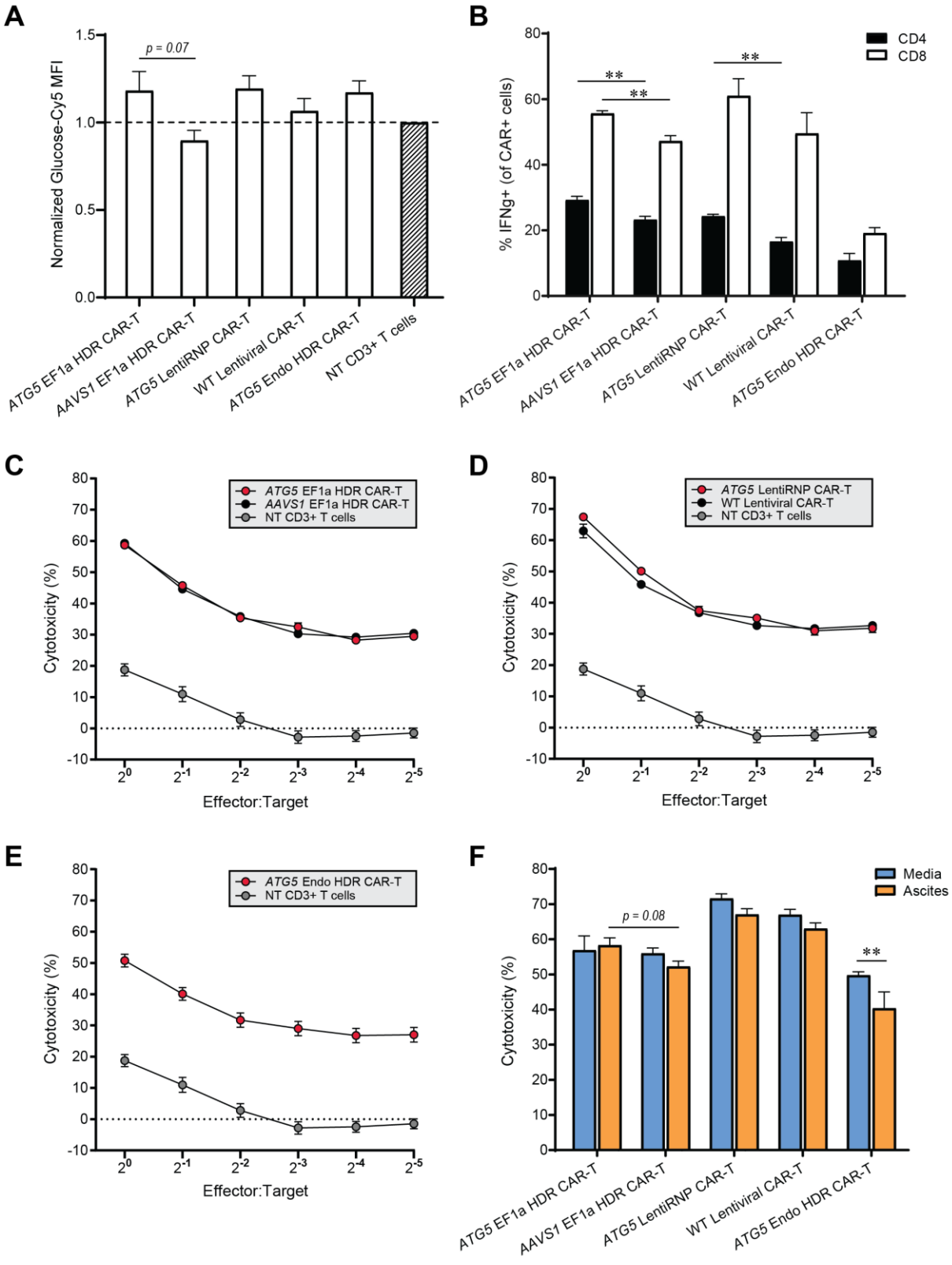
A
Normalized Glucose-Cy5 MFI
p = 0.07
ATG5 EF1a HDR CAR-T
AAVS1 EF1a HDR CAR-T
ATG5 LentiRNP CAR-T
WT Lentiviral CAR-T
ATG5 Endo HDR CAR-T
NT CD3+ T cells
B
% IFNg+ (of CAR+ cells)
CD4
CD8
**
**
**
C
ATG5 EF1a HDR CAR-T
AAVS1 EF1a HDR CAR-T
NT CD3+ T cells
Cytotoxicity (%)
Effector:Target
D
ATG5 LentiRNP CAR-T
WT Lentiviral CAR-T
NT CD3+ T cells
Cytotoxicity (%)
Effector:Target
E
ATG5 Endo HDR CAR-T
NT CD3+ T cells
Cytotoxicity (%)
Effector:Target
F
Media
Ascites
p = 0.08
**
Cytotoxicity (%)

Figure 13. Deletion of *ATG5* enhances *in vitro* glucose uptake and effector function.
(A) Bar graph showing normalized glucose uptake by each CAR-T cell condition. Glucose uptake was quantified as median fluorescence intensity (MFI) of Cy5-labelled glucose after a 30-minute time period. MFI for each CAR-T condition was normalized to MFI for non-transduced T cells within each individual experiment to allow for comparison between experiments. Results are from two healthy donors, n = 2 independent experiments per donor, 2 technical replicates per experiment. **(B)** Bar graph showing percent of CAR-T cells positive for the cytokine interferon gamma after 24h co-culture with SKOV3 ovarian tumor cells at a 2:1 effector-to-target cell ratio, grouped by CD4 (black bars) and CD8 (white bars). Results are from one healthy donor, n = 2 independent experiments, 2 technical replicates per experiment. **(C-E)** Scatter plots showing percent cytotoxicity of luciferase-expressing SKOV3 ovarian tumor cells after 24h co-culture with CAR-T cells at the indicated E:T ratios. Assays were performed in 50/50 RPMI and TexMACS media. Results are from two healthy donors, n = 2 independent experiments per donor, 4 technical replicates per experiment. **(F)** Bar graph showing percent cytotoxicity of luciferase-expressing SKOV3 ovarian tumor cells after 24h co-culture with CAR-T cells at an E:T ratio of 1:1. Assays were performed in 50/50 RPMI and TexMACS media (blue bars) or patient-derived ascites supernatant (orange bars). Results are from two healthy donors, n = 1 experiment per donor, 4 technical replicates per experiment. All error bars represent +SEM. P values were determined by one-way ANOVA (A, B) or two-way ANOVA (F); *$p<0.05$, **$p<0.01$.

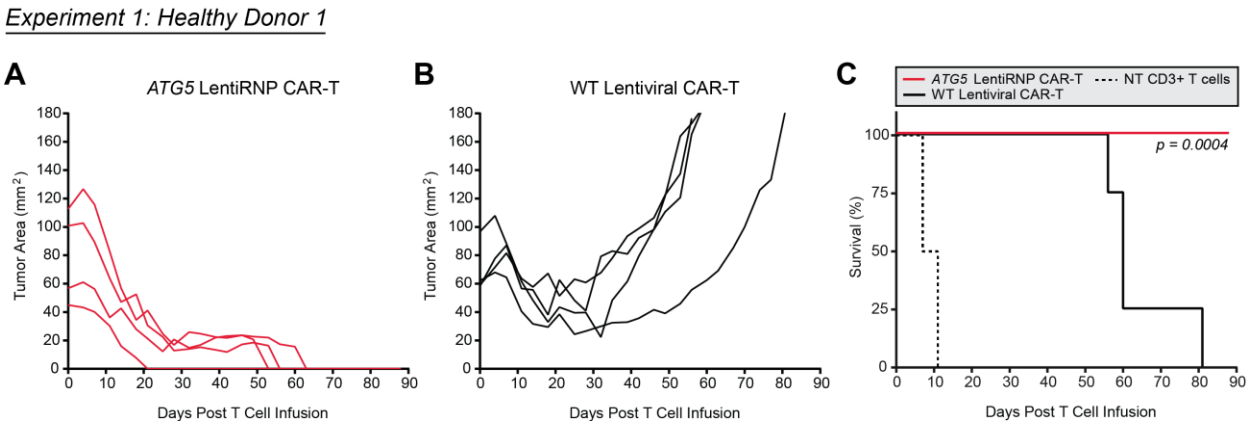

Figure 14. *ATG5* LentiRNP CAR-T cells from Donor 1 demonstrate superior *in vivo* cytotoxicity as compared to WT Lentiviral CAR-T cells.

(A-B) Growth curves for Experiment 1. NSG mice were implanted with human OVCAR3 tumors and treated with $5.0x10^6$ *ATG5* LentiRNP (A) or WT Lentiviral (B) CAR-T cells (n = 4 mice per group; one line = one mouse). Tumors were measured twice per week using digital calipers, and area (length x width) was used to quantify tumor burden. Mice were euthanized upon reaching humane endpoint (tumor area greater than $180mm^2$). **(C)** Survival curves for Experiment 1. Groups were compared by log-rank test.

Experiment 2: Healthy Donor 2

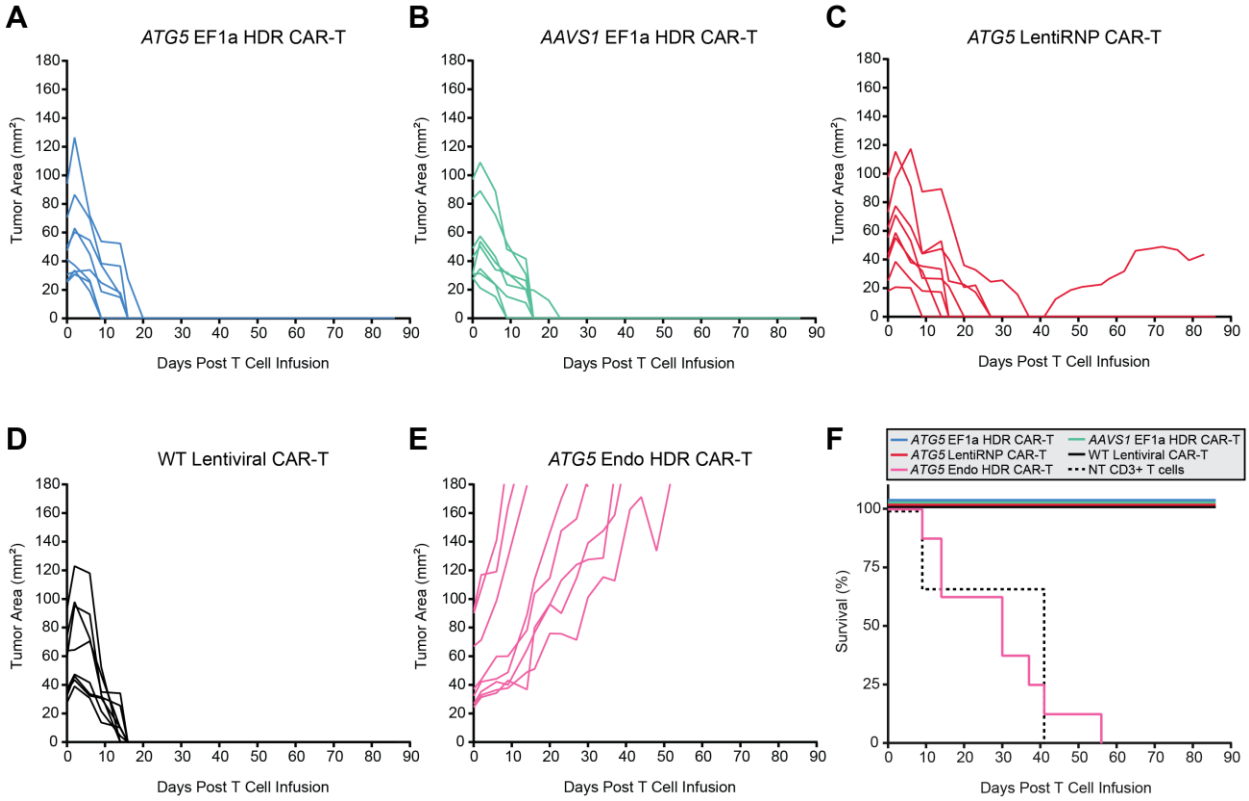

Figure 15. *ATG5*-knockout CAR-T cells from Donor 2 show similar *in vivo* efficacy to control CAR-T cells.

(A-E) Growth curves for Experiment 2. NSG mice were implanted with human OVCAR3 tumors and treated with $5.0x10^6$ *ATG5* EF1α HDR (A), *AAVS1* EF1α HDR (B), *ATG5* LentiRNP (C), WT Lentiviral (D), or *ATG5* Endo HDR (E) CAR-T cells (n = 8 mice per group; one line = one mouse). Tumors were measured twice per week using digital calipers, and area (length x width) was used to quantify tumor burden. Mice were euthanized upon reaching humane endpoint (tumor area greater than $180mm^2$). **(F)** Survival curves for Experiment 2.

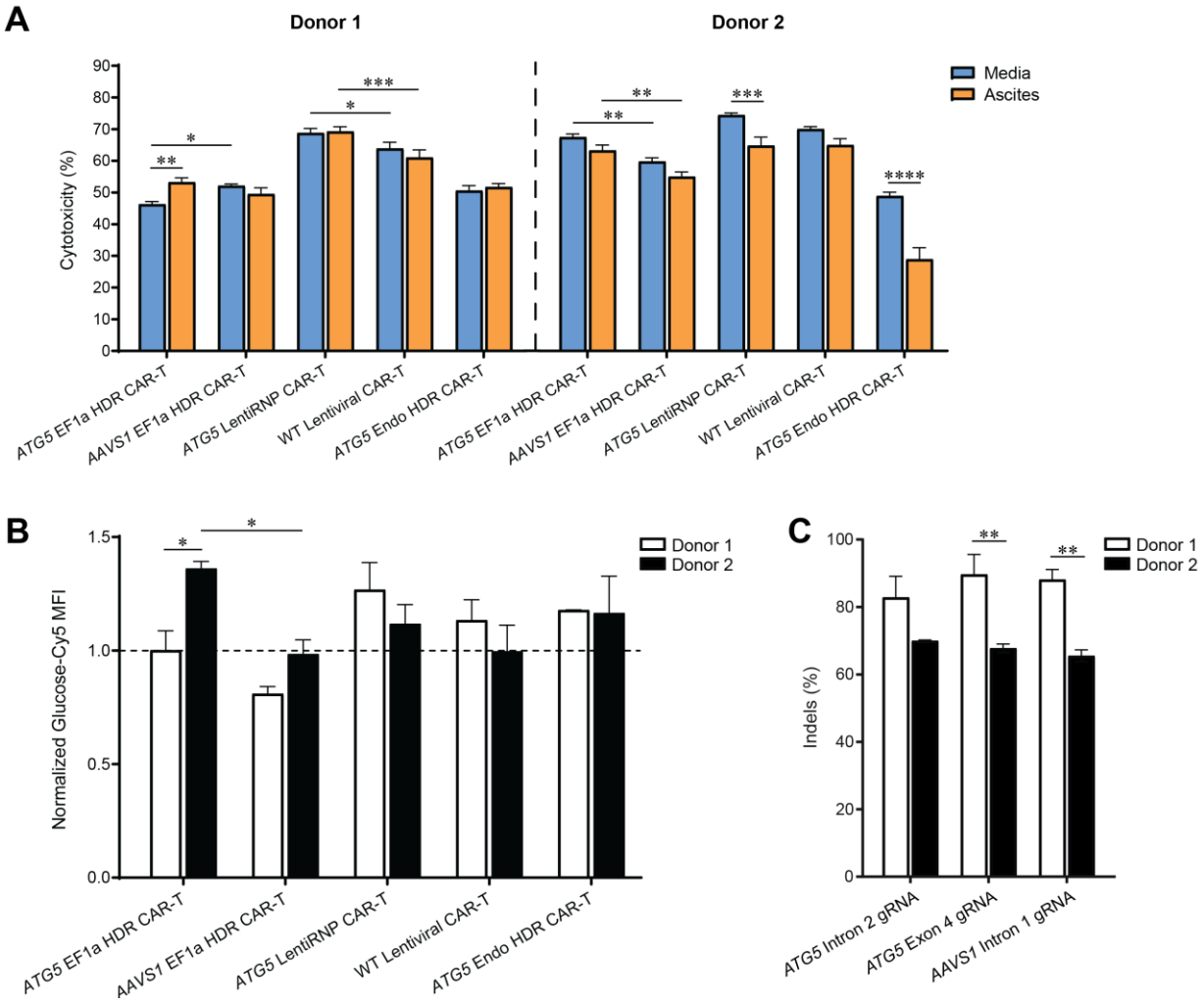

Figure 16. CAR-T cell cytotoxicity is influenced by heterogeneity between donors.
(A) Bar graph showing percent cytotoxicity of luciferase-expressing SKOV3 ovarian tumor cells after 24h co-culture with CAR-T cells from Donor 1 (left) or Donor 2 (right) at an E:T ratio of 1:1. Assays were conducted in 50/50 RPMI and TexMACS media (blue bars) or patient-derived ascites supernatant (orange bars). Results are from 1 experiment per donor, 4 technical replicates per experiment. **(B)** Bar graph showing normalized glucose uptake by CAR-T cells made from Donor 1 (open bars) or Donor 2 (shaded bars). Results are from 2 experiments per donor, 2 technical replicates per experiment. **(C)** Indel quantification as determined by TIDE analysis. CD3+ T cells from Donor 1 (white bars) or Donor 2 (black bars) were electroporated on the with HiFiCas9 RNPs and genomic DNA was harvested three days post-electroporation. Results are from 2 independent experiments. All error bars represent +SEM. P values were determined by two-way ANOVA (*p<0.05, **p<0.01, ***p<0.001, ****p<0.0001).

3.5 Results

3.5.1 Engineering autophagy-deficient CAR-T cells using CRISPR-Cas9

To evaluate the role of autophagy deletion on CAR-T cell function, we engineered *ATG5*-knockout CAR-T cells using three distinct CRISPR-Cas9 genome editing approaches. Our first method used lentiviral CAR transduction followed by RNP-mediated deletion of *ATG5* (targeting exon 4) to produce autophagy-deficient αFR CAR-T cells in a two-step editing process ("*ATG5* LentiRNP CAR-T"; Fig. 9A). To ensure that the majority of edited cells would be CAR-positive and limit the possibility of deleting *ATG5* in untransduced T cells, we also performed an enrichment step before electroporation. As a control for this method, we performed electroporations without a targeting RNP to generate autophagy-competent lentiviral CAR-T cells ("WT Lentiviral CAR-T"). Of note, the lentiviral construct used for both of these CAR-T cells included an EF1α core promoter to express the CAR.

The second and third method used HDR-mediated gene trapping to integrate the CAR directly into intron 2 of *ATG5* in a single-step editing process using AAV6 as a donor template (Fig. 9B, C). However, we varied the composition of each donor sequence to generate two functionally distinct CAR-T cell products, one with a full-length EF1α promoter inserted upstream of the CAR ("*ATG5* EF1α HDR CAR-T"; Fig. 9B), and one where the CAR would be placed under transcriptional control of the endogenous *ATG5* promoter as described in Chapter 2 (*"ATG5* Endo HDR CAR-T"; Fig. 9C). To generate an autophagy-competent control, we integrated the EF1α CAR construct into intron 1 of the safe-harbor locus *AAVS1* ("*AAVS1* EF1α HDR CAR-T"). Unfortunately, due to challenges with manufacturing we were unable to generate AAV6 for an *AAVS1*-targeting donor without the added EF1α promoter sequence. Therefore, we used the matched EF1α HDR CAR-T cells to represent the single-step editing process when making comparisons between different editing approaches.

3.5.2 Metabolite profiling uncovers key metabolites elevated in autophagy-knockout CAR-T cells

After generating each CAR-T product, we wanted to investigate whether *ATG5* deletion could reprogram metabolic phenotype under non-autophagy inducing conditions. To answer this question, we used high-resolution liquid chromatography mass spectrometry (LC-MS) to profile metabolites in autophagy-knockout and autophagy-competent CAR-T cells at the end of *in vitro* expansion. After constructing a heatmap of normalized metabolite abundances, we observed a clear separation in metabolite profiles between the *ATG5* and *AAVS1* EF1α HDR CAR-T cells, with minimal variation between donors (Fig. 10A). This separation was less distinct between the *ATG5* LentiRNP and WT Lentiviral CAR-T cells, although a similar pattern could be visualized for key metabolites like glucose and glutamine which were elevated in both the EF1α HDR and LentiRNP *ATG5*-knockout CAR-T cells. Interestingly, there was notable variability in the *ATG5* Endo HDR CAR-T group, which could indicate differences in promoter activity between donors. This result suggests that activity of the CAR itself plays a role in determining CAR-T cell metabolism, and that using a non-constitutive endogenous promoter to regulate CAR signaling is susceptible to donor heterogeneity.

Next, we used linear modeling to quantify metabolites that were differentially enriched in CAR-T cells deleted for autophagy. The *ATG5* Endo HDR CAR-T group was excluded from this analysis due to lack of a matched control. After adjusting for gene-editing method (CRISPR HDR vs. LentiRNP/Lentiviral) and including donor as a random effect, we identified 37 significantly differing metabolites between autophagy-knockout and autophagy-competent CAR-T cells ($P_{adj}<0.05$; Table 3). This was a surprising result given the lack of autophagy-inducing stimuli during *ex vivo* culture. The most differentially abundant metabolites identified in this analysis were glucose and glutamine, and both were significantly enriched in CAR-T cells deleted for *ATG5* (Fig. 11A, B). When we probed downstream metabolites in the glucose and glutamine pathways, we discovered that the tricarboxylic acid (TCA) cycle intermediates malate and citrate were significantly reduced in *ATG5*-knockout CAR-T cells, while the glycolytic metabolite pyruvate was significantly increased (Table 3). This pattern of metabolite enrichment indicates that *ATG5*-knockout CAR-T cells undergo a metabolic shift from mitochondrial oxidation to aerobic glycolysis that occurs independently of nutrient deprivation or hypoxia. Of

note, while glucose was significantly elevated in both *ATG5*-knockout CAR-T groups, the difference relative to autophagy-competent controls was much higher for CAR-T cells made using the single-step editing process (Fig. 11A). This could indicate that deleting *ATG5* using targeted CAR integration, rather than RNP knockout, facilitates a stronger metabolic phenotype in the context of glucose uptake as compared to control CAR-T cells.

Unexpectedly, our analysis also uncovered notable differences in amino acid abundance between autophagy-knockout and autophagy-competent CAR-T cells. In particular, we observed significant enrichment of the essential amino acids methionine, leucine, and phenylalanine, suggesting that *ATG5* deletion could be facilitating increased amino acid uptake (Fig. 12C-E; Table 3). While further investigation is required, this result is in line with recent reports demonstrating that basal ATG5 activity promotes ubiquitination and proteasomal degradation of the transcription factor Myc, a known positive regulator of the amino acid transporters ASCT2 and LAT1[157]. Overall, our metabolomics analysis indicates that deletion of *ATG5* induces metabolic reprogramming in CAR-T cells, and this effect occurs under non-restrictive conditions and is consistent across donors and editing method.

3.5.3 CAR-T immune phenotype is significantly influenced by the editing process

Given the notable differences in metabolic phenotype, we next wanted to determine whether *ATG5* deletion would influence the immunological phenotype of CAR-T cells expanded *ex vivo*. To our surprise, there was no significant effect of *ATG5* deletion on CAR expression, CD4/CD8 ratio, or percentage of CAR-T cells positive for the activation marker CD137 or the exhaustion marker PD1 (Fig. 12A-D). Similarly, when we stained for CCR7 and CD45RO to identify central memory (T_{cm}) CAR-T cells, we again saw no significant effect of *ATG5* deletion (Fig. 12E). These results suggest that under non-restricted conditions, there is no impact of *ATG5* deletion on CAR-T cell immune phenotype.

However, significant differences began to emerge when we compared the three *ATG5*-knockout CAR-T groups to each other. As expected, there was a wide range in CAR expression, with the *ATG5* Endo HDR CAR-T cells exhibiting the lowest CAR median fluorescence intensity (Fig. 12A). Unexpectedly, the *ATG5* EF1α HDR CAR-T cells had significantly higher CD137 (in the

CD8+ compartment; Fig. 12C) and PD1 (in the CD4+ compartment; Fig. 12D) as compared to the *ATG5* LentiRNP CAR-T cells. Similar differences were observed when we compared the autophagy-competent CAR-T cells (*AAVS1* EF1α HDR vs. WT Lentiviral), with significantly increased CD8+/CD137+ and CD4+/PD1+ CAR-T cells in the EF1α HDR group. Taken together, these data indicate that CAR-T immune phenotype during *ex vivo* culture is influenced by editing method and choice of promoter, rather than autophagy status.

3.5.4 Autophagy-knockout CAR-T cells demonstrate superior antitumor effector responses *in vitro*

Although we did not observe any differences in immune phenotype due to *ATG5* deletion, we wondered whether the metabolic reprogramming from mitochondrial oxidation to glycolytic metabolism would translate to superior *in vitro* function. First, we used a flow cytometry-based assay to quantify *in vitro* uptake of fluorescently-labelled glucose. Encouragingly, we saw a trend towards increased glucose uptake by autophagy-knockout CAR-T groups, which validated the results of our metabolite profiling experiments (Fig. 13A). Next, we used a co-culture assay with αFR-expressing SKOV3 ovarian tumor cells to stimulate production of the effector cytokine IFN-γ, and observed significantly higher IFN-γ expression in the *ATG5* EF1α HDR CAR-T cells (both CD4+ and CD8+) as compared to the *AAVS1* EF1α HDR CAR-T cells (Fig. 13B). Interestingly, IFN-γ expression by the *ATG5* LentiRNP CAR-T cells was significantly higher for the CD4+ compartment only (Fig. 13B). As production of IFN-γ is linked to glycolytic metabolism[49,158], this result could be attributed to our earlier observation that glucose is less significantly enriched in *ATG5*-knockout CAR-T cells made using the two-step editing strategy (Fig. 11A). However, the increased IFN-γ production did not translate into significant improvements in cytotoxicity for the *ATG5* EF1α HDR CAR-T group or the *ATG5* LentiRNP CAR-T group (Fig. 13C, D). In contrast, the *ATG5* Endo HDR CAR-T cells had the lowest IFN-γ expression and *in vitro* cytotoxicity of all CAR-T groups (Fig. 13B, E), which could indicate that the beneficial effect of *ATG5* deletion on cytokine production is constrained by using the endogenous *ATG5* promoter.

As we did not see measurable improvements in antitumor activity under non-restricted conditions, we wanted to determine whether deletion of *ATG5* would prove advantageous in a

restricted environment. To answer this question, we used patient-derived ascites fluid to simulate the immune-suppressive conditions of the ovarian TME. Similar to the solid TME, the ascites contains numerous suppressive cell types such as disseminated tumor cells, CAFs, TAMs, and MDSCs[159]. Importantly, immune-inhibitory factors in the ascites such as chemokines, cytokines, growth factors, and metabolites are retained in the acellular fraction, which has been shown to exert direct and indirect suppressive effects on T cells[160,161]. Furthermore, we previously demonstrated that ascites fluid contains significantly reduced glutamine and glucose as compared to most T-cell media formulations[156]. We took advantage of these features and repeated our cytotoxicity assays in cell-free ascites supernatant collected from an HGSOC patient with known glucose- and glutamine-restricted ascites. Although our results did not reach statistical significance, we saw reduced cytotoxicity when CAR-T cells were cultured in ascites supernatant, with the exception of the *ATG5* EF1α HDR CAR-T group where similar results were obtained in both media and ascites (Fig. 13F). In line with this, we saw a trend towards increased cytotoxicity in ascites by the *ATG5* EF1α HDR CAR-T cells as compared to the *AAVS1* EF1α HDR CAR-T cells, suggesting that *ATG5* deletion has a beneficial effect on CAR-T cell function in the suppressive milieu of the ascites TME. However, similar to previous experiments, the *ATG5* Endo HDR CAR-T cells were the least cytotoxic of all the *ATG5*-knockout CAR-T groups, and exhibited a significant reduction in cytotoxicity when cultured in ascites supernatant (Fig. 13F).

Taken together, our *in vitro* assays suggest that although deletion of *ATG5* enhances glucose uptake and cytokine production in the absence of autophagy-inducing stimuli, a suppressive environment may be needed to see functional benefits. However, using the endogenous *ATG5* promoter to drive CAR expression attenuates the beneficial effects of *ATG5* deletion regardless of the environment.

3.5.5 Autophagy-knockout CAR-T cells are effective against ovarian tumors *in vivo*

Lastly, we wanted to determine whether the beneficial effects of autophagy deletion observed *in vitro* would translate to effective tumor control *in vivo*. To test this, we used immunodeficient mice implanted with αFR-expressing OVCAR3 human ovarian tumors. Of note, we chose the OVCAR3 cell line due to its close genetic similarity with known high-grade serous ovarian

tumor samples[162]. We began by conducting a small-scale preliminary experiment to determine whether a dose of $5.0x10^6$ CAR-T cells would allow us to see differences in tumor regression between groups ("Experiment 1"; Table 4). We used the *ATG5* LentiRNP and WT Lentiviral CAR-T cells for this experiment, as these CAR-T cells had demonstrated the highest *in vitro* cytotoxicity in ascites supernatant (Fig. 13F). After infusing $5.0x10^6$ *ATG5* LentiRNP or WT Lentiviral CAR-T cells per mouse, we saw immediate decreases in tumor size across all treated mice, regardless of group (Fig. 14A, B). However, a clear separation began to emerge three weeks post-infusion, when tumors in the WT Lentiviral CAR-T group began to increase in size again while the *ATG5* LentiRNP group continued to regress. This translated to significant differences in survival by the end of the experiment, with all mice in the *ATG5* LentiRNP CAR-T group remaining tumor-free at 86 days post-infusion (Fig. 14C).

Building on the success of our first experiment, we conducted a larger *in vivo* study to compare efficacy across all CAR-T groups ("Experiment 2"; Table 5). We treated tumor-bearing mice with $5.0x10^6$ CAR-T cells per mouse and again saw an immediate effect of treatment across all groups, with the exception of the *ATG5* Endo HDR CAR-T group where we did not observe any tumor control (Fig. 15A-E). However, unlike in the first experiment, we saw prolonged tumor control in all other CAR-T groups regardless of autophagy status. This culminated in no significant differences in survival between the *ATG5* and *AAVS1* EF1α HDR CAR-T groups, nor the *ATG5* LentiRNP and WT Lentiviral CAR-T groups (Fig. 15F). For mice treated with the *ATG5* Endo HDR CAR-T cells, survival was not significantly different from mice treated with untransduced T cells, which aligned with our *in vitro* observations wherein the *ATG5* Endo HDR CAR-T cells demonstrated limited cytotoxicity in ascites supernatant.

3.5.6 Donor heterogeneity influences editing efficiency and CAR-T cell cytotoxicity

As we did not see the same beneficial effect of *ATG5* deletion in our second *in vivo* experiment, we wondered whether differences between healthy donors could be influencing the functionality of our CAR-T product. To answer this question, we assessed *in vitro* cytotoxicity for CAR-T cells made from Donor 1 (*in vivo* Experiment 1) and CAR-T cells made from Donor 2 (Experiment 2). Interestingly, the *ATG5* LentiRNP CAR-T cells from Donor 1 exhibited superior cytotoxicity in both media and ascites supernatant as compared to the WT Lentiviral CAR-T

cells from Donor 1, a result that paralleled our first *in vivo* experiment (Fig. 16A). However, when the *ATG5* LentiRNP CAR-T cells were made from Donor 2, the beneficial effect of *ATG5* deletion observed in media was not apparent, and in fact, cytotoxicity was suppressed by ascites supernatant (Fig. 16A). In contrast, when we examined CAR-T cells from Donor 2 made using the CRISPR HDR method, the *ATG5* EF1α HDR CAR-T cells demonstrated superior cytotoxicity in both media and ascites supernatant, as well as increased glucose uptake as compared to *AAVS1* EF1α HDR CAR-T cells (Fig. 16B).

Of note, we observed significantly lower editing efficiency in Donor 2 as compared to Donor 1 (Fig. 16C), which aligned with genomic analysis showing reduced indels at *ATG5* for the LentiRNP CAR-T cells from our second *in vivo* experiment (Table 5). This suggests that there is a minimum threshold of *ATG5* deletion required to elicit improvements in *in vivo* efficacy over autophagy-competent CAR-T cells. However, using a two-step editing process like the LentiRNP strategy limits enrichment of edited cells and is therefore more susceptible to donor differences in editing efficiency. This is a crucial consideration for metabolic engineering strategies that require a high frequency of gene deletion to yield functional benefits.

3.6 Discussion

A key mechanism underscoring the resistance of ovarian cancer to immunotherapy is metabolic suppression, in which tumor cells, cancer-associated fibroblasts, and suppressive immune cells consume key nutrients and release inhibitory metabolites into the TME. Limited glucose and amino acid availability is particularly concerning for antitumor immunity, as depletion of these essential nutrients can lead to autophagy induction and the suppression of T-cell effector responses[84–86]. Therefore, the development of successful T cell-based therapies for ovarian cancer requires strategies to overcome downregulation of effector responses due to nutrient deprivation in the ovarian TME.

Here, we deleted the essential autophagy gene *ATG5* in αFR CAR-T cells, and used LC-MS to measure metabolite abundances in *ATG5*-knockout and *ATG5*-wildtype CAR-T cells cultured *in vitro*. Although we previously reported metabolic differences in tumor-infiltrating lymphocytes

(TIL) harvested from *Atg5*-knockout mice[86], we did not expect to see such distinct metabolic phenotypes for CAR-T cells cultured under nutrient-replete conditions. While this result could be attributed to differences in autophagy-mediated degradation of metabolic enzymes, which has been shown to occur under basal conditions in tumor cells[163], it could also indicate a possible non-canonical role for ATG5 in regulating T cell metabolism.

In line with this hypothesis, recent work has shown that ATG5 interacts with the E3 ubiquitin-protein ligase FBXW7 to facilitate degradation of the transcription factor Myc through a mechanism independent of ATG12-ATG5 conjugation. Notably, ATG5-mediated regulation of Myc was shown to occur only under non-starvation conditions, and the effect was lost upon serum starvation[157]. Myc is a key transcription factor for the regulation of amino acid import in T cells, and deletion of Myc has been shown to downregulate expression of the transporters ASCT2 (*SLC1A5*) and LAT1 (*SLC7A5*)[164]. Although we did not investigate either of these transporters, our LC-MS profiling of *ATG5*-knockout CAR-T cells revealed significant enrichment of glutamine (imported by ASCT2), and methionine and leucine (imported by LAT1). Furthermore, we also detected a pattern of metabolite abundance indicating a shift from mitochondrial oxidation to glycolysis in *ATG5*-knockout CAR-T cells, and Myc is a known positive regulator of glycolytic enzymes such as glyceraldehyde-3-phosphate dehydrogenase (GAPDH) and hexokinase[165]. While further investigation is required to confirm this hypothesis, it is possible that the effects of *ATG5* deletion on amino acid import and glucose metabolism are mediated by increased expression of Myc-regulated metabolic genes under non-starvation conditions.

Aerobic glycolysis is essential for T cell effector function, and inhibition of the glycolytic pathway has been shown to limit cytokine production and cytolytic activity[32,158]. Accordingly, *ATG5*-knockout CAR-T cells expressed high levels of IFN-γ after co-culture with target tumor cells. However, when we conducted *in vitro* cytotoxicity assays under non-restricted conditions, there was no improvement in tumor killing as compared to autophagy-competent CAR-T cells. Interestingly, while it was previously shown that treatment with 2-deoxy-D-glucose (2-DG, an inhibitor of glycolysis) completely inhibited production of IFN-γ, expression of the cytolytic molecule perforin was only partially inhibited by 2-DG, and there was no effect of 2-DG

treatment on expression of IL-2[49]. In line with these results, a recent report investigating the benefits of GLUT1 overexpression in CD19 CAR-T cells found that functional enhancement was only detected when glucose was restricted, and in standard culture medium, this effect was lost[166]. Taken together, these observations indicate that there is a wide range of glucose dependencies exhibited by different elements of the T cell effector response, and that alternate mechanisms regulate cytolysis when glucose availability is high. This would explain why the notable differences observed in glucose metabolism and IFN-γ production failed to translate into improved cytotoxicity under non-restricted conditions, and suggests that a suppressive environment is required to see the benefits of *ATG5* deletion.

Ascites fluid from patients with ovarian cancer is a useful medium for assessing the efficacy of engineered CAR-T cells under immune-suppressive conditions, as immune-inhibitory factors such as transforming growth factor beta (TGF-β), interleukin-10 (IL-10), and kynurenine are retained in the fluid fraction after sample processing[137,139,142]. Furthermore, we previously demonstrated that ascites from patients with HGSOC contains significantly reduced glucose and glutamine as compared to standard cell culture medium, and inhibits T cell effector responses *in vitro*[156]. Accordingly, when we performed cytotoxicity assays in ascites fluid from a patient with known glucose- and glutamine-restricted ascites, we saw global reductions in CAR-T cell cytotoxicity, indicating immune suppression. However, in line with our hypothesis that deletion of *ATG5* would prove advantageous in a restricted environment, we observed superior cytotoxicity by *ATG5*-knockout CAR-T cells as compared to autophagy-competent CAR-T cells, although the extent of this effect varied between healthy donors. While this result could be attributed solely to the changes in glucose metabolism and IFN-γ production in *ATG5*-knockout CAR-T cells, it is important to note that amino acid starvation is the canonical stimulus for autophagy[167].

Under non-starvation conditions, autophagy mediates the degradation of specific intracellular cargo through a mechanism termed selective autophagy, which uses cargo receptors such as sequestosome-1 (SQSTM1; also known as p62) to bind ubiquitinated substrates and deliver them to the autophagosome for degradation[168]. Selective autophagy is crucial for cellular homeostasis, and common substrates include damaged organelles, peroxisomes, protein aggregates, ferritin,

and cytosolic bacteria[169]. In contrast, while starvation-induced autophagy was initially described as a bulk recycling process, there is a growing body of evidence to indicate that cargo selectivity is maintained under starvation conditions[170,171]. This suggests that the autophagy-induced attenuation of T cell effector function previously demonstrated by our group and others[84–86] could result from a specific degradative program. Indeed, this hypothesis is supported by a recent preprint in which the authors used mass spectrometry-based proteomics to identify over 3800 proteins downregulated in T cells exposed to amino acid starvation. Strikingly, inhibition of autophagy repressed starvation-induced degradation of effector molecules such as granzymes and perforin, as well as glucose and amino transporters, but had no effect on mitochondrial proteins involved in the electron transport chain[172]. While further investigation is required, these results suggest that glutamine deprivation in the ovarian ascites TME causes specific degradation of proteins required for a robust effector response, and this process is inhibited in CAR-T cells deleted for *ATG5*.

3.7 Limitations and future directions

Broadly, this chapter demonstrates that deletion of *ATG5* in CAR-T cells supports effective tumor control under immune-suppressive conditions. Taken together with other reports from the field, our results support a model in which deletion of *ATG5* prevents downregulation of CAR-T cell effector responses when exposed to glucose and glutamine deprivation. However, several questions remain unanswered. First, although we proposed that the elevated glutamine abundance in *ATG5*-knockout CAR-T cells was due to increased uptake through amino acid transporters, this could also stem from reduced glutamine consumption by downstream metabolic processes. As LC-MS metabolite profiling only detects static metabolite abundances (a limitation of this method), we would need to use a different approach to investigate this hypothesis, such as isotope-tracing analysis. Isotope-tracing analysis is a well-established method for quantifying metabolic flux, and 13C-labelled glutamine in particular has already been used to monitor glutamine metabolism in tumor cells and adipocytes[173–175]. Therefore, a follow-up *in vitro* tracing study with 13C-labelled glutamine could allow us to gain a deeper understanding of the effects of *ATG5* deletion on glutamine utilization in CAR-T cells.

Second, although we showed that *ATG5* deletion had beneficial effects on CAR-T function in ascites supernatant, given that the ascites sample was restricted in both glutamine and glucose, the precise contribution of each metabolite is still unclear. As we previously showed that glucose restriction reduces the upregulation of IFN-γ in murine T cells deleted for *Atg5*[86], it is possible that *ATG5*-knockout CAR-T cells are resistant to glutamine but not glucose deprivation. To answer this question, we could repeat our cytotoxicity assays in ascites supernatant supplemented with exogenous glucose or glutamine, which would allow us to determine the individual role of each metabolite while still exposing *ATG5*-knockout CAR-T cells to other soluble factors in the ascites. Importantly, the results of this investigation could be used to identify other cancer types in which to explore the therapeutic potential of *ATG5*-knockout CAR-T cells. For example, glucose deprivation has also been shown in stomach cancer, colon cancer, and glioblastoma[176–178], while both glucose and glutamine are implicated in acute myeloid leukemia (AML)[179]. Interestingly, the development of an effective CAR-T cell therapy for AML has remained elusive, in direct contrast to the rapid success achieved in the treatment of B-cell malignancies. Therefore, if follow-up studies indicate that *ATG5*-knockout CAR-T cells are resistant to both glutamine and glucose deprivation, a future clinical path for this project could be to evaluate *ATG5* deletion as a strategy to improve CAR-T efficacy in AML.

3.8 Technological considerations

Lastly, we also used this chapter to assess three distinct gene-editing methods for generating *ATG5*-knockout CAR-T cells, with the goal of answering two additional questions: first, could the endogenous *ATG5* promoter be used to mediate a successful antitumor response *in vivo*; and second, were there any functional differences between CAR-T products that would favor one editing process over another. To answer the first question, we compared two iterations of the single-step CRISPR HDR strategy developed in Chapter 2, one where the CAR was expressed by an exogenous EF1α promoter, and one where the CAR was expressed by the endogenous *ATG5* promoter. While we originally hypothesized that using the endogenous *ATG5* promoter would support enhanced CAR activity in restricted conditions due to the presence of autophagy-inducing stimuli, this strategy actually proved detrimental to CAR-T function and constrained antitumor responses *in vivo*. Given the vastly reduced CAR MFI we observed in the *ATG5* Endo

HDR CAR-T cells, a simple explanation for this result could be that the CAR surface density was too low to facilitate an effective cytolytic response. A second, but related, explanation could be attributed to promoter dynamics, with the *ATG5* promoter unable to support rapid internalization and re-expression of the CAR in response to antigen.

To answer the second question, we compared *ATG5* EF1α HDR CAR-T cells made using the single-step CRISPR HDR method to *ATG5* LentiRNP CAR-T cells made using a two-step editing process. Although both groups effectively controlled tumors *in vivo*, one of the mice in the *ATG5* LentiRNP CAR-T group eventually experienced a recurrence, while all mice in the *ATG5* EF1α HDR CAR-T group remained tumor-free. When we re-evaluated the results of our *in vitro* assays, we saw donor-dependent variability in cytotoxic function for the *ATG5* LentiRNP CAR-T group, which we attributed to differences in the extent of *ATG5* knockout mediated by RNP electroporation. As the two-step editing approach limits enrichment of edited cells, CAR-T cells made using this process are more susceptible to donor differences in editing efficiency, which is a crucial consideration when a high frequency of gene deletion is needed for functional benefits. In contrast, the single-step editing process enables selection of edited cells during the CAR enrichment step, which yields a CAR-T product with a higher frequency of *ATG5* deletion and superior *in vivo* function.

Chapter 4: Process development for nonviral manufacturing of clinical-grade CD22 CAR-T cells for the treatment of B-cell malignancies

Authors:

Gillian Carleton[1,2], Scott McComb[3,4,5], Tyler Dyer[2], and Julian J. Lum[1,2]

Affiliations:

1. Department of Biochemistry and Microbiology, University of Victoria, Victoria, BC.
2. Trev and Joyce Deeley Research Centre, BC Cancer, Victoria, BC.
3. Human Health Therapeutics Research Centre, National Research Council, Ottawa, ON.
4. Department of Biochemistry, Microbiology, and Immunology, University of Ottawa, Ottawa, ON.
5. Centre for Infection, Immunity, and Inflammation, University of Ottawa, Ottawa, ON.

Author contributions:

G.A.C designed and performed experiments, analyzed the data, and wrote the text. G.A.C and S.M. designed the CAR donor template. S.M. created Figure 17A. T.D developed and optimized the *in vitro* cytotoxicity assay. G.A.C. created all other figures. G.A.C and J.J.L edited the text.

4.1 Abstract

There is growing interest in the Canadian cell therapy space in moving towards nonviral approaches for clinical-grade production of CAR-T cells. Here, we devised a strategy for nonviral manufacturing of CD22 CAR-T cells using targeted integration of a linear dsDNA template at the T cell receptor alpha chain (*TRAC*) locus. Using *in vitro* cytotoxicity assays, we showed that nonviral CD22 CAR-T cells exhibited comparable antitumor activity to lentiviral CD22 CAR-T cells. We validated three strategies for improving overall CAR-T yield – an antibody-based method for selective expansion of CAR-positive cells, a magnetic bead method for enrichment of CAR-positive cells, and a pharmaceutical method to increase CAR knock-in through treatment with small molecule inhibitors. Lastly, we demonstrated how each method could be integrated within the pre-installed T cell engineering protocol for clinical CAR-T manufacturing on the Miltenyi CliniMACS Prodigy and Electroporator system. The results of this study establish feasibility for nonviral CAR-T manufacturing within the current Canadian cell therapy infrastructure, and lay the groundwork for future development of allogeneic CAR-T therapies.

4.2 Introduction

The development of a non-commercial platform for production of Canadian-made CD19 CAR-T cells has increased access to this life-changing therapy for numerous patients with B-cell malignancies[88]. However, over 30% of patients receiving CD19 CAR-T therapy eventually relapse with antigen-negative disease, leaving them with a high disease burden and few viable treatment options[180,181]. To support the development of CAR-T therapies for CD19-negative disease, alternative B-cell antigens such as CD22 are currently being evaluated for efficacy and toxicity. CD22 is a sialoglycoprotein that is highly expressed on the surface of B cells, and an antibody-drug conjugate targeting CD22 was recently approved for the treatment of pediatric patients with acute lymphoblastic leukemia[182]. While CAR-T cells targeting CD22 have yet to be approved by the FDA, CD22 CAR-T cells have demonstrated similar efficacy and safety as CD19 CAR-T cells in several clinical studies to date[183,184]. To that end, The National Research

Council of Canada recently developed a single-domain CD22 CAR for use in an upcoming clinical trial for patients with relapsed CD19-negative disease.

Similar to the FDA-approved CAR therapies, which are manufactured by lentiviral or gammaretroviral CAR transduction[2], the Canadian platform uses GMP-grade lentivirus for CAR delivery[88]. However, viral delivery methods are associated with safety risks, such as the potential for malignant transformation due to random integration at oncogenic loci[185]. Viral manufacturing at the scale required for clinical application is also costly and time-consuming, which adds operational complexity. In contrast, genome editing with CRISPR-Cas9 can be exploited to facilitate site-specific CAR integration without the need for viral vectors. Furthermore, this approach has already been tested in the clinical setting, with results from the first nonviral CD19 CAR-T trial showing objective responses in all patients and a manageable toxicity profile[186].

Here, we present a gene-editing method for nonviral integration of the clinical CD22 CAR construct at the *TRAC* locus. By using a linear dsDNA donor to deliver the CAR, our approach mitigates potential adverse events linked to randomly-integrating viral vectors and reduces challenges associated with virus manufacturing. Furthermore, deletion of *TRAC* prevents antigen recognition by the endogenous TCR and eliminates the potential of graft-vs-host disease (GVHD)[187], thereby providing an avenue towards future development of a Canadian-made allogeneic CAR-T product.

4.3 Materials and Methods

4.3.1 Cell line culture

Luciferase-expressing CD22-positive K562 human leukemia cells (K562-CD22-Luc) were grown in RPMI 1640 (ThermoFisher) supplemented with 10% heat-inactivated fetal bovine serum (FBS; Sigma), 2 mM L-glutamine (ThermoFisher), 1% penicillin-streptomycin (ThermoFisher), and 1 μg/ml puromycin (Gibco).

4.3.2 Design and synthesis of genome editing components

The *TRAC*-targeting guide RNA (TRAC-1a) was previously designed by Scott McComb[188]. Guide RNA was synthesized by IDT (Alt-R sgRNA), resuspended in nuclease-free water to 100 μM, and stored at -80°C. The gRNA sequence can be found in Supplementary Table 6.

The TRAC-CD22 CAR donor template was designed around a published CD22-CAR construct[189]. The CAR comprised a CD28 leader sequence, a camelid-derived single-domain antibody targeting human CD22, a CD8 hinge domain, a CD28 transmembrane domain, a 4-1BB costimulatory domain, and a CD3ζ intracellular domain. The full donor sequence was synthesized by Twist Bioscience in a standard cloning vector, and included a 2A self-cleaving peptide (2A) sequence immediately upstream of the CAR, a bovine growth hormone polyadenylation (pA) sequence immediately downstream of the CAR, and 1 kb of genomic *TRAC* sequence at both the 5' and 3' ends.

TRAC-CD22 linear dsDNA donors were generated by PCR amplification with KAPA-HiFi polymerase (Roche). In brief, primers were designed to amplify 500 bp of genomic *TRAC* as homology arms (TRAC-CD22 donor). A second set of primers was designed to generate 500 bp homology arms with truncated Cas targeting sequences (TRAC-CD22-tCTS donor) as previously described[19]. PCR reactions were concentrated and purified using KAPA magnetic beads (Roche) at a 1:1 volumetric ratio. Purified dsDNA donors were quantified by NanoDrop (ThermoFisher) and normalized to 2 μg/μl with nuclease-free water. All donor sequences can be found in Supplementary Table 7. PCR primer sequences can be found in Supplementary Table 8.

4.3.3 Lentivirus production

The CD22-CAR lentivirus was a gift from Julie Nielson, and was prepared in-house as previously described[17]. In brief, the CD22-CAR sequence was commercially synthesized and cloned into a lentiviral expression vector, downstream of an elongation factor 1 alpha (EF1α) long promoter sequence. CD22-CAR vector was co-transfected with packaging and envelope plasmids into HEK293T cells (CRL-11268, ATCC) using TransIT-LT1 (Mirus, MIR2305).

Virus-containing supernatant was collected, filtered, and concentrated by ultra-centrifugation at 25,000 rpm for 90 minutes at 4ºC. Viral pellets were resuspended in D-PBS and stored at -80ºC.

4.3.4 T cell isolation and culture

Peripheral blood mononuclear cells (PBMCs) were isolated from healthy donor leukapheresis products (STEMCELL) by Ficoll gradient density centrifugation. CD3+ T cells were isolated from PBMCs using positive selection CD3 microbeads (Miltenyi) as per the manufacturer's protocol. T cells were activated with 25 μl Immunocult CD3/CD28 T cell activators (STEMCELL) per 1 million cells and cultured in Immunocult-XF medium (STEMCELL) supplemented with 1% penicillin-streptomycin, 2 mM L-glutamine, and 300 U/ml IL-2 (Peprotech).

4.3.5 T cell electroporation

RNPs were prepared as previously described[110]. In brief, sgRNA (100 μM, IDT) was mixed in a 2:1:1 molar ratio with poly-l-glutamic acid (PGA; 100 mg/ml, Sigma) and SpCas9 nuclease (10 mg/ml, IDT), and incubated for 15 minutes at 37ºC. After RNP formation, dsDNA donors (2-3 μg DNA/50 pmol RNP on a Cas9 basis) were mixed with RNPs and incubated for an additional 5 minutes at room temperature. T cells were resuspended in electroporation buffer P3 (Lonza), mixed with dsDNA/RNPs at a ratio of $1x10^6$ cells/50 pmol RNP, and electroporated in 16-well nucleocuvette strips on the 4D-Nucleofector X Unit (Lonza) using pulse code EO115 or EH115 as indicated. Immediately post-electroporation, 80 μl of pre-warmed T cell medium (no IL-2) was added to each well and the nucleocuvette strip was returned to the incubator for 15 minutes at 37ºC. After 15 minutes, T cells were transferred to a 48-well plate at a density of $1x10^6$ cells/ml in complete T cell medium. For experiments using small-molecule inhibitors ("TSA/Ned"), T cells were plated in complete T cell medium supplemented with 0.05 μM Trichostatin A (Cayman Chemicals) and 1.0 μM Nedisertib (Selleck). Inhibitors were removed by medium exchange 24 hours post-electroporation.

4.3.6 Magnetic bead enrichment

Cells were collected, centrifuged for 5 minutes at 1500 rpm and 4°C, and washed once prior to staining for 30 minutes at room temperature with AF647-conjugated anti-V_HH antibody (in-house) diluted 1:50 in PBS. After staining, cells were washed twice, then incubated for 15 minutes at 4°C with anti-AF647 microbeads (Miltenyi) at a ratio of 10 μl beads per 5 million cells in cell-enrichment buffer (PBS supplemented with 0.5% heat-inactivated human serum (Sigma)). Cells were washed once with cell-enrichment buffer, then passed through an MS column (Miltenyi) for positive enrichment of labelled cells.

4.3.7 CAR-T cell restimulation

CAR-positive cells were plated at 50,000-250,000 cells/ml (10,000 to 50,000 cells per well) in a 96 well flat-bottom plate coated in 50 μg/ml unlabeled anti-V_HH antibody (in-house). After 2 days of re-stimulation, CAR-T cells were moved to standard tissue culture plates. For the remaining culture period, CAR-T cells were maintained at 500,000 to 1 million cells/ml and transferred to larger culture vessels as needed.

4.3.8 CAR-T cell production – Lentiviral CAR-T cells

T cells were isolated and activated on Day 0 as per section 4.3.4, and transduced on Day 1 with concentrated CD22-CAR lentivirus at an MOI of 0.1. CAR-T cells (“Lentiviral CD22-CAR-T”) were enriched on Day 5 by magnetic bead enrichment as per section 4.3.6, restimulated on Day 8 as per section 4.3.7, and expanded for an additional 8-10 days.

4.3.9 CAR-T cell production – Nonviral CAR-T cells

T cells were isolated and activated on Day 0 as per section 4.3.4, and electroporated on Day 3 as per section 4.3.5 with either TRAC-CD22 or TRAC-CD22-tCTS donors, as indicated. CAR-T cells (“*TRAC* CD22-CAR-T”) were enriched on Day 8 by magnetic bead enrichment as per section 4.3.6, restimulated on Day 8 as per section 4.3.7, and expanded for an additional 8-10 days.

4.3.10 Flow cytometry analysis

Percentage of CAR-positive cells was determined by multicolor flow cytometry 5 days post-electroporation. T cells were washed, stained with fixable viability dye eF506 (1/2000; Invitrogen #65-0844-14) for 15 minutes at 4°C, washed again, then stained for 20 minutes at room temperature with the following antibody cocktail diluted in flow cytometry staining buffer: CD3-BV750 (1/100; Biolegend #344845) and CAR-AF647 (1/50; in-house). Cells were resuspended in flow cytometry staining buffer prior to acquisition on a Cytek Aurora spectral flow cytometer. Cytometry data were analyzed using SpectroFlo (Cytek) and FlowJo v10.10 (BD Life Sciences). A detailed list of all antibodies can be found in Supplementary Table 9.

4.3.11 *In vitro* cytotoxicity assay

A luciferase-based assay was used to measure CAR-T cell cytotoxicity. In brief, CAR-T cells were co-cultured in a 96-well plate with luciferase-expressing, CD22-positive K562 (K562-CD22-Luc) cells at the indicated effector-to-target (E:T) cell ratios. K562-CD22-Luc cells were also cultured alone to determine the maximum luciferase expression (RLU_{max}), while medium-only wells were used to account for background luminescence ($RLU_{background}$). After 24 hours, D-Luciferin (1/20; Revvity Health Sciences) was added to each well, mixed by pipetting, and the plate was incubated in the dark for 5 minutes. Luminescence was measured on a Varioskan Lux plate reader (Thermo Scientific), and specific tumor cell lysis calculated as $(RLU_{sample}/((RLU_{max}-RLU_{background})) \times 100$.

4.4 Figures and Tables

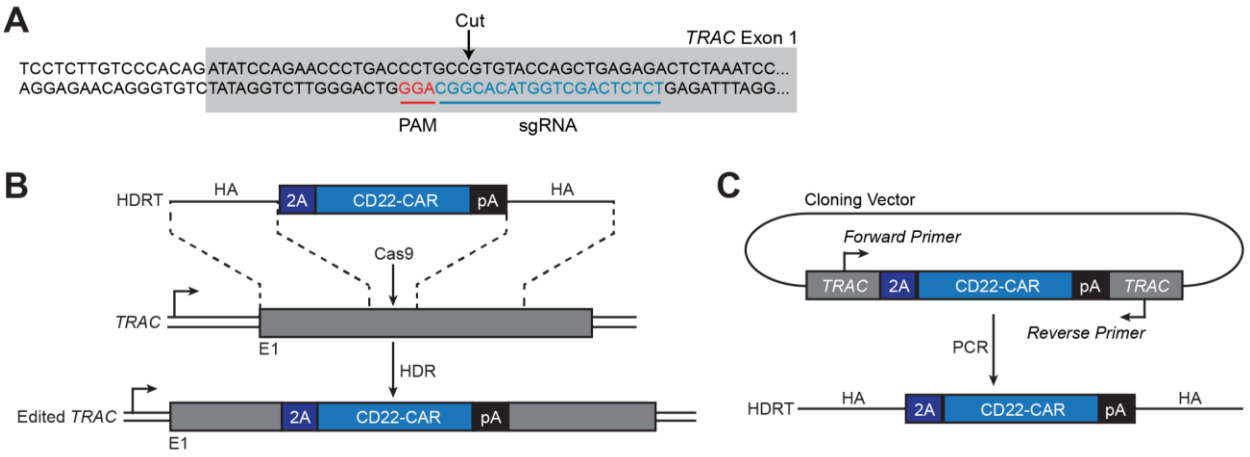

Figure 17. Genome editing strategy for nonviral production of *TRAC* CD22-CAR-T cells. **(A)** Closeup view of the Cas9 cut site in exon 1 of *TRAC* (grey box), with the protospacer adjacent motif (PAM) highlighted in red and the sgRNA sequence in blue. **(B)** Schematic of the dsDNA donor template (HDRT) and *TRAC* exon 1 (E1) after CAR integration. The donor template contains a 2A sequence, CD22-CAR cassette, polyadenylation sequence (pA), and homology arms (HA). **(C)** Diagram showing the PCR amplification process for *TRAC*-CD22 donor production.

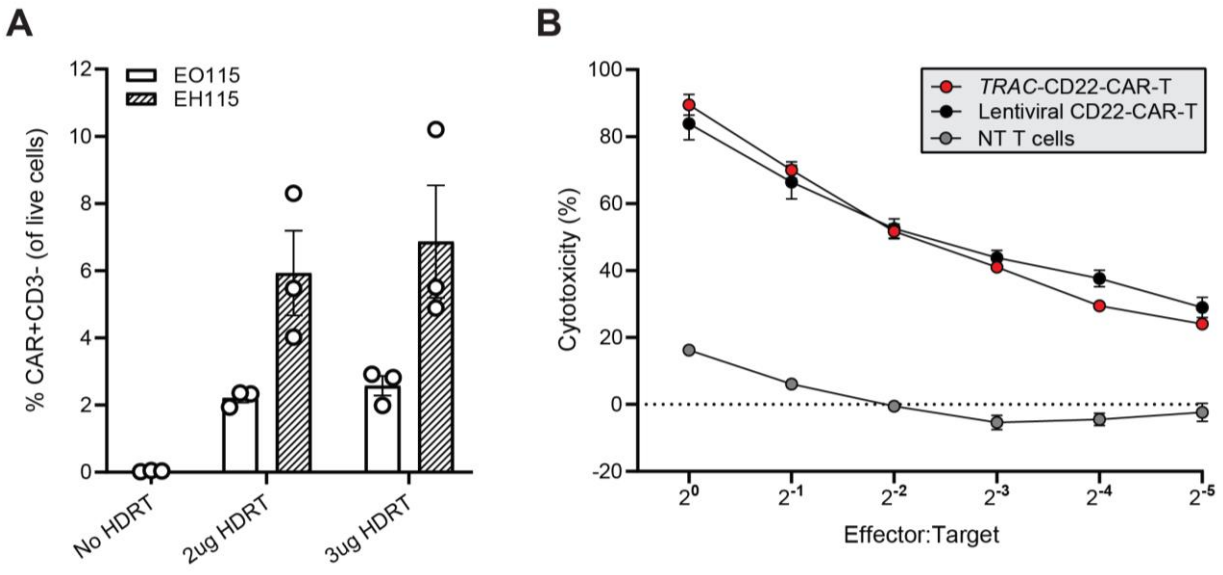

Figure 18. RNP/dsDNA co-electroporation generates functional *TRAC* CD22-CAR-T cells. **(A)** Bar graph showing percentage of CAR-positive cells five days post-electroporation with *TRAC*-targeting RNPs and dsDNA HDRTs at the indicated dose, using the Lonza 4D pulse code EO115 or EH115. Results are from three different healthy donors. **(B)** Scatter plot showing percent cytotoxicity of luciferase-expressing CD22-positive K562 cells after 24h co-culture with *TRAC*-CD22-CAR-T cells (red) and lentiviral CD22-CAR-T cells (black) at the indicated E:T ratios. Results are from one healthy donor, n = 2 independent experiments, 4 technical replicates per experiment.

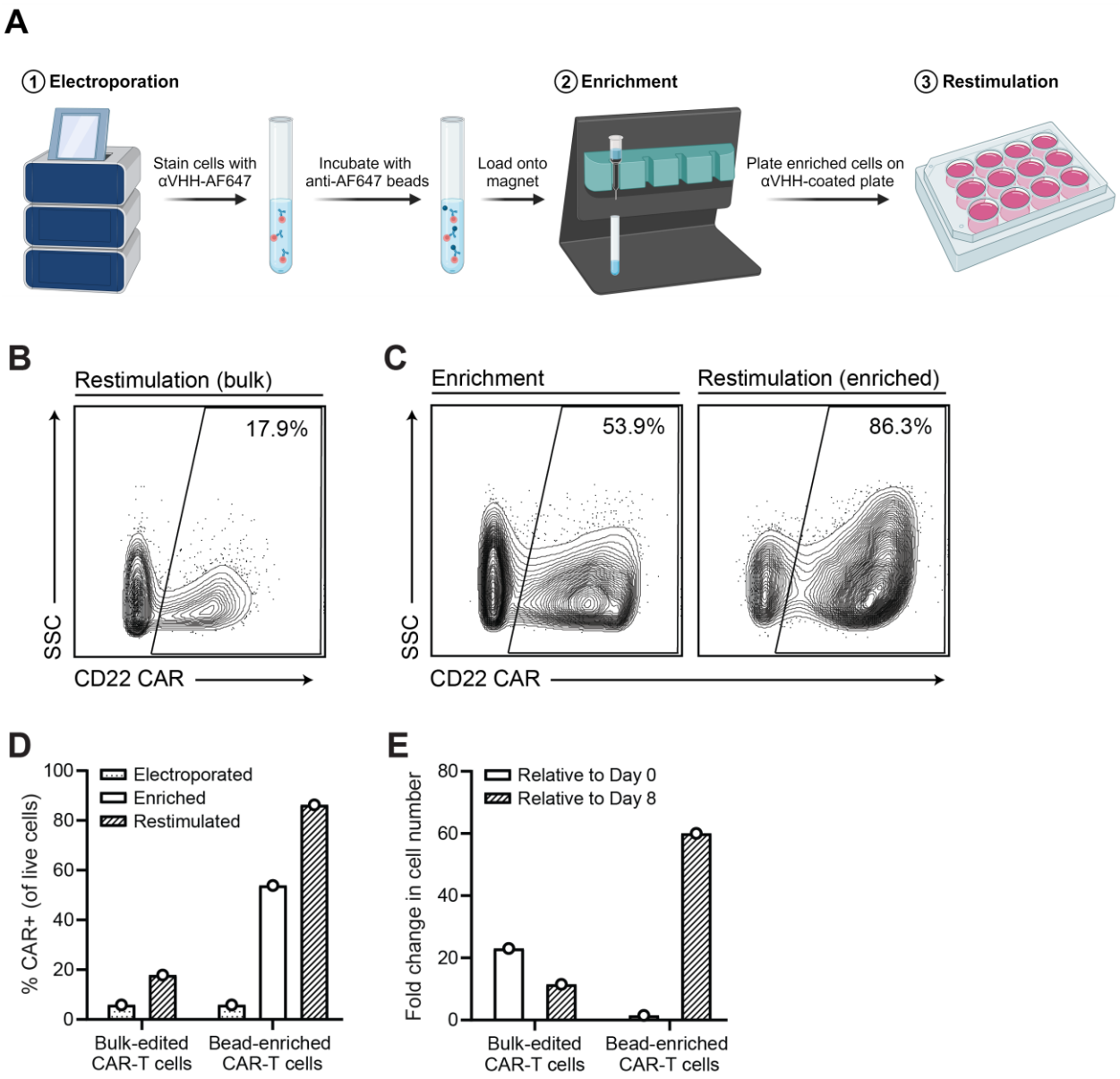

Figure 19. A method for enrichment and selective expansion of edited CAR-T cells.
(A) Schematic showing complete process of electroporation, bead enrichment, and anti-V_HH restimulation. Image was created with Biorender.com. **(B)** Flow cytometry contour plot showing percentage of CAR-positive cells after anti-V_HH restimulation of the bulk population. **(C)** Flow cytometry contour plots showing percentage of CAR-positive cells immediately after bead-enrichment (left) and after anti-V_HH restimulation of the enriched population. **(D)** Bar graph quantifying results illustrated in (B-C). **(E)** Bar graph showing fold change in cell number relative to number of cells at start of experiment (Day 0, open bars), and relative to number of

cells at start of restimulation (Day 8, shaded bars). Cells were electroporated with 3 μg HDRT using pulse code EH115, enriched by magnetic bead selection, restimulated with anti-V_HH antibody, and expanded for ten days. Results are from one healthy donor, n = 1 experiment.

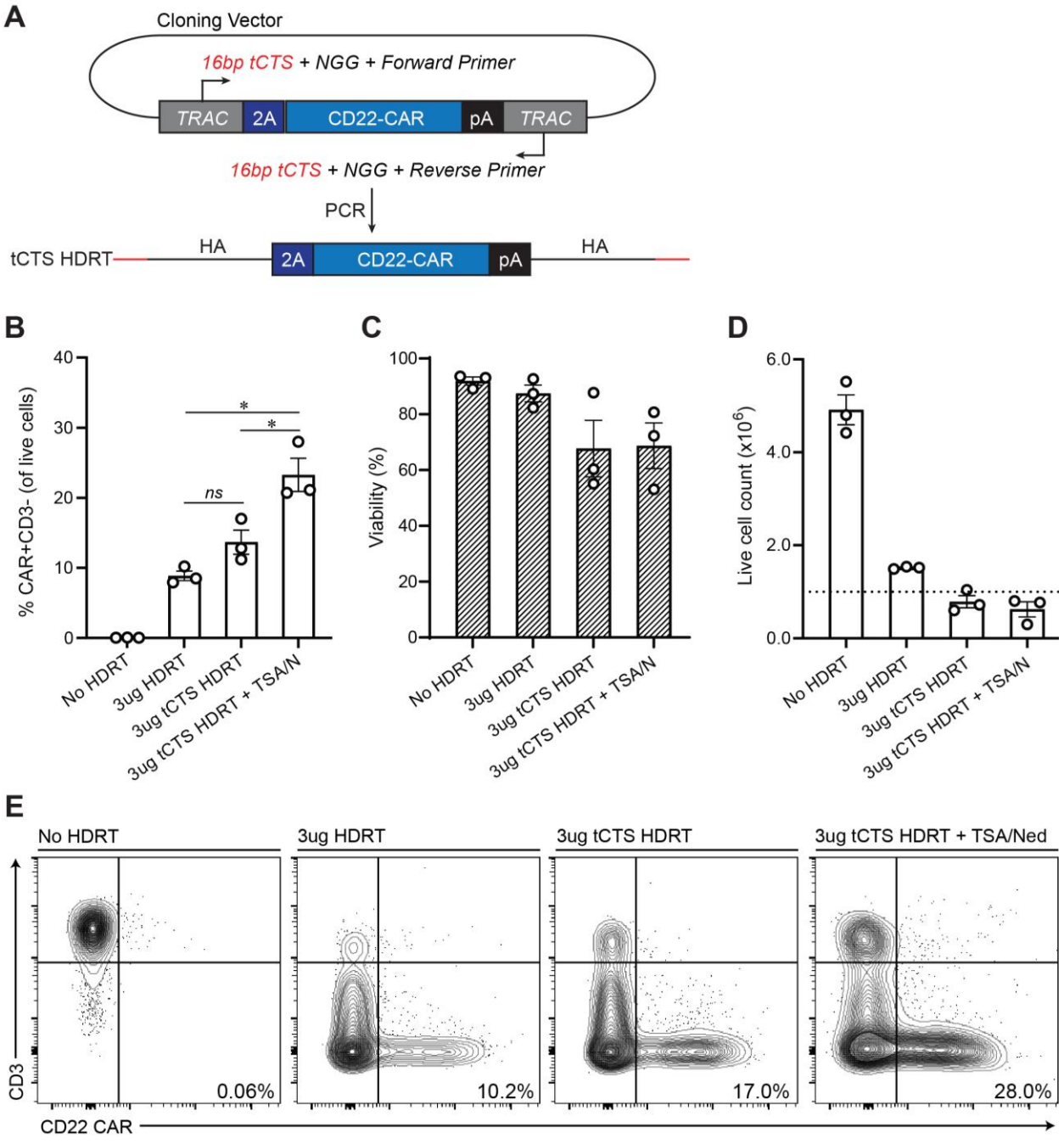

Figure 20. Modifications to the editing process increase CAR integration at *TRAC*.
(A) Diagram showing PCR amplification with primers containing truncated Cas targeting sequences (tCTS) for TRAC-CD22-tCTS donor production. **(B-D)** Bar graphs showing percentage of CAR-positive cells (B), percent viability (C), and live cell counts (D) five days post-electroporation with *TRAC*-targeting RNPs and dsDNA HDRTs at the indicated dose, using pulse code EH115. The dotted line in (D) indicates a starting number of $1x10^6$ live cells per

electroporation. Cells in the TSA/N condition were treated with 0.05 μM Trichostatin A and 1.0 μM Nedisertib for 24h immediately following electroporation. Results are from one healthy donor, n = 3 independent experiments. All error bars represent +/- SEM. P values were determined by Welch's *t* test (*p<0.05). **(E)** Flow cytometry contour plots from one of the experiments in (B-D) showing percentage of CAR-positive cells after each modification made to the editing process.

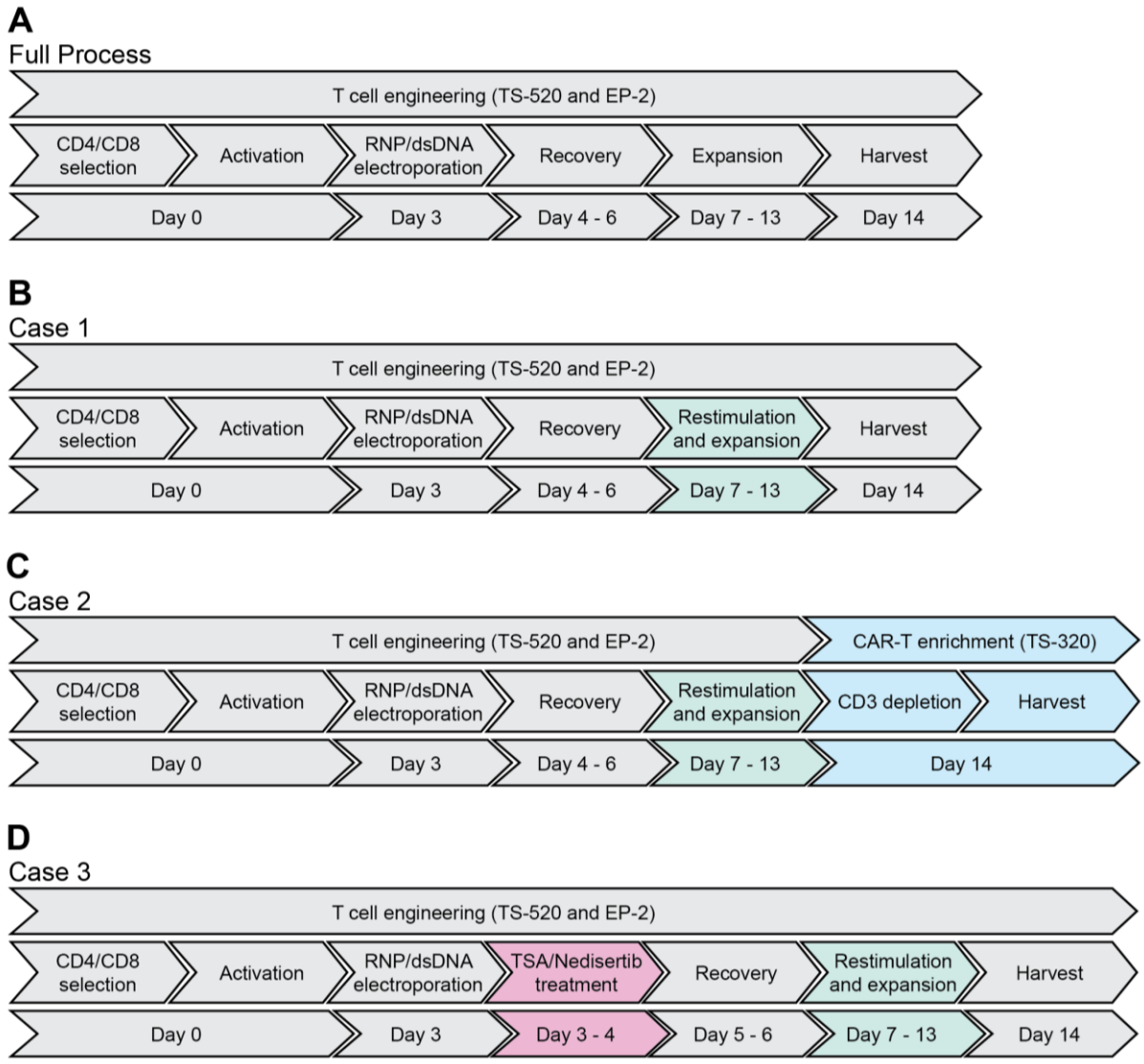

Figure 21. Closed-system manufacturing of nonviral CAR-T cells.

(A) Overview of the full T cell engineering process using the Miltenyi CliniMACS Prodigy and Electroporator. **(B)** Overview of a process option to add an anti-V_HH restimulation reagent to the cultivation chamber on Day 7. **(C)** Same as (B) but with an added separation process on Day 14 to deplete unedited, CD3-positive cells from the final product. **(D)** Same as (B) but with small molecule inhibitors added to the cultivation chamber immediately post-electroporation on Day 3. TS-520, Prodigy Tubing Set 520; EP-2, Electroporation Tubing Set 2; TS-320, Separation Tubing Set 320.

4.5 Results

4.5.1 Nonviral integration at *TRAC* generates functional CD22 CAR-T cells

Using a single-domain CD22 CAR recently developed by the National Research Council[189], we devised a strategy for targeted integration at *TRAC*. We selected *TRAC* based on previous work showing that integration at this locus allows for optimal regulation of CAR expression by the endogenous promoter[104]. Our editing approach was inspired by the original CD19 CAR knock-in pioneered by Eyquem *et al.*[104], but rather than inserting the CAR into the first intron of *TRAC*, we selected a guide RNA sequence with a PAM site in exon 1 (Fig. 17A). This eliminated the need for a splice acceptor on the donor template (Fig. 17B). We used high-fidelity PCR amplification to produce a linear dsDNA donor containing 500bp homology arms of genomic *TRAC* sequence flanking the CAR repair construct (Fig. 17C). To generate *TRAC*-integrated CD22 CAR-T cells, we combined RNPs and dsDNA donors and electroporated them simultaneously into CD3+ T cells. In contrast to the AAV6 experiments described in Chapters 2 and 3, we found that the Lonza pulse code EH115 yielded the highest rate of CAR knock-in (Fig. 18A). Efficiency was further improved by increasing the HDRT dose from 2 μg to 3 μg of dsDNA, although there was some variability in CAR integration between the three donors tested (Fig. 18A). We used the healthy donor with the highest knock-in to generate CAR-T cells for functional assays, and as a standard for comparison, we made CD22 CAR-T cells using a research-grade version of the lentivirus for the upcoming CLIC-02 trial. In head-to-head cytotoxicity assays, *TRAC*-integrated CD22 CAR-T cells demonstrated equivalent cytotoxicity to lentiviral CD22 CAR-T cells (Fig. 18B), thereby establishing proof-of-concept for our nonviral engineering approach.

4.5.2 Magnetic bead selection and anti-V_HH restimulation generate a highly-enriched CAR-T product

After functional validation, we sought to improve the percentage of CAR-positive cells in our final product. Of note, durable responses have been seen in patients where the infusion product was less than 20% CAR-positive[11]. However, given the high number of CAR-T cells required to achieve a therapeutic dose ($1x10^6$ CAR-positive cells per kg), improving CAR positivity

increases the likelihood of meeting dose requirements. This is especially crucial considering the temporary loss in viability that occurs post-electroporation. To that end, we developed a method to selectively expand CAR-positive cells after electroporation (Fig. 19A).

We hypothesized that restimulation could be used to both overcome the electroporation-induced loss in cell number and also selectively expand the edited cells. We restimulated cells post-electroporation with an anti-V_HH antibody specific for the single-domain CD22 CAR, and after ten days of expansion we saw an increase in the percentage of CAR-positive cells to 17.9% (Fig. 19B, D). While this was an improvement, we rationalized that adding an enrichment step before restimulation would yield a more significant increase. To avoid the cell stress commonly induced by fluorescence-activated cell sorting (FACS)[190], we enriched CAR-T cells from the bulk population using magnetic bead selection. This method increased CAR positivity to 53.9% immediately after selection, which was further improved by anti-V_HH restimulation to 86.3% (Fig. 19C, D). However, while the enriched population expanded 60-fold relative to the start of restimulation on Day 8, the overall increase in cell number relative to Day 0 was only 1.5-fold when using this method, as compared to 23-fold for the restimulated bulk population (Fig. 19E). From these data, we concluded that successful implementation of our enrichment strategy would require either a higher rate of CAR knock-in, or significant scale-up in starting cell number.

4.5.3 Post-electroporation treatment with Trichostatin A and Nedisertib increases CAR integration at *TRAC*

Given our challenges in isolating a sufficient number of CAR-positive cells, we turned our attention towards improving the efficiency of the editing process. We began by adding truncated Cas targeting sites (tCTSs) to our dsDNA donor to improve Cas9 and HDRT binding. Each tCTS comprised 16 nucleotides from the *TRAC* sgRNA sequence, followed by the PAM sequence, with 4 mismatched nucleotides added to the 5’ end of the sgRNA. These sequences were appended to both homology arms in the PAM “In” orientation recommended by Shy *et al*.[19] (Fig. 20A). After RNP/dsDNA co-electroporation with tCTS HDRTs, we saw a moderate improvement in CAR knock-in as compared to the original HDRT, although this effect was not statistically significant (Fig. 20B).

We next explored the possibility of using tCTS HDRTs in combination with small molecule inhibitors to further increase CAR integration. Both histone deacetylase (HDAC) and DNA-dependent protein kinase (DNA-PK) inhibitors have been tested extensively in this context[19,191–193]. We performed RNP/dsDNA co-electroporation with tCTS donors as above, then treated the cells with Trichostatin A (TSA; HDAC inhibitor) and Nedisertib (DNA-PK inhibitor) for a 24-hour period immediately following electroporation. This method significantly increased CAR knock-in relative to the untreated tCTS condition and to the original HDRT, with the highest-performing experiment achieving 28.0% CAR+/CD3- cells as detected by flow cytometry (Fig. 20B, E). Furthermore, as we completely removed the inhibitors by media exchange after 24 hours, there was only a small decrease in viability and proliferation as compared to the untreated tCTS condition (Fig. 20C, D). Taken together, these results confirm that treatment with TSA and Nedisertib is an effective method of increasing CAR integration, and could be used in combination with anti-V_HH restimulation to achieve a therapeutic dose of CD22 CAR-T cells without the need for additional enrichment.

4.5.4 Adapting benchtop gene-editing methodologies to clinical-grade, closed-system manufacturing of nonviral CAR-T cells

After evaluating different methods of increasing CAR positivity in small-scale experiments, we last sought to integrate each method into a clinical protocol for CAR-T cell production. As the CLIC-01 trial uses the Miltenyi CliniMACS Prodigy for CD19 CAR-T manufacturing, we wanted to ensure that our nonviral gene-editing approach could be adapted for use with the Prodigy. With the addition of an electroporator module, manufacturing of gene-edited CAR-T cells on the Prodigy is accomplished using a pre-installed T Cell Engineering (TCE) process (Fig. 21A). We used the TCE process as a framework to design three hypothetical protocols updated to include anti-V_HH restimulation (“Case 1”), restimulation combined with magnetic bead enrichment (“Case 2”), and restimulation combined with TSA/Nedisertib treatment (“Case 3”).

Case 1 follows the standard TCE process until anti-V_HH restimulation on Day 7, which is accomplished by adding restimulation reagent to a new medium bag and performing a complete medium exchange (Fig. 21B). As this is considered a “functionally open” step, the bag

containing the restimulation reagent must be prepared in a Grade A isolator to maintain sterility. Case 2 adds a Day 14 enrichment step to the restimulation protocol described for Case 1. In brief, this involves harvesting the cells into buffer, sterile welding a second tubing set (TS320) onto the Prodigy, and then loading the cells back onto the machine for depletion of CD3-positive cells using Miltenyi's GMP-grade TCRα/β magnetic beads (Fig. 21C). The final product is then harvested and formulated as usual. Lastly, Case 3 incorporates TSA/Nedisertib treatment on Day 3 in addition to the restimulation protocol outlined in Case 1. As the TCE process is already programmed for a 24-hour post-electroporation recovery period, this step is easily accomplished by using a Grade A isolator to add inhibitors to the bag containing the recovery medium. After 24 hours of treatment, a complete medium exchange is performed to remove the inhibitors from the cultivation chamber, and the protocol proceeds as usual to restimulation, expansion, and harvest (Fig. 21D).

4.6 Discussion

The development of a nonviral CAR-T manufacturing pipeline is an integral step on the path towards safer, more affordable cell therapies. In this chapter, we established proof-of-concept for nonviral, site-specific insertion of a CD22 CAR at the *TRAC* locus. Our engineering approach generates CD22 CAR-T cells that are deficient for the endogenous TCR, which eliminates the potential of GVHD and is therefore a necessary prerequisite for development of future allogeneic CAR-T therapies. Furthermore, our nonviral *TRAC*-integrated CD22 CAR-T cells exhibited comparable *in vitro* cytotoxicity to lentiviral CD22 CAR-T cells. These results demonstrate that the endogenous *TRAC* promoter can be used to generate a highly-functional CAR-T cell without the need for an exogenous promoter. This is advantageous for several reasons. First, from a technical standpoint, eliminating the need for an exogenous promoter sequence reduces the overall size of the donor template. As HDR efficiency decreases with longer dsDNA templates[16] while toxicity increases[17], minimizing template size is crucial for maintaining a high level of transgene integration and post-editing viability. Second, using the *TRAC* promoter facilitates intrinsic regulation of CAR expression, which could improve antitumor efficacy by limiting premature CAR-T exhaustion caused by constitutive activation. Indeed, Eyquem *et al.* previously showed that terminal differentiation and exhaustion are delayed in *TRAC*-encoded CAR-T cells,

a feature that is associated with superior antitumor activity *in vivo*[104]. However, another possible benefit of intrinsic CAR regulation is the potential to decrease systemic inflammatory toxicity, a common and serious side effect of CAR-T therapy that is triggered by high levels of CAR-T activation and cytokine secretion[194]. Although much attention has been given to engineering molecular switches to regulate CAR expression and prevent toxicity[195–197], these on/off approaches fail to provide a nuanced response to the characteristics of the tumor microenvironment. Conversely, placing the CAR under transcriptional control of the *TRAC* promoter enables dynamic patterning of CAR internalization and re-expression. While further investigation is required, integration at *TRAC* could facilitate a more balanced cytokine response leading to reduced CAR-mediated cytotoxicity.

Nonviral manufacturing techniques generate comparably fewer CAR-T cells than traditional viral methods. This can be attributed to lower rates of CAR knock-in as well as toxicity induced by the process of electroporation with DNA donors. While it is possible to overcome both of these limiting factors by simply doubling or tripling the number of electroporated cells, the financial burden associated with additional reagents and consumables would be prohibitive, especially in the context of a publicly-funded healthcare system. In this study, we showed that overall CAR-T yield could be increased by selectively expanding CAR-positive cells through restimulation with an anti-V_HH antibody. We also demonstrated that the same antibody, when coupled to a magnetic bead selection system, could be used to enrich CAR-T cells without the need for FACS. Lastly, we showed that CAR knock-in could be improved by adding truncated Cas targeting sites to our HDRTs, and treating the cells with Trichostatin A and Nedisertib for 24 hours post-electroporation.

However, further validation studies will be required to ensure that fidelity of the CAR-T product is maintained using these updating manufacturing practices. In particular, it is currently unknown whether restimulation through the CAR will have any detrimental effects on CAR-T persistence *in vivo*. The general consensus in the field is that repeated antigen exposure leads CAR-T cells to adopt an exhausted phenotype[198], but this phenomenon could also be partially attributed to the strong exogenous promoters used to express most CARs. In the case of our *TRAC*-integrated CD22 CAR-T cells, the physiological cost of CAR restimulation could be much less. Similarly,

although transient dosing with small molecule inhibitors has been shown to have no deleterious effects on *in vitro* CAR-T killing[19], this would need to be validated extensively *in vivo*.

From a clinical implementation perspective, both restimulation and inhibitor treatment could be seamlessly integrated into the current manufacturing workflow on the Miltenyi CliniMACS Prodigy using a flexible process option in the TCE protocol. Assuming a starting population of $1x10^8$ CD4/CD8 cells on Day 0, and RNP/dsDNA co-electroporation with tCTS HDRTs, a clinical expansion using Case 1 (restimulation protocol) could easily yield a therapeutic dose ($1x10^6$ CAR-T cells per kg) by Day 14, albeit with the lowest percentage of CAR-positive cells. However, as inhibitor treatment showed the lowest live cell counts post-electroporation in our small-scale experiments, a clinical expansion using Case 3 (inhibitor treatment) would benefit from loading a higher volume of apheresis product to increase the starting cell number. This would require an additional column and CD4/CD8 beads for the initial T cell isolation, plus a proportionate increase in HDRTs and Cas9, but would yield a higher percentage of CAR-positive cells in the final product.

Methods to enrich the CAR-positive population are rarely used in clinical production as they add manufacturing complexity, increase cost, and for autologous CAR-T cells, there is no need to infuse a purified population as long as the minimum dose of CAR-positive cells is met. However, in the case of an allogeneic CAR-T therapy, an enrichment step is necessary to prevent contamination of the infusion product with unedited cells. Therefore, we designed Case 2 (enrichment) for the specific purpose of allogeneic CAR-T manufacturing. While our original small-scale experiments included an enrichment step immediately after electroporation, we realized that this method would require multiple TS520 tubing sets, one for pre-enrichment, and one for post-enrichment. This would be in addition to the separate TS320 tubing set required for the enrichment process, bringing the overall increase in cost to over $10,000CAD. Furthermore, using the CAR as a target for enrichment increases the chance of carrying over magnetic beads into the final product. To overcome these issues, we adjusted the protocol to incorporate the enrichment step at the end of the expansion process, and modified the method of enrichment from positive selection with an anti-CAR antibody to depletion with an anti-CD3 antibody. This method would prevent bead contamination in the enriched product while also limiting

unnecessary repeated stimulation through the CAR. Using this approach, enrichment of an allogeneic CAR-T can be easily accomplished on the Prodigy in a cost-effective manner and with minimal added complexity.

For future considerations, a logical follow-on to this work is to generate a fully allogeneic CAR-T cell by multiplexing our *TRAC* knock-in with a second deletion at beta-2-microglobulin (*B2M*) to eliminate the potential of host-mediated graft rejection[199]. A second avenue of interest is to determine whether site-specific insertion at *TRAC* can be used to mitigate CAR-mediated systemic inflammatory toxicity without the need for extrinsic methods of CAR regulation. Lastly, it is important to note that the results presented here were achieved with dsDNA donors, which are the least efficient and most toxic. With research-grade ssDNA now available for commercial synthesis, we will evaluate our updated manufacturing practices in the context of ssDNA donors, and expect to see further improvements in CAR knock-in and overall CAR-T yield.

In conclusion, our study establishes proof-of-concept for a nonviral CAR-T engineering process that can be seamlessly incorporated into current clinical manufacturing practices. Furthermore, this work lays the groundwork for future development of affordable, Canadian-made allogeneic CAR-T cells.

Chapter 5: Concluding Remarks

5.1 Summary

To address metabolic restriction in the tumor microenvironment, we devised a single-step engineering method to combine targeted CAR integration with concomitant silencing of a metabolic gene of interest. This method was described in detail in Chapter 2, where as proof-of-concept, we deleted the essential autophagy gene *ATG5* in CAR-T cells for ovarian cancer immunotherapy. We also conducted an off-target risk assessment to demonstrate the safety of our engineering approach. In Chapter 3, we performed a comprehensive metabolic and functional analysis and showed that deletion of *ATG5* led to alterations in glucose and glutamine metabolism and enhanced CAR-T cell efficacy under nutrient-restricted conditions *in vitro* and *in vivo*.

To mitigate safety concerns and operational complexities associated with viral transduction methods, we developed a pipeline for nonviral manufacturing of Canadian-made CAR-T therapies. We demonstrated feasibility of this approach in Chapter 5, where we delivered a CAR targeting the hematological antigen CD22 to the *TRAC* locus, and showed comparable *in vitro* cytotoxicity to lentiviral CD22 CAR-T cells. We also explored strategies for improving CAR-T enrichment, expansion, and editing efficiency, and designed three engineering protocols for clinical-grade nonviral manufacturing on the Miltenyi CliniMACS Prodigy.

In summary, the work presented in this dissertation illustrates how genome editing with CRISPR-Cas9 can be used to overcome current limitations in the field of CAR-T cell therapy and improve outcomes for patients with cancer.

5.2 Perspective and future directions

In a 1977 publication in *Scientific American*, the father of modern tumor immunology Lloyd J. Old stated “there is something unique about a cancer cell that distinguishes it from normal cells, and this difference can be recognized by the body’s immune system”[200]. Old’s prediction that

immunotherapy would become a pillar of cancer treatment was finally realized in 2010, when the first immune checkpoint inhibitor was approved for clinical use[201]. Since then, the arsenal of FDA-approved immunotherapeutics has rapidly expanded to include six CAR-T therapies for B-cell malignancies and TIL therapy for melanoma[2,202]. However, despite many successes, the immunotherapy field is still hindered by a number of unresolved issues.

The most prominent of these challenges is the resistance of solid tumors to adoptive cell therapies like CAR-T cells[203]. While numerous strategies have been proposed to address this issue, we believe that targeting CAR-T metabolism is the closest thing to a universal approach for enhancing efficacy in solid tumors. This is due to the overwhelming body of evidence for metabolic dysregulation as a hallmark shared by most, if not all cancers[204–208]. That said, the complexity of restrictive and suppressive mechanisms in the TME means that modifying a single metabolic gene is unlikely to yield significant survival benefits. In our Perspective article in *Nature Metabolism*, we introduced the concept of bioengineering metabolic networks, wherein multiple genes in the same pathway (a "micro-network") or across related pathways (a "macro-network") are targeted for modification[209]. A recent example of micro-network engineering comes from Fultang *et al*., where CAR-T cells were engineered to overexpress both argininosuccinate synthase and ornithine transcarbamylase as a strategy to address arginine deficiency in acute myeloid leukemia[210]. Macro-network engineering has yet to be tested in the preclinical setting, but with recent advances in multiplex genome editing[211,212], it is now possible to simultaneously modify pathways involved in nutrient restriction (i.e. glucose or glutamine) and metabolite suppression (i.e. adenosine, kynurenine). This approach should enable CAR-T cells to overcome a wider range of metabolic obstacles, and will hopefully yield more significant survival benefits for patients with solid tumors.

Although much attention has been paid to the immunotherapy firewall posed by solid tumors, it is also important to note that hematological CAR-T therapies have their own share of unresolved problems – notably, the high incidence rate of CAR-mediated toxicity. The most common treatment-related adverse event is cytokine release syndrome (CRS), which was shown by a recent meta-analysis to occur in 77% of patients enrolled across 84 CAR-T trials targeting CD19 or BCMA[213]. The second is immune effector-cell associated neurotoxicity syndrome (ICANS),

which can occur concurrently with CRS or shortly thereafter[214]. Complications from these adverse events can be life-threatening, but even mild cases pose a serious concern for patient quality of life[215–217]. While the development and severity of CRS and ICANS is largely attributed to patient- and disease-related factors, the CAR-T therapy itself also plays a role. For this reason, numerous efforts are underway to engineer next-generation CAR-T cells with improved safety profiles. Prominent examples include co-expressing the CAR with a suicide gene like inducible caspase 9, and modifying CAR-T cells to secrete soluble antagonists against CRS-associated cytokines[218,219]. However, these strategies target the downstream effects of uncontrolled CAR-T cell activation, whereas a more direct approach could be to modulate the strength of the effector response and the CAR-T activation kinetics. Interestingly, it was noted in the original *Nature* publication by Eyqeum *et al*. that *TRAC*-integrated CD19 CAR-T cells secrete less cytokines than retroviral CD19 CAR-T cells, and engage in antigen-induced CAR downregulation and re-expression similar to the endogenous TCR[104]. This raises the question of whether integration at the *TRAC* locus could be a strategy to reduce excessive CAR activation and limit associated inflammatory responses.

While site-specific insertion of a CAR at the *TRAC* locus has never been evaluated in the context of reducing CRS, if effective, it could provide additional rationale for incorporating nonviral genome editing into current CAR-T manufacturing practices. This is a salient (and timely) consideration for the Canadian cell therapy field, given that the target demographic for the upcoming CD22 CAR-T trial includes patients with relapsed CD19-negative disease, whose high tumor burden puts them at an increased risk of developing CRS. Therefore, another follow-on for our nonviral CAR-T project will be to uncover any differences in development and severity of CRS between lentiviral and *TRAC*-integrated CAR-T cells. We believe that this work has the potential to yield significant quality of life benefits to Canadian patients, and truly underscores the promise of genome editing as a tool for creating safer, more effective CAR-T therapies.

References

1. Labanieh L, Mackall CL. CAR immune cells: design principles, resistance and the next generation. *Nature*. 2023;614(7949):635-648. doi:10.1038/s41586-023-05707-3

2. Mitra A, Barua A, Huang L, Ganguly S, Feng Q, He B. From bench to bedside: the history and progress of CAR T cell therapy. *Front Immunol*. 2023;14:1188049. doi:10.3389/fimmu.2023.1188049

3. Benmebarek MR, Karches CH, Cadilha BL, Lesch S, Endres S, Kobold S. Killing Mechanisms of Chimeric Antigen Receptor (CAR) T Cells. *Int J Mol Sci*. 2019;20(6):1283. doi:10.3390/ijms20061283

4. Chmielewski M, Hombach AA, Abken H. Antigen-Specific T-Cell Activation Independently of the MHC: Chimeric Antigen Receptor-Redirected T Cells. *Front Immunol*. 2013;4:371. doi:10.3389/fimmu.2013.00371

5. Bove C, Maher J, Glover M. The role of CD4+ CAR T cells in cancer immunotherapy. *Transl Cancer Res*. 2024;13(5). doi:10.21037/tcr-23-2044

6. Huppa JB, Davis MM. T-cell-antigen recognition and the immunological synapse. *Nat Rev Immunol*. 2003;3(12):973-983. doi:10.1038/nri1245

7. Cappell KM, Kochenderfer JN. Long-term outcomes following CAR T cell therapy: what we know so far. *Nat Rev Clin Oncol*. 2023;20(6):359-371. doi:10.1038/s41571-023-00754-1

8. Müller F, Taubmann J, Bucci L, et al. CD19 CAR T-Cell Therapy in Autoimmune Disease — A Case Series with Follow-up. *N Engl J Med*. 2024;390(8):687-700. doi:10.1056/NEJMoa2308917

9. Garneau JE, Dupuis MÈ, Villion M, et al. The CRISPR/Cas bacterial immune system cleaves bacteriophage and plasmid DNA. *Nature*. 2010;468(7320):67-71. doi:10.1038/nature09523

10. Stadtmauer EA, Fraietta JA, Davis MM, et al. CRISPR-engineered T cells in patients with refractory cancer. *Science*. 2020;367(6481):eaba7365. doi:10.1126/science.aba7365

11. Zhang J, Hu Y, Yang J, et al. Non-viral, specifically targeted CAR-T cells achieve high safety and efficacy in B-NHL. *Nature*. 2022;609(7926):369-374. doi:10.1038/s41586-022-05140-y

12. Jinek M, Chylinski K, Fonfara I, Hauer M, Doudna JA, Charpentier E. A programmable dual RNA-guided DNA endonuclease in adaptive bacterial immunity. *Science*. 2012;337(6096):816-821. doi:10.1126/science.1225829

13. Wang JH, Gessler DJ, Zhan W, Gallagher TL, Gao G. Adeno-associated virus as a delivery vector for gene therapy of human diseases. *Signal Transduct Target Ther*. 2024;9(1):1-33. doi:10.1038/s41392-024-01780-w

14. Delivery technologies for T cell gene editing: Applications in cancer immunotherapy - eBioMedicine. Accessed August 10, 2024. https://www.thelancet.com/journals/ebiom/article/PIIS2352-3964(21)00147-X/fulltext

15. McGuirk JP, Tam CS, Kröger N, et al. CTX110 Allogeneic CRISPR-Cas9-Engineered CAR T Cells in Patients (Pts) with Relapsed or Refractory (R/R) Large B-Cell Lymphoma (LBCL): Results from the Phase 1 Dose Escalation Carbon Study. *Blood*. 2022;140(Supplement 1):10303-10306. doi:10.1182/blood-2022-166432

16. Paludan SR, Reinert LS, Hornung V. DNA-stimulated cell death: implications for host defence, inflammatory diseases and cancer. *Nat Rev Immunol*. 2019;19(3):141-153. doi:10.1038/s41577-018-0117-0

17. DiNapoli SE, Martinez-McFaline R, Gribbin CK, et al. Synthetic CRISPR/Cas9 reagents facilitate genome editing and homology directed repair. *Nucleic Acids Res*. 2020;48(7):e38. doi:10.1093/nar/gkaa085

18. Kath J, Du W, Pruene A, et al. Pharmacological interventions enhance virus-free generation of TRAC-replaced CAR T cells. *Mol Ther Methods Clin Dev*. 2022;25:311-330. doi:10.1016/j.omtm.2022.03.018

19. Shy BR, Vykunta VS, Ha A, et al. High-yield genome engineering in primary cells using a hybrid ssDNA repair template and small-molecule cocktails. *Nat Biotechnol*. 2023;41(4):521-531. doi:10.1038/s41587-022-01418-8

20. Pacesa M, Lin CH, Cléry A, et al. Structural basis for Cas9 off-target activity. *Cell*. 2022;185(22):4067-4081.e21. doi:10.1016/j.cell.2022.09.026

21. Bravo JPK, Liu MS, Hibshman GN, et al. Structural basis for mismatch surveillance by CRISPR–Cas9. *Nature*. 2022;603(7900):343-347. doi:10.1038/s41586-022-04470-1

22. Concordet JP, Haeussler M. CRISPOR: intuitive guide selection for CRISPR/Cas9 genome editing experiments and screens. *Nucleic Acids Res*. 2018;46(W1):W242-W245. doi:10.1093/nar/gky354

23. Vakulskas CA, Dever DP, Rettig GR, et al. A high-fidelity Cas9 mutant delivered as a ribonucleoprotein complex enables efficient gene editing in human hematopoietic stem and progenitor cells. *Nat Med*. 2018;24(8):1216-1224. doi:10.1038/s41591-018-0137-0

24. Human Gene Therapy Products Incorporating Human Genome Editing; Guidance for Industry.

25. Malinin NL, Lee G, Lazzarotto CR, et al. Defining genome-wide CRISPR-Cas genome-editing nuclease activity with GUIDE-seq. *Nat Protoc*. 2021;16(12):5592-5615. doi:10.1038/s41596-021-00626-x

26. Sterner RC, Sterner RM. CAR-T cell therapy: current limitations and potential strategies. *Blood Cancer J*. 2021;11(4):1-11. doi:10.1038/s41408-021-00459-7

27. Xu M, Zhang T, Xia R, Wei Y, Wei X. Targeting the tumor stroma for cancer therapy. *Mol Cancer*. 2022;21(1):208. doi:10.1186/s12943-022-01670-1

28. Beckermann KE, Dudzinski SO, Rathmell JC. Dysfunctional T cell metabolism in the tumor microenvironment. *Cytokine Growth Factor Rev*. 2017;35:7-14. doi:10.1016/j.cytogfr.2017.04.003

29. Chang CH, Qiu J, O'Sullivan D, et al. Metabolic Competition in the Tumor Microenvironment Is a Driver of Cancer Progression. *Cell*. 2015;162(6):1229-1241. doi:10.1016/j.cell.2015.08.016

30. Sugiura A, Rathmell JC. Metabolic Barriers to T Cell Function in Tumors. *J Immunol Baltim Md 1950*. 2018;200(2):400-407. doi:10.4049/jimmunol.1701041

31. Gubser PM, Bantug GR, Razik L, et al. Rapid effector function of memory CD8+ T cells requires an immediate-early glycolytic switch. *Nat Immunol*. 2013;14(10):1064-1072. doi:10.1038/ni.2687

32. Chang CH, Curtis JD, Maggi LB, et al. Posttranscriptional control of T cell effector function by aerobic glycolysis. *Cell*. 2013;153(6):1239-1251. doi:10.1016/j.cell.2013.05.016

33. Wellen KE, Hatzivassiliou G, Sachdeva UM, Bui TV, Cross JR, Thompson CB. ATP-Citrate Lyase Links Cellular Metabolism to Histone Acetylation. *Science*. 2009;324(5930):1076-1080. doi:10.1126/science.1164097

34. Yaqoob P, Calder PC. Glutamine requirement of proliferating T lymphocytes. *Nutr Burbank Los Angel Cty Calif*. 1997;13(7-8):646-651. doi:10.1016/s0899-9007(97)83008-0

35. Sinclair LV, Rolf J, Emslie E, Shi YB, Taylor PM, Cantrell DA. Control of amino-acid transport by antigen receptors coordinates the metabolic reprogramming essential for T cell differentiation. *Nat Immunol*. 2013;14(5):500-508. doi:10.1038/ni.2556

36. Corrado M, Pearce EL. Targeting memory T cell metabolism to improve immunity. *J Clin Invest*. 132(1):e148546. doi:10.1172/JCI148546

37. Rangel Rivera GO, Knochelmann HM, Dwyer CJ, et al. Fundamentals of T Cell Metabolism and Strategies to Enhance Cancer Immunotherapy. *Front Immunol*. 2021;12:645242. doi:10.3389/fimmu.2021.645242

38. Early TCR Signaling Induces Rapid Aerobic Glycolysis Enabling Distinct Acute T Cell Effector Functions. *Cell Rep*. 2018;22(6):1509-1521. doi:10.1016/j.celrep.2018.01.040

39. The Mammalian Target of Rapamycin: Linking T Cell Differentiation, Function, and Metabolism. *Immunity*. 2010;33(3):301-311. doi:10.1016/j.immuni.2010.09.002

40. Kawalekar OU, O'Connor RS, Fraietta JA, et al. Distinct Signaling of Coreceptors Regulates Specific Metabolism Pathways and Impacts Memory Development in CAR T Cells. *Immunity*. 2016;44(2):380-390. doi:10.1016/j.immuni.2016.01.021

41. Connolly JL, Schnitt SJ, Wang HH, Longtine JA, Dvorak A, Dvorak HF. Tumor Structure and Tumor Stroma Generation. In: *Holland-Frei Cancer Medicine. 6th Edition*. BC Decker; 2003. Accessed August 9, 2024. https://www.ncbi.nlm.nih.gov/books/NBK13447/

42. Bremnes RM, Dønnem T, Al-Saad S, et al. The Role of Tumor Stroma in Cancer Progression and Prognosis: Emphasis on Carcinoma-Associated Fibroblasts and Non-small Cell Lung Cancer. *J Thorac Oncol*. 2011;6(1):209-217. doi:10.1097/JTO.0b013e3181f8a1bd

43. Elia I, Haigis MC. Metabolites and the tumor microenvironment: from cellular mechanisms to systemic metabolism. *Nat Metab*. 2021;3(1):21-32. doi:10.1038/s42255-020-00317-z

44. Ganapathy V, Thangaraju M, Prasad PD. Nutrient transporters in cancer: relevance to Warburg hypothesis and beyond. *Pharmacol Ther*. 2009;121(1):29-40. doi:10.1016/j.pharmthera.2008.09.005

45. Shi LZ, Wang R, Huang G, et al. HIF1alpha-dependent glycolytic pathway orchestrates a metabolic checkpoint for the differentiation of TH17 and Treg cells. *J Exp Med*. 2011;208(7):1367-1376. doi:10.1084/jem.20110278

46. Li Z, Sun C, Qin Z. Metabolic reprogramming of cancer-associated fibroblasts and its effect on cancer cell reprogramming. *Theranostics*. 2021;11(17):8322-8336. doi:10.7150/thno.62378

47. M de-Brito N, Duncan-Moretti J, C da-Costa H, et al. Aerobic glycolysis is a metabolic requirement to maintain the M2-like polarization of tumor-associated macrophages. *Biochim Biophys Acta Mol Cell Res*. 2020;1867(2):118604. doi:10.1016/j.bbamcr.2019.118604

48. Jian SL, Chen WW, Su YC, et al. Glycolysis regulates the expansion of myeloid-derived suppressor cells in tumor-bearing hosts through prevention of ROS-mediated apoptosis. *Cell Death Dis*. 2017;8(5):e2779. doi:10.1038/cddis.2017.192

49. Cham CM, Driessens G, O'Keefe JP, Gajewski TF. Glucose Deprivation Inhibits Multiple Key Gene Expression Events and Effector Functions in CD8+ T Cells. *Eur J Immunol*. 2008;38(9):2438-2450. doi:10.1002/eji.200838289

50. Rodriguez PC, Quiceno DG, Zabaleta J, et al. Arginase I production in the tumor microenvironment by mature myeloid cells inhibits T-cell receptor expression and antigen-specific T-cell responses. *Cancer Res*. 2004;64(16):5839-5849. doi:10.1158/0008-5472.CAN-04-0465

51. Akinjiyan FA, Ibitoye Z, Zhao P, et al. DDR2-regulated arginase activity in ovarian cancer-associated fibroblasts promotes collagen production and tumor progression. *Oncogene*. 2024;43(3):189-201. doi:10.1038/s41388-023-02884-3

52. Geiger R, Rieckmann JC, Wolf T, et al. L-Arginine Modulates T Cell Metabolism and Enhances Survival and Anti-tumor Activity. *Cell*. 2016;167(3):829-842.e13. doi:10.1016/j.cell.2016.09.031

53. Distinct Regulation of Th17 and Th1 Cell Differentiation by Glutaminase-Dependent Metabolism - PubMed. Accessed August 9, 2024. https://pubmed.ncbi.nlm.nih.gov/30392958/

54. Oh MH, Sun IH, Zhao L, et al. Targeting glutamine metabolism enhances tumor-specific immunity by modulating suppressive myeloid cells. *J Clin Invest*. 2020;130(7):3865-3884. doi:10.1172/JCI131859

55. Targeting glutamine metabolism as a therapeutic strategy for cancer | Experimental & Molecular Medicine. Accessed August 9, 2024. https://www.nature.com/articles/s12276-023-00971-9

56. Giatromanolaki A, Harris AL, Koukourakis MI. The prognostic and therapeutic implications of distinct patterns of argininosuccinate synthase 1 (ASS1) and arginase-2 (ARG2) expression by cancer cells and tumor stroma in non-small-cell lung cancer. *Cancer Metab*. 2021;9(1):28. doi:10.1186/s40170-021-00264-7

57. Frontiers | Crosstalk Between Tumor-Associated Microglia/Macrophages and CD8-Positive T Cells Plays a Key Role in Glioblastoma. Accessed August 9, 2024. https://www.frontiersin.org/journals/immunology/articles/10.3389/fimmu.2021.650105/full

58. Young A, Ngiow SF, Barkauskas DS, et al. Co-inhibition of CD73 and A2AR Adenosine Signaling Improves Anti-tumor Immune Responses. *Cancer Cell*. 2016;30(3):391-403. doi:10.1016/j.ccell.2016.06.025

59. Munn DH, Shafizadeh E, Attwood JT, Bondarev I, Pashine A, Mellor AL. Inhibition of T Cell Proliferation by Macrophage Tryptophan Catabolism. *J Exp Med*. 1999;189(9):1363-1372.

60. Rattigan YI, Patel BB, Ackerstaff E, et al. Lactate is a mediator of metabolic cooperation between stromal carcinoma associated fibroblasts and glycolytic tumor cells in the tumor microenvironment. *Exp Cell Res*. 2012;318(4):326-335. doi:10.1016/j.yexcr.2011.11.014

61. Bunse L, Pusch S, Bunse T, et al. Suppression of antitumor T cell immunity by the oncometabolite (R)-2-hydroxyglutarate. *Nat Med*. 2018;24(8):1192-1203. doi:10.1038/s41591-018-0095-6

62. Kilgour MK, MacPherson S, Zacharias LG, et al. 1-Methylnicotinamide is an immune regulatory metabolite in human ovarian cancer. *Sci Adv*. 2021;7(4):eabe1174. doi:10.1126/sciadv.abe1174

63. Ohta A, Gorelik E, Prasad SJ, et al. A2A adenosine receptor protects tumors from antitumor T cells. *Proc Natl Acad Sci*. 2006;103(35):13132-13137. doi:10.1073/pnas.0605251103

64. Deaglio S, Dwyer KM, Gao W, et al. Adenosine generation catalyzed by CD39 and CD73 expressed on regulatory T cells mediates immune suppression. *J Exp Med*. 2007;204(6):1257-1265. doi:10.1084/jem.20062512

65. Campesato LF, Budhu S, Tchaicha J, et al. Blockade of the AHR restricts a Treg-macrophage suppressive axis induced by L-Kynurenine. *Nat Commun*. 2020;11(1):4011. doi:10.1038/s41467-020-17750-z

66. Fischer K, Hoffmann P, Voelkl S, et al. Inhibitory effect of tumor cell–derived lactic acid on human T cells. *Blood*. 2007;109(9):3812-3819. doi:10.1182/blood-2006-07-035972

67. Zhang Y, Zhai Z, Duan J, et al. Lactate: The Mediator of Metabolism and Immunosuppression. *Front Endocrinol*. 2022;13:901495. doi:10.3389/fendo.2022.901495

68. Baumann T, Dunkel A, Schmid C, et al. Regulatory myeloid cells paralyze T cells through cell–cell transfer of the metabolite methylglyoxal. *Nat Immunol*. 2020;21(5):555-566. doi:10.1038/s41590-020-0666-9

69. Luengo A, Gui DY, Vander Heiden MG. Targeting Metabolism for Cancer Therapy. *Cell Chem Biol*. 2017;24(9):1161-1180. doi:10.1016/j.chembiol.2017.08.028

70. Jacobs SR, Herman CE, MacIver NJ, et al. Glucose Uptake Is Limiting in T Cell Activation and Requires CD28-Mediated Akt-Dependent and Independent Pathways. *J Immunol Baltim Md 1950*. 2008;180(7):4476-4486.

71. Scharping NE, Menk AV, Moreci RS, et al. The Tumor Microenvironment Represses T Cell Mitochondrial Biogenesis to Drive Intratumoral T Cell Metabolic Insufficiency and Dysfunction. *Immunity*. 2016;45(2):374-388. doi:10.1016/j.immuni.2016.07.009

72. Nagahama Y, Shimoda M, Mao G, et al. Regnase-1 controls colon epithelial regeneration via regulation of mTOR and purine metabolism. *Proc Natl Acad Sci*. 2018;115(43):11036-11041. doi:10.1073/pnas.1809575115

73. Wei J, Long L, Zheng W, et al. Targeting REGNASE-1 programs long-lived effector T cells for cancer therapy. *Nature*. 2019;576(7787):471-476. doi:10.1038/s41586-019-1821-z

74. Mai D, Johnson O, Reff J, et al. Combined disruption of T cell inflammatory regulators Regnase-1 and Roquin-1 enhances antitumor activity of engineered human T cells. *Proc Natl Acad Sci*. 2023;120(12):e2218632120. doi:10.1073/pnas.2218632120

75. Giuffrida L, Sek K, Henderson MA, et al. CRISPR/Cas9 mediated deletion of the adenosine A2A receptor enhances CAR T cell efficacy. *Nat Commun*. 2021;12(1):3236. doi:10.1038/s41467-021-23331-5

76. Rabinowitz JD, White E. Autophagy and Metabolism. *Science*. 2010;330(6009):1344-1348. doi:10.1126/science.1193497

77. Eng CH, Yu K, Lucas J, White E, Abraham RT. Ammonia Derived from Glutaminolysis Is a Diffusible Regulator of Autophagy. *Sci Signal*. 2010;3(119):ra31-ra31. doi:10.1126/scisignal.2000911

78. Nascimbeni AC, Codogno P, Morel E. Phosphatidylinositol-3-phosphate in the regulation of autophagy membrane dynamics. *FEBS J*. 2017;284(9):1267-1278. doi:10.1111/febs.13987

79. The ATG conjugation systems in autophagy. *Curr Opin Cell Biol*. 2020;63:1-10. doi:10.1016/j.ceb.2019.12.001

80. Dikic I, Elazar Z. Mechanism and medical implications of mammalian autophagy. *Nat Rev Mol Cell Biol*. 2018;19(6):349-364. doi:10.1038/s41580-018-0003-4

81. Fujii S, Mitsunaga S, Yamazaki M, et al. Autophagy is activated in pancreatic cancer cells and correlates with poor patient outcome. *Cancer Sci*. 2008;99(9):1813-1819. doi:10.1111/j.1349-7006.2008.00893.x

82. Luo T, Fu J, Xu A, et al. PSMD10/gankyrin induces autophagy to promote tumor progression through cytoplasmic interaction with ATG7 and nuclear transactivation of ATG7 expression. *Autophagy*. 2015;12(8):1355-1371. doi:10.1080/15548627.2015.1034405

83. Liu M, Jiang L, Fu X, et al. Cytoplasmic liver kinase B1 promotes the growth of human lung adenocarcinoma by enhancing autophagy. *Cancer Sci*. 2018;109(10):3055-3067. doi:10.1111/cas.13746

84. Wei H, Wei S, Gan B, Peng X, Zou W, Guan JL. Suppression of autophagy by FIP200 deletion inhibits mammary tumorigenesis. *Genes Dev*. 2011;25(14):1510-1527. doi:10.1101/gad.2051011

85. Salah FS, Ebbinghaus M, Muley VY, et al. Tumor suppression in mice lacking GABARAP, an Atg8/LC3 family member implicated in autophagy, is associated with alterations in cytokine secretion and cell death. *Cell Death Dis*. 2016;7(4):e2205-e2205. doi:10.1038/cddis.2016.93

86. DeVorkin L, Pavey N, Carleton G, et al. Autophagy Regulation of Metabolism Is Required for CD8+ T Cell Anti-tumor Immunity. *Cell Rep*. 2019;27(2):502-513.e5. doi:10.1016/j.celrep.2019.03.037

87. Villeneuve PJA, Bredeson C. CAR-T Cells in Canada; Perspective on How to Ensure We Get Our Value's Worth. *Curr Oncol*. 2023;30(4):4033-4040. doi:10.3390/curroncol30040305

88. Kekre N, Hay KA, Webb JR, et al. CLIC-01: Manufacture and distribution of non-cryopreserved CAR-T cells for patients with CD19 positive hematologic malignancies. *Front Immunol*. 2022;13:1074740. doi:10.3389/fimmu.2022.1074740

89. Kohn DB, Chen YY, Spencer MJ. Successes and challenges in clinical gene therapy. *Gene Ther*. 2023;30(10):738-746. doi:10.1038/s41434-023-00390-5

90. Shah NN, Qin H, Yates B, et al. Clonal expansion of CAR T cells harboring lentivector integration in the CBL gene following anti-CD22 CAR T-cell therapy. *Blood Adv*. 2019;3(15):2317-2322. doi:10.1182/bloodadvances.2019000219

91. Levine BL, Pasquini MC, Connolly JE, et al. Unanswered questions following reports of secondary malignancies after CAR-T cell therapy. *Nat Med*. 2024;30(2):338-341. doi:10.1038/s41591-023-02767-w

92. Suran M. FDA Adds Boxed Warning to CAR T-Cell Therapies, but Says Benefits Outweigh Risks of Secondary Cancers. *JAMA*. 2024;331(10):818-820. doi:10.1001/jama.2024.1011

93. Fraietta JA, Lacey SF, Orlando EJ, et al. Determinants of response and resistance to CD19 chimeric antigen receptor (CAR) T cell therapy of chronic lymphocytic leukemia. *Nat Med*. 2018;24(5):563-571. doi:10.1038/s41591-018-0010-1

94. Chen GM, Chen C, Das RK, et al. Integrative Bulk and Single-Cell Profiling of Premanufacture T-cell Populations Reveals Factors Mediating Long-Term Persistence of CAR T-cell Therapy. *Cancer Discov*. 2021;11(9):2186-2199. doi:10.1158/2159-8290.CD-20-1677

95. Locke FL, Rossi JM, Neelapu SS, et al. Tumor burden, inflammation, and product attributes determine outcomes of axicabtagene ciloleucel in large B-cell lymphoma. *Blood Adv*. 2020;4(19):4898-4911. doi:10.1182/bloodadvances.2020002394

96. Das RK, Vernau L, Grupp SA, Barrett DM. Naïve T-cell Deficits at Diagnosis and after Chemotherapy Impair Cell Therapy Potential in Pediatric Cancers. *Cancer Discov*. 2019;9(4):492-499. doi:10.1158/2159-8290.CD-18-1314

97. Singh N, Perazzelli J, Grupp SA, Barrett DM. Early memory phenotypes drive T cell proliferation in patients with pediatric malignancies. *Sci Transl Med*. 2016;8(320):320ra3. doi:10.1126/scitranslmed.aad5222

98. Balke-Want H, Keerthi V, Cadinanos-Garai A, et al. Non-viral chimeric antigen receptor (CAR) T cells going viral. *Immuno-Oncol Technol*. 2023;18:100375. doi:10.1016/j.iotech.2023.100375

99. Labbé RP, Vessillier S, Rafiq QA. Lentiviral Vectors for T Cell Engineering: Clinical Applications, Bioprocessing and Future Perspectives. *Viruses*. 2021;13(8):1528. doi:10.3390/v13081528

100. Du Y, Spence SE, Jenkins NA, Copeland NG. Cooperating cancer-gene identification through oncogenic-retrovirus–induced insertional mutagenesis. *Blood*. 2005;106(7):2498-2505. doi:10.1182/blood-2004-12-4840

101. Carter M, Shieh J. Chapter 11 - Gene Delivery Strategies. In: Carter M, Shieh J, eds. *Guide to Research Techniques in Neuroscience (Second Edition)*. Academic Press; 2015:239-252. doi:10.1016/B978-0-12-800511-8.00011-3

102. Kumar M, Keller B, Makalou N, Sutton RE. Systematic determination of the packaging limit of lentiviral vectors. *Hum Gene Ther*. 2001;12(15):1893-1905. doi:10.1089/104303401753153947

103. Mansilla-Soto J, Eyquem J, Haubner S, et al. HLA-independent T cell receptors for targeting tumors with low antigen density. *Nat Med*. 2022;28(2):345-352. doi:10.1038/s41591-021-01621-1

104. Eyquem J, Mansilla-Soto J, Giavridis T, et al. Targeting a CAR to the TRAC locus with CRISPR/Cas9 enhances tumour rejection. *Nature*. 2017;543(7643):113-117. doi:10.1038/nature21405

105. Guschin DY, Waite AJ, Katibah GE, Miller JC, Holmes MC, Rebar EJ. A rapid and general assay for monitoring endogenous gene modification. *Methods Mol Biol Clifton NJ*. 2010;649:247-256. doi:10.1007/978-1-60761-753-2_15

106. Agudelo D, Duringer A, Bozoyan L, et al. Marker-free coselection for CRISPR-driven genome editing in human cells. *Nat Methods*. 2017;14(6):615-620. doi:10.1038/nmeth.4265

107. Dalvai M, Loehr J, Jacquet K, et al. A Scalable Genome-Editing-Based Approach for Mapping Multiprotein Complexes in Human Cells. *Cell Rep*. 2015;13(3):621-633. doi:10.1016/j.celrep.2015.09.009

108. Mali P, Yang L, Esvelt KM, et al. RNA-guided human genome engineering via Cas9. *Science*. 2013;339(6121):823-826. doi:10.1126/science.1232033

109. Song DG, Ye Q, Poussin M, Liu L, Figini M, Powell DJ. A fully human chimeric antigen receptor with potent activity against cancer cells but reduced risk for off-tumor toxicity. *Oncotarget*. 2015;6(25):21533-21546.

110. Nguyen DN, Roth TL, Li PJ, et al. Polymer-stabilized Cas9 nanoparticles and modified repair templates increase genome editing efficiency. *Nat Biotechnol*. 2020;38(1):44-49. doi:10.1038/s41587-019-0325-6

111. Brinkman EK, Chen T, Amendola M, van Steensel B. Easy quantitative assessment of genome editing by sequence trace decomposition. *Nucleic Acids Res*. 2014;42(22):e168. doi:10.1093/nar/gku936

112. Clement K, Rees H, Canver MC, et al. CRISPResso2 provides accurate and rapid genome editing sequence analysis. *Nat Biotechnol*. 2019;37(3):224-226. doi:10.1038/s41587-019-0032-3

113. Tsai SQ, Zheng Z, Nguyen NT, et al. GUIDE-seq enables genome-wide profiling of off-target cleavage by CRISPR-Cas nucleases. *Nat Biotechnol*. 2015;33(2):187-197. doi:10.1038/nbt.3117

114. Bloh K, Kanchana R, Bialk P, et al. Deconvolution of Complex DNA Repair (DECODR): Establishing a Novel Deconvolution Algorithm for Comprehensive Analysis of CRISPR-Edited Sanger Sequencing Data. *CRISPR J*. 2021;4(1):120-131. doi:10.1089/crispr.2020.0022

115. Nassar LR, Barber GP, Benet-Pagès A, et al. The UCSC Genome Browser database: 2023 update. *Nucleic Acids Res*. 2023;51(D1):D1188-D1195. doi:10.1093/nar/gkac1072

116. Martin LP, Konner JA, Moore KN, et al. Characterization of folate receptor alpha (FRα) expression in archival tumor and biopsy samples from relapsed epithelial ovarian cancer patients: A phase I expansion study of the FRα-targeting antibody-drug conjugate mirvetuximab soravtansine. *Gynecol Oncol*. 2017;147(2):402-407. doi:10.1016/j.ygyno.2017.08.015

117. Kandalaft LE, Powell DJ, Coukos G. A phase I clinical trial of adoptive transfer of folate receptor-alpha redirected autologous T cells for recurrent ovarian cancer. *J Transl Med*. 2012;10:157. doi:10.1186/1479-5876-10-157

118. Kershaw MH, Westwood JA, Parker LL, et al. A Phase I Study on Adoptive Immunotherapy Using Gene-Modified T Cells for Ovarian Cancer. *Clin Cancer Res Off J Am Assoc Cancer Res*. 2006;12(20 Pt 1):6106-6115. doi:10.1158/1078-0432.CCR-06-1183

119. Xu L, Lahiri P, Skowronski J, Bhatia N, Lattanzi A, Porteus MH. Molecular dynamics of genome editing with CRISPR-Cas9 and rAAV6 virus in human HSPCs to treat sickle cell disease. *Mol Ther Methods Clin Dev*. 2023;30:317-331. doi:10.1016/j.omtm.2023.07.009

120. Ravikumar B, Sarkar S, Davies JE, et al. Regulation of mammalian autophagy in physiology and pathophysiology. *Physiol Rev*. 2010;90(4):1383-1435. doi:10.1152/physrev.00030.2009

121. Sambamoorthy G, Raman K. Understanding the evolution of functional redundancy in metabolic networks. *Bioinformatics*. 2018;34(17):i981-i987. doi:10.1093/bioinformatics/bty604

122. Srivastava A. In vivo tissue-tropism of adeno-associated viral vectors. *Curr Opin Virol*. 2016;21:75-80. doi:10.1016/j.coviro.2016.08.003

123. CRISPR-Mediated Integration of Large Gene Cassettes Using AAV Donor Vectors. *Cell Rep*. 2017;20(3):750-756. doi:10.1016/j.celrep.2017.06.064

124. Rogers GL, Huang C, Clark RDE, Seclén E, Chen HY, Cannon PM. Optimization of AAV6 transduction enhances site-specific genome editing of primary human lymphocytes. *Mol Ther Methods Clin Dev*. 2021;23:198-209. doi:10.1016/j.omtm.2021.09.003

125. Sather BD, Romano Ibarra GS, Sommer K, et al. Efficient modification of CCR5 in primary human hematopoietic cells using a megaTAL nuclease and AAV donor template. *Sci Transl Med*. 2015;7(307):307ra156. doi:10.1126/scitranslmed.aac5530

126. Bijlani S, Pang KM, Sivanandam V, Singh A, Chatterjee S. The Role of Recombinant AAV in Precise Genome Editing. *Front Genome Ed*. 2022;3. doi:10.3389/fgeed.2021.799722

127. Haeussler M, Schönig K, Eckert H, et al. Evaluation of off-target and on-target scoring algorithms and integration into the guide RNA selection tool CRISPOR. *Genome Biol*. 2016;17(1):148. doi:10.1186/s13059-016-1012-2

128. Hsu PD, Scott DA, Weinstein JA, et al. DNA targeting specificity of RNA-guided Cas9 nucleases. *Nat Biotechnol*. 2013;31(9):827-832. doi:10.1038/nbt.2647

129. Liu M, Zhang W, Xin C, et al. Global detection of DNA repair outcomes induced by CRISPR–Cas9. *Nucleic Acids Res*. 2021;49(15):8732-8742. doi:10.1093/nar/gkab686

130. Daei Sorkhabi A, Mohamed Khosroshahi L, Sarkesh A, et al. The current landscape of CAR T-cell therapy for solid tumors: Mechanisms, research progress, challenges, and counterstrategies. *Front Immunol*. 2023;14:1113882. doi:10.3389/fimmu.2023.1113882

131. Torre LA, Trabert B, DeSantis CE, et al. Ovarian cancer statistics, 2018. *CA Cancer J Clin*. 2018;68(4):284-296. doi:10.3322/caac.21456

132. Kandalaft LE, Dangaj Laniti D, Coukos G. Immunobiology of high-grade serous ovarian cancer: lessons for clinical translation. *Nat Rev Cancer*. 2022;22(11):640-656. doi:10.1038/s41568-022-00503-z

133. Tanyi J, Haas A, Aggarwal C, et al. Phase I study of autologous T cells bearing fully-humanized chimeric antigen receptors targeting mesothelin in mesothelin- expressing cancers (314). *Gynecol Oncol*. 2022;166:S164-S165. doi:10.1016/S0090-8258(22)01537-2

134. Pang N, Shi J, Qin L, et al. IL-7 and CCL19-secreting CAR-T cell therapy for tumors with positive glypican-3 or mesothelin. *J Hematol OncolJ Hematol Oncol*. 2021;14(1):118. doi:10.1186/s13045-021-01128-9

135. Castelletti L, Yeo D, van Zandwijk N, Rasko JEJ. Anti-Mesothelin CAR T cell therapy for malignant mesothelioma. *Biomark Res*. 2021;9(1):11. doi:10.1186/s40364-021-00264-1

136. Kumar S, Acharya S, Karthikeyan M, Biswas P, Kumari S. Limitations and potential of immunotherapy in ovarian cancer. *Front Immunol*. 2024;14. doi:10.3389/fimmu.2023.1292166

137. Giuntoli RL, Webb TJ, Zoso A, et al. Ovarian cancer-associated ascites demonstrates altered immune environment: implications for antitumor immunity. *Anticancer Res*. 2009;29(8):2875-2884.

138. Single-cell analyses implicate ascites in remodeling the ecosystems of primary and metastatic tumors in ovarian cancer | Nature Cancer. Accessed August 14, 2024. https://www.nature.com/articles/s43018-023-00599-8

139. Kampan NC, Madondo MT, McNally OM, Stephens AN, Quinn MA, Plebanski M. Interleukin 6 Present in Inflammatory Ascites from Advanced Epithelial Ovarian Cancer Patients Promotes Tumor Necrosis Factor Receptor 2-Expressing Regulatory T Cells. *Front Immunol*. 2017;8:1482. doi:10.3389/fimmu.2017.01482

140. Kerslake R, Panfilov S, Mustafa N, et al. Elevated Circulating Lactate Levels and Widespread Expression of Its Cognate Receptor, Hydroxycarboxylic Acid Receptor 1 (HCAR1), in Ovarian Cancer. *J Clin Med*. 2022;12(1):217. doi:10.3390/jcm12010217

141. Mendler AN, Hu B, Prinz PU, Kreutz M, Gottfried E, Noessner E. Tumor lactic acidosis suppresses CTL function by inhibition of p38 and JNK/c-Jun activation. *Int J Cancer*. 2012;131(3):633-640. doi:10.1002/ijc.26410

142. Grobben Y, den Ouden JE, Aguado C, van Altena AM, Kraneveld AD, Zaman GJR. Amino Acid-Metabolizing Enzymes in Advanced High-Grade Serous Ovarian Cancer Patients: Value of Ascites as Biomarker Source and Role for IL4I1 and IDO1. *Cancers*. 2023;15(3):893. doi:10.3390/cancers15030893

143. Song M, Sandoval TA, Chae CS, et al. IRE1α-XBP1 controls T cell function in ovarian cancer by regulating mitochondrial activity. *Nature*. 2018;562(7727):423-428. doi:10.1038/s41586-018-0597-x

144. Laasik M, Hynninen J, Forsback S, Noponen T, Seppänen M, Hietanen S. The feasibility of [18F]EF5-PET/CT to image hypoxia in ovarian tumors: a clinical study. *EJNMMI Res*. 2020;10(1):103. doi:10.1186/s13550-020-00689-z

145. Guo N, Yang A, Farooq FB, et al. CD8 + T cell infiltration is associated with improved survival and negatively correlates with hypoxia in clear cell ovarian cancer. *Sci Rep*. 2023;13(1):6530. doi:10.1038/s41598-023-30655-3

146. Kim KS, Sengupta S, Berk M, et al. Hypoxia enhances lysophosphatidic acid responsiveness in ovarian cancer cells and lysophosphatidic acid induces ovarian tumor metastasis in vivo. *Cancer Res*. 2006;66(16):7983-7990. doi:10.1158/0008-5472.CAN-05-4381

147. Vignali PDA, DePeaux K, Watson MJ, et al. Hypoxia drives CD39-dependent suppressor function in exhausted T cells to limit antitumor immunity. *Nat Immunol*. 2023;24(2):267-279. doi:10.1038/s41590-022-01379-9

148. Townsend KN, Spowart JE, Huwait H, et al. Markers of T cell infiltration and function associate with favorable outcome in vascularized high-grade serous ovarian carcinoma. *PloS One*. 2013;8(12):e82406. doi:10.1371/journal.pone.0082406

149. White E, Mehnert JM, Chan CS. Autophagy, Metabolism, and Cancer. *Clin Cancer Res*. 2015;21(22):5037-5046. doi:10.1158/1078-0432.CCR-15-0490

150. Tasdogan A, Faubert B, Ramesh V, et al. Metabolic heterogeneity confers differences in melanoma metastatic potential. *Nature*. 2020;577(7788):115-120. doi:10.1038/s41586-019-1847-2

151. Faubert B, Tasdogan A, Morrison SJ, Mathews TP, DeBerardinis RJ. Stable isotope tracing to assess tumor metabolism in vivo. *Nat Protoc*. 2021;16(11):5123-5145. doi:10.1038/s41596-021-00605-2

152. DeVilbiss AW, Zhao Z, Martin-Sandoval MS, et al. Metabolomic profiling of rare cell populations isolated by flow cytometry from tissues. *eLife*. 10:e61980. doi:10.7554/eLife.61980

153. Karpievitch YV, Nikolic SB, Wilson R, Sharman JE, Edwards LM. Metabolomics Data Normalization with EigenMS. *PLOS ONE*. 2014;9(12):e116221. doi:10.1371/journal.pone.0116221

154. Pang Z, Zhou G, Ewald J, et al. Using MetaboAnalyst 5.0 for LC–HRMS spectra processing, multi-omics integration and covariate adjustment of global metabolomics data. *Nat Protoc*. 2022;17(8):1735-1761. doi:10.1038/s41596-022-00710-w

155. Ritchie ME, Phipson B, Wu D, et al. limma powers differential expression analyses for RNA-sequencing and microarray studies. *Nucleic Acids Res*. 2015;43(7):e47. doi:10.1093/nar/gkv007

156. MacPherson S, Keyes S, Kilgour MK, et al. Clinically relevant T cell expansion media activate distinct metabolic programs uncoupled from cellular function. *Mol Ther Methods Clin Dev*. 2022;24:380-393. doi:10.1016/j.omtm.2022.02.004

157. A nonautophagic role of ATG5 in regulating cell growth by targeting c-Myc for proteasome-mediated degradation. *iScience*. 2021;24(11):103296. doi:10.1016/j.isci.2021.103296

158. Ho PC, Bihuniak JD, Macintyre AN, et al. Phosphoenolpyruvate Is a Metabolic Checkpoint of Anti-tumor T Cell Responses. *Cell*. 2015;162(6):1217-1228. doi:10.1016/j.cell.2015.08.012

159. Zheng X, Wang X, Cheng X, et al. Single-cell analyses implicate ascites in remodeling the ecosystems of primary and metastatic tumors in ovarian cancer. *Nat Cancer*. 2023;4(8):1138-1156. doi:10.1038/s43018-023-00599-8

160. Tran E, Nielsen JS, Wick DA, et al. Polyfunctional T-Cell Responses Are Disrupted by the Ovarian Cancer Ascites Environment and Only Partially Restored by Clinically Relevant Cytokines. *PLOS ONE*. 2010;5(12):e15625. doi:10.1371/journal.pone.0015625

161. Nunes D, Ricardo S. Ovarian Cancer Ascites as a Liquid Tumor Microenvironment. In: Lele S, ed. *Ovarian Cancer*. Exon Publications; 2022. Accessed August 14, 2024. http://www.ncbi.nlm.nih.gov/books/NBK585986/

162. Domcke S, Sinha R, Levine DA, Sander C, Schultz N. Evaluating cell lines as tumour models by comparison of genomic profiles. *Nat Commun*. 2013;4(1):2126. doi:10.1038/ncomms3126

163. Jiao L, Zhang HL, Li DD, et al. Regulation of glycolytic metabolism by autophagy in liver cancer involves selective autophagic degradation of HK2 (hexokinase 2). *Autophagy*. 2017;14(4):671-684. doi:10.1080/15548627.2017.1381804

164. Marchingo JM, Sinclair LV, Howden AJ, Cantrell DA. Quantitative analysis of how Myc controls T cell proteomes and metabolic pathways during T cell activation. *eLife*. 2020;9:e53725. doi:10.7554/eLife.53725

165. Wang R, Dillon CP, Shi LZhichang, et al. The transcription factor Myc controls metabolic reprogramming upon T lymphocyte activation. *Immunity*. 2011;35(6):871-882. doi:10.1016/j.immuni.2011.09.021

166. Shi Y, Kotchetkov IS, Dobrin A, et al. GLUT1 overexpression enhances CAR T cell metabolic fitness and anti-tumor efficacy. *Mol Ther*. 2024;32(7):2393-2405. doi:10.1016/j.ymthe.2024.05.006

167. Hosokawa N, Hara T, Kaizuka T, et al. Nutrient-dependent mTORC1 Association with the ULK1–Atg13–FIP200 Complex Required for Autophagy. *Mol Biol Cell*. 2009;20(7):1981-1991. doi:10.1091/mbc.e08-12-1248

168. Lamark T, Johansen T. Mechanisms of Selective Autophagy.

169. Recruitment and Activation of the ULK1/Atg1 Kinase Complex in Selective Autophagy. *J Mol Biol*. 2020;432(1):123-134. doi:10.1016/j.jmb.2019.07.027

170. Khaminets A, Heinrich T, Mari M, et al. Regulation of endoplasmic reticulum turnover by selective autophagy. *Nature*. 2015;522(7556):354-358. doi:10.1038/nature14498

171. Zellner S, Schifferer M, Behrends C. Systematically defining selective autophagy receptor-specific cargo using autophagosome content profiling. *Mol Cell*. 2021;81(6):1337-1354.e8. doi:10.1016/j.molcel.2021.01.009

172. Sinclair LV, Youdale T, Spinelli L, et al. Autophagy repression by antigen and cytokines shapes mitochondrial, migration and effector machinery in CD8 T cells. Published online June 11, 2024:2024.06.10.598276. doi:10.1101/2024.06.10.598276

173. Jang C, Chen L, Rabinowitz JD. Metabolomics and isotope tracing. *Cell*. 2018;173(4):822-837. doi:10.1016/j.cell.2018.03.055

174. Metallo CM, Gameiro PA, Bell EL, et al. Reductive glutamine metabolism by IDH1 mediates lipogenesis under hypoxia. *Nature*. 2011;481(7381):380-384. doi:10.1038/nature10602

175. Yoo H, Antoniewicz MR, Stephanopoulos G, Kelleher JK. Quantifying reductive carboxylation flux of glutamine to lipid in a brown adipocyte cell line. *J Biol Chem*. 2008;283(30):20621-20627. doi:10.1074/jbc.M706494200

176. Hirayama A, Kami K, Sugimoto M, et al. Quantitative metabolome profiling of colon and stomach cancer microenvironment by capillary electrophoresis time-of-flight mass spectrometry. *Cancer Res*. 2009;69(11):4918-4925. doi:10.1158/0008-5472.CAN-08-4806

177. Roslin M, Henriksson R, Bergström P, Ungerstedt U, Bergenheim AT. Baseline levels of glucose metabolites, glutamate and glycerol in malignant glioma assessed by stereotactic microdialysis. *J Neurooncol*. 2003;61(2):151-160. doi:10.1023/a:1022106910017

178. Marcus HJ, Carpenter KLH, Price SJ, Hutchinson PJ. In vivo assessment of high-grade glioma biochemistry using microdialysis: a study of energy-related molecules, growth factors and cytokines. *J Neurooncol*. 2010;97(1):11-23. doi:10.1007/s11060-009-9990-5

179. Musharraf SG, Siddiqui AJ, Shamsi T, Choudhary MI, Rahman A ur. Serum metabonomics of acute leukemia using nuclear magnetic resonance spectroscopy. *Sci Rep*. 2016;6:30693. doi:10.1038/srep30693

180. Xu X, Sun Q, Liang X, et al. Mechanisms of Relapse After CD19 CAR T-Cell Therapy for Acute Lymphoblastic Leukemia and Its Prevention and Treatment Strategies. *Front Immunol*. 2019;10. doi:10.3389/fimmu.2019.02664

181. Plaks V, Rossi JM, Chou J, et al. CD19 target evasion as a mechanism of relapse in large B-cell lymphoma treated with axicabtagene ciloleucel. *Blood*. 2021;138(12):1081-1085. doi:10.1182/blood.2021010930

182. Shah NN, Sokol L. Targeting CD22 for the Treatment of B-Cell Malignancies. *ImmunoTargets Ther*. 2021;10:225-236. doi:10.2147/ITT.S288546

183. Fry TJ, Shah NN, Orentas RJ, et al. CD22-targeted CAR T cells induce remission in B-ALL that is naive or resistant to CD19-targeted CAR immunotherapy. *Nat Med*. 2018;24(1):20-28. doi:10.1038/nm.4441

184. Pan J, Niu Q, Deng B, et al. CD22 CAR T-cell therapy in refractory or relapsed B acute lymphoblastic leukemia. *Leukemia*. 2019;33(12):2854-2866. doi:10.1038/s41375-019-0488-7

185. Modlich U, Navarro S, Zychlinski D, et al. Insertional Transformation of Hematopoietic Cells by Self-inactivating Lentiviral and Gammaretroviral Vectors. *Mol Ther*. 2009;17(11):1919-1928. doi:10.1038/mt.2009.179

186. Hu Y, Zu C, Zhang M, et al. Safety and efficacy of CRISPR-based non-viral PD1 locus specifically integrated anti-CD19 CAR-T cells in patients with relapsed or refractory Non-Hodgkin's lymphoma: a first-in-human phase I study. *eClinicalMedicine*. 2023;60. doi:10.1016/j.eclinm.2023.102010

187. Lonez C, Breman E. Allogeneic CAR-T Therapy Technologies: Has the Promise Been Met? *Cells*. 2024;13(2):146. doi:10.3390/cells13020146

188. Bloemberg D, Sosa-Miranda CD, Nguyen T, Weeratna RD, McComb S. Self-Cutting and Integrating CRISPR Plasmids Enable Targeted Genomic Integration of Genetic Payloads for Rapid Cell Engineering. *CRISPR J*. 2021;4(1):104-119. doi:10.1089/crispr.2020.0090

189. McComb S, Arbabi-Ghahroudi M, Hay KA, et al. Discovery and preclinical development of a therapeutically active nanobody-based chimeric antigen receptor targeting human CD22. *Mol Ther Oncol*. 2024;32(1). doi:10.1016/j.omton.2024.200775

190. Pfister G, Toor SM, Sasidharan Nair V, Elkord E. An evaluation of sorter induced cell stress (SICS) on peripheral blood mononuclear cells (PBMCs) after different sort conditions - Are your sorted cells getting SICS? *J Immunol Methods*. 2020;487:112902. doi:10.1016/j.jim.2020.112902

191. Riesenberg S, Maricic T. Targeting repair pathways with small molecules increases precise genome editing in pluripotent stem cells. *Nat Commun*. 2018;9(1):2164. doi:10.1038/s41467-018-04609-7

192. Robert F, Barbeau M, Éthier S, Dostie J, Pelletier J. Pharmacological inhibition of DNA-PK stimulates Cas9-mediated genome editing. *Genome Med*. 2015;7(1):93. doi:10.1186/s13073-015-0215-6

193. Liu B, Chen S, Rose AL, et al. Inhibition of histone deacetylase 1 (HDAC1) and HDAC2 enhances CRISPR/Cas9 genome editing. *Nucleic Acids Res*. 2020;48(2):517-532. doi:10.1093/nar/gkz1136

194. Sheth VS, Gauthier J. Taming the beast: CRS and ICANS after CAR T-cell therapy for ALL. *Bone Marrow Transplant*. 2021;56(3):552-566. doi:10.1038/s41409-020-01134-4

195. Wu CY, Roybal KT, Puchner EM, Onuffer J, Lim WA. Remote control of therapeutic T cells through a small molecule-gated chimeric receptor. *Science*. 2015;350(6258):aab4077. doi:10.1126/science.aab4077

196. Cho JH, Collins JJ, Wong WW. Universal Chimeric Antigen Receptors for Multiplexed and Logical Control of T Cell Responses. *Cell*. 2018;173(6):1426-1438.e11. doi:10.1016/j.cell.2018.03.038

197. Morsut L, Roybal KT, Xiong X, et al. Engineering Customized Cell Sensing and Response Behaviors Using Synthetic Notch Receptors. *Cell*. 2016;164(4):780-791. doi:10.1016/j.cell.2016.01.012

198. Selli ME, Landmann JH, Arveseth C, Singh N. Inducing T cell dysfunction by chronic stimulation of CAR-engineered T cells targeting cancer cells in suspension cultures. *STAR Protoc*. 2023;4(1):101954. doi:10.1016/j.xpro.2022.101954

199. Ren J, Liu X, Fang C, Jiang S, June CH, Zhao Y. Multiplex Genome Editing to Generate Universal CAR T Cells Resistant to PD1 Inhibition. *Clin Cancer Res Off J Am Assoc Cancer Res*. 2017;23(9):2255-2266. doi:10.1158/1078-0432.CCR-16-1300

200. Old LJ. Cancer Immunology. *Sci Am*. 1977;236(5):62-79.

201. Shiravand Y, Khodadadi F, Kashani SMA, et al. Immune Checkpoint Inhibitors in Cancer Therapy. *Curr Oncol*. 2022;29(5):3044-3060. doi:10.3390/curroncol29050247

202. Kochenderfer JN. FDA approval of the first cellular therapy for a solid (non-hematologic) cancer. *Mol Ther*. 2024;32(4):857-858. doi:10.1016/j.ymthe.2024.03.012

203. Guzman G, Reed MR, Bielamowicz K, Koss B, Rodriguez A. CAR-T Therapies in Solid Tumors: Opportunities and Challenges. *Curr Oncol Rep*. 2023;25(5):479-489. doi:10.1007/s11912-023-01380-x

204. Sedlak JC, Yilmaz ÖH, Roper J. Metabolism and Colorectal Cancer. *Annu Rev Pathol*. 2023;18:467-492. doi:10.1146/annurev-pathmechdis-031521-041113

205. Mossmann D, Müller C, Park S, et al. Arginine reprograms metabolism in liver cancer via RBM39. *Cell*. 2023;186(23):5068-5083.e23. doi:10.1016/j.cell.2023.09.011

206. Sun H, Zhang L, Wang Z, et al. Single-cell transcriptome analysis indicates fatty acid metabolism-mediated metastasis and immunosuppression in male breast cancer. *Nat Commun*. 2023;14(1):5590. doi:10.1038/s41467-023-41318-2

207. Cheu JWS, Chiu DKC, Kwan KKL, et al. Hypoxia-inducible factor orchestrates adenosine metabolism to promote liver cancer development. *Sci Adv*. 2023;9(18):eade5111. doi:10.1126/sciadv.ade5111

208. Hanahan D. Hallmarks of Cancer: New Dimensions. *Cancer Discov*. 2022;12(1):31-46. doi:10.1158/2159-8290.CD-21-1059

209. McPhedran SJ, Carleton GA, Lum JJ. Metabolic engineering for optimized CAR-T cell therapy. *Nat Metab*. 2024;6(3):396-408. doi:10.1038/s42255-024-00976-2

210. Fultang L, Booth S, Yogev O, et al. Metabolic engineering against the arginine microenvironment enhances CAR-T cell proliferation and therapeutic activity. *Blood*. 2020;136(10):1155-1160. doi:10.1182/blood.2019004500

211. Tieu V, Sotillo E, Bjelajac JR, et al. A versatile CRISPR-Cas13d platform for multiplexed transcriptomic regulation and metabolic engineering in primary human T cells. *Cell*. 2024;187(5):1278-1295.e20. doi:10.1016/j.cell.2024.01.035

212. Hunt MS, Yang SJ, Mortensen E, et al. Dual-locus, dual-HDR editing permits efficient generation of antigen-specific regulatory T cells with robust suppressive activity. *Mol Ther*. 2023;31(10):2872-2886. doi:10.1016/j.ymthe.2023.07.016

213. Lei W, Xie M, Jiang Q, et al. Treatment-Related Adverse Events of Chimeric Antigen Receptor T-Cell (CAR T) in Clinical Trials: A Systematic Review and Meta-Analysis. *Cancers*. 2021;13(15):3912. doi:10.3390/cancers13153912

214. Santomasso BD, Nastoupil LJ, Adkins S, et al. Management of Immune-Related Adverse Events in Patients Treated With Chimeric Antigen Receptor T-Cell Therapy: ASCO Guideline. *J Clin Oncol*. 2021;39(35):3978-3992. doi:10.1200/JCO.21.01992

215. Flugel CL, Majzner RG, Krenciute G, et al. Overcoming on-target, off-tumour toxicity of CAR T cell therapy for solid tumours. *Nat Rev Clin Oncol*. 2023;20(1):49-62. doi:10.1038/s41571-022-00704-3

216. Gust J, Ponce R, Liles WC, Garden GA, Turtle CJ. Cytokines in CAR T Cell–Associated Neurotoxicity. *Front Immunol*. 2020;11. doi:10.3389/fimmu.2020.577027

217. Morris EC, Neelapu SS, Giavridis T, Sadelain M. Cytokine release syndrome and associated neurotoxicity in cancer immunotherapy. *Nat Rev Immunol*. 2022;22(2):85-96. doi:10.1038/s41577-021-00547-6

218. Diaconu I, Ballard B, Zhang M, et al. Inducible Caspase-9 Selectively Modulates the Toxicities of CD19-Specific Chimeric Antigen Receptor-Modified T Cells. *Mol Ther J Am Soc Gene Ther*. 2017;25(3):580-592. doi:10.1016/j.ymthe.2017.01.011

219. Xue L, Yi Y, Xu Q, et al. Chimeric antigen receptor T cells self-neutralizing IL6 storm in patients with hematologic malignancy. *Cell Discov*. 2021;7(1):84. doi:10.1038/s41421-021-00299-6

Supplementary Material

Supplementary Table 6. Guide RNA sequences.

Guide RNA name	Target	Sequence
ATG5-I2A-696	*ATG5* Intron 2	GTAATCTGACTTTCCGTAGC
ATG5-I2A-719	*ATG5* Intron 2	GCTACGGAAAGTCAGATTAC
ATG5-I2A-824	*ATG5* Intron 2	GCACCGAGTAGTACCACTTG
ATG5-I2A-950	*ATG5* Intron 2	AAGTTCGGCAATCTTGTTAC
ATG5-I2B-905	*ATG5* Intron 2	CGGATCGCTGCCTAATGTTA
ATG5-I2B-945	*ATG5* Intron 2	CCGTTTATGTATCCTTAGTC
ATG5-I2C-710	*ATG5* Intron 2	GTCACGTTCTCCTACCTAGT
ATG5-E4-56	*ATG5* Exon 4	CATCAAGTTCAGCTCTTCCT
AAVS1-I1[108]	*AAVS1* Intron 1	GGGGCCACTAGGGACAGGAT
TRAC-1a[188]	*TRAC* Exon 1	TCTCTCAGCTGGTACACGGC

Supplementary Table 7. Donor DNA sequences.

Donor name	DNA sequence
ATP1A1-Q118R-N129D	AATGTTACTGTGGATTGGAGCGATTCTTTGTTTCTTGGCTTATAGCATCCGGGCTGCTA CAGAAGAGGAACCTCAAAACGATGACGTGAGTTCTGGAATTCTCTATATGGATTTGTA GTACACATCAGATATCTTCTCCGTCTTTGTCTCCCAC
ATG5-mScarlet-I_NLS	GGCTGTGCCTTCTAGTTGCCAGCCATCTGTTGTTTGCCCCTCCCCCGTGCCTTCCTTGA CCCTGGAAGGTGCCACTCCCACTGTCCTTTCCTAATAAAATGAGGAAATTGCATCGCA TTGTCTGAGTAGGTGTCATTCTATTCTGGGGGGTGGGGTGGGGCAGGACAGCAAGGG GGAGGATTGGGAAGACAATAGCAGGCATGCTGGGGATGCGGTGGGCTCTATGGGTCG ACGTGGTACTACTCGGTGCATGAATGTTTCCCCAGGCTCATGTTGGGATTTTGTTTGAA ATCATCTTTATGGGTTTTCTTACTAGAAATGATAGTTTTAGAGAAGTTCGGCAATCTTG TTACTGGTACTCAAGCTTATATACACGTGAGTAATCTTAACTTTGGAAATATCAACCG TTTTCTGTCTAGAAAAACATCCACAGTTAAAAACCAAGTATGGTCATAGTTTTATTTTT AGAAGAATTTCATTTGTTAGAGGTATTTTTTCTGTTCTTGTTCTGTAATATAGGTTAGG ATACCATTTTTTTTTTCCAAACAAGTTTTTGCTGTTTTAATTACAACTTTTAACCTTCAT TGGCTTTGTAATAGTATATAAGAGTATGTGAGAGTATAAGAGTATATTTGGCCAAATT GACAACAACTGGAATTCTGCATTAATGAATCGGCCAACGCGCGGGGAGAGGCGGTTT GCGTATTGGGCGCTCTTCCGCTTCCTCGCTCACTGACTCGCTGCGCTCGGTCGTTCGGC TGCGGCGAGCGGTATCAGCTCACTCAAAGGCGGTAATACGGTTATCCACAGAATCAG GGGATAACGCAGGAAAGAACATGTGAGCAAAAGGCCAGCAAAAGGCCAGGAACCGT AAAAAGGCCGCGTTGCTGGCGTTTTTCCATAGGCTCCGCCCCCCTGACGAGCATCACA AAAATCGACGCTCAAGTCAGAGGTGGCGAAACCCGACAGGACTATAAAGATACCAGG CGTTTCCCCCTGGAAGCTCCCTCGTGCGCTCTCCTGTTCCGACCCTGCCGCTTACCGGA TACCTGTCCGCCTTTCTCCCTTCGGGAAGCGTGGCGCTTTCTCATAGCTCACGCTGTAG GTATCTCAGTTCGGTGTAGGTCGTTCGCTCCAAGCTGGGCTGTGTGCACGAACCCCCC GTTCAGCCCGACCGCTGCGCCTTATCCGGTAACTATCGTCTTGAGTCCAACCCGGTAA GACACGACTTATCGCCACTGGCAGCAGCCACTGGTAACAGGATTAGCAGAGCGAGGT ATGTAGGCGGTGCTACAGAGTTCTTGAAGTGGTGGCCTAACTACGGCTACACTAGAA GGACAGTATTTGGTATCTGCGCTCTGCTGAAGCCAGTTACCTTCGGAAAAAGAGTTGG TAGCTCTTGATCCGGCAAACAAACCACCGCTGGTAGCGGTGGTTTTTTTGTTTGCAAG CAGCAGATTACGCGCAGAAAAAAAGGATCTCAAGAAGATCCTTTGATCTTTTCTACGG GGTCTGACGCTCAGTGGAACGAAAACTCACGTTAAGGGATTTTGGTCATGAGATTATC AAAAAGGATCTTCACCTAGATCCTTTTAAATTAAAAATGAAGTTTTAAATCAATCTAA AGTATATATGAGTAAACTTGGTCTGACAGTTACCAATGCTTAATCAGTGAGGCACCTA TCTCAGCGATCTGTCTATTTCGTTCATCCATAGTTGCCTGACTCCCCGTCGTGTAGATA ACTACGATACGGGAGGGCTTACCATCTGGCCCCAGTGCTGCAATGATACCGCGAGAC CCACGCTCACCGGCTCCAGATTTATCAGCAATAAACCAGCCAGCCGGAAGGGCCGAG CGCAGAAGTGGTCCTGCAACTTTATCCGCCTCCATCCAGTCTATTAATTGTTGCCGGG AAGCTAGAGTAAGTAGTTCGCCAGTTAATAGTTTGCGCAACGTTGTTGCCATTGCTAC AGGCATCGTGGTGTCACGCTCGTCGTTTGGTATGGCTTCATTCAGCTCCGGTTCCCAAC GATCAAGGCGAGTTACATGATCCCCCATGTTGTGCAAAAAAGCGGTTAGCTCCTTCGG TCCTCCGATCGTTGTCAGAAGTAAGTTGGCCGCAGTGTTATCACTCATGGTTATGGCA GCACTGCATAATTCTCTTACTGTCATGCCATCCGTAAGATGCTTTTCTGTGACTGGTGA GTACTCAACCAAGTCATTCTGAGAATAGTGTATGCGGCGACCGAGTTGCTCTTGCCCG GCGTCAATACGGGATAATACCGCGCCACATAGCAGAACTTTAAAAGTGCTCATCATTG GAAAACGTTCTTCGGGGCGAAAACTCTCAAGGATCTTACCGCTGTTGAGATCCAGTTC GATGTAACCCACTCGTGCACCCAACTGATCTTCAGCATCTTTTACTTTCACCAGCGTTT CTGGGTGAGCAAAAACAGGAAGGCAAAATGCCGCAAAAAAGGGAATAAGGGCGACA CGGAAATGTTGAATACTCATACTCTTCCTTTTTCAATATTATTGAAGCATTTATCAGGG TTATTGTCTCATGAGCGGATACATATTTGAATGTATTTAGAAAAATAAACAAATAGGG GTTCCGCGCACATTTCCCCGAAAAGTGCCACCTGACGTCTAAGAAACCATTATTATCA TGACATTAACCTATAAAAATAGGCGTATCACGAGGCCCTTTCGTCTCGCGCGTTTCGG TGATGACGGTGAAAACCTCTGACACATGCAGCTCCCGGAGACGGTCACAGCTTGTCTG TAAGCGGATGCCGGGAGCAGACAAGCCCGTCAGGGCGCGTCAGCGGGTGTTGGCGGG TGTCGGGGCTGGCTTAACTATGCGGCATCAGAGCAGATTGTACTGAGAGTGCACCATA TGGCTCGAAACCGGACGGAGCCATTGCTCTCGCAGAGGGAGGAGCGCTTCCGGCTAG CGCACATAGACTTGCAGGTGTGAGTTAATGGATTATGTATTTTACAAACACTTTTCAA ATGTCTTCTGATTTTGGTGTGCTTTGTTTCCCTTTTCTAAGTGCATGTATAATCCCAGTT TATGCCTCTGTCAGAGATGACATCCTGCCTGTTCACTGAATAGCCCATAATAGGCAAA GATATTCTCAATTGTCGTTACTGTTTTTTCTTTTTGTGTCTCAGGTATGCATTCTAGTGT TTACCTGGAGATGATGTGGAAAAGTAGAAGTGTATTTGTGATGAGGAAATGCTTCTTC TGTTTCACTTTAATGAAGTCTGCCCTTTGCTTTCCCCCTCATCTCTCTGAGAGGCAGTG CTGCTCCTCAGCCTGCTCCAGCTACGGAAAGTCAGATTACTGGAGGAAGCTACTTATT AAGGAGCCCATTCGCTCACTTTTTGGGTATAGGACTGTTTTTTTGTTTTTGTTTTCCTCT GTGCATCCTCAGCATCTGGCACAGGCTCCTCAAAAGCTTCTGACCTCTTCTCTTCCTCC

CACAGGGCCTCGAGAGATCTGCCACCATGGTGAGCAAGGGCGAGGCAGTGATCAAGG
AGTTCATGCGGTTCAAGGTGCACATGGAGGGCTCCATGAACGGCCACGAGTTCGAGA
TCGAGGGCGAGGGCGAGGGCCGCCCCTACGAGGGCACCCAGACCGCCAAGCTGAAG
GTGACCAAGGGTGGCCCCCTGCCCTTCTCCTGGGACATCCTGTCCCCTCAGTTCATGT
ACGGCTCCAGGGCCTTCATCAAGCACCCCGCCGACATCCCCGACTACTATAAGCAGTC
CTTCCCCGAGGGCTTCAAGTGGGAGCGCGTGATGAACTTCGAGGACGGCGGCGCCGT
GACCGTGACCCAGGACACCTCCCTGGAGGACGGCACCCTGATCTACAAGGTGAAGCT
CCGCGGCACCAACTTCCCTCCTGACGGCCCCGTAATGCAGAAGAAGACAATGGGCTG
GGAAGCATCCACCGAGCGGTTGTACCCCGAGGACGGCGTGCTGAAGGGCGACATTAA
GATGGCCCTGCGCCTGAAGGACGGCGGCCGCTACCTGGCGGACTTCAAGACCACCTA
CAAGGCCAAGAAGCCCGTGCAGATGCCCGGCGCCTACAACGTCGACCGCAAGTTGGA
CATCACCTCCCACAACGAGGACTACACCGTGGTGGAACAGTACGAACGCTCCGAGGG
CCGCCACTCCACCGGCGGCATGGACGAGCTGTACAAGAAAAGGCCGGCGGCCACGAA
AAAGGCCGGCCAGGCAAAAAAGAAAAAGTGATAACTCGAGCGGCCGCGTTTAAACC
CTGCA

AAVS1_Puro_PGK1_ATG5_cDNA TTAAGCTTATGACAGATGACAAAGATGTGCTTCGAGATGTGTGGTTTGGACGAATTCC
AACTTGTTTCACGCTATATCAGGATGAGATAACTGAAAGGGAAGCAGAACCATACTA
TTTGCTTTTGCCAAGAGTAAGTTATTTGACGTTGGTAACTGACAAAGTGAAAAAGCAC
TTTCAGAAGGTTATGAGACAAGAAGACATTAGTGAGATATGGTTTGAATATGAAGGC
ACACCACTGAAATGGCATTATCCAATTGGTTTGCTATTTGATCTTCTTGCATCAAGTTC
AGCTCTTCCTTGGAACATCACAGTACATTTTAAGAGTTTTCCAGAAAAAGACCTTCTG
CACTGTCCATCTAAGGATGCAATTGAAGCTCATTTTATGTCATGTATGAAAGAAGCTG
ATGCTTTAAAACATAAAAGTCAAGTAATCAATGAAATGCAGAAAAAAGATCACAAGC
AACTCTGGATGGGATTGCAAAATGACAGATTTGACCAGTTTTGGGCCATCAATCGGAA
ACTCATGGAATATCCTGCAGAAGAAAATGGATTTCGTTATATCCCCTTTAGAATATAT
CAGACAACGACTGAAAGACCTTTCATTCAGAAGCTGTTTCGTCCTGTGGCTGCAGATG
GACAGTTGCACACACTAGGAGATCTCCTCAAAGAAGTTTGTCCTTCTGCTATTGATCC
TGAAGATGGGGAAAAAAAGAATCAAGTGATGATTCATGGAATTGAGCCAATGTTGGA
AACACCTCTGCAGTGGCTGAGTGAACATCTGAGCTACCCGGATAATTTTCTTCATATT
AGTATCATCCCACAGCCAACAGATTGAGGATCCACTAGTCCAGTGTGGTGGAATTCTG
CAGATATCCAGCACAGTGGCGGCCGCTCGAGTCTAGACGTTTAAACCCTGCAGGCTGT
GCCTTCTAGTTGCCAGCCATCTGTTGTTTGCCCCTCCCCCGTGCCTTCCTTGACCCTGG
AAGGTGCCACTCCCACTGTCCTTTCCTAATAAAATGAGGAAATTGCATCGCATTGTCT
GAGTAGGTGTCATTCTATTCTGGGGGGTGGGGTGGGGCAGGACAGCAAGGGGGAGGA
TTGGGAAGACAATAGCAGGCATGCTGGGGATGCGGTGGGCTCTATGGGTCGACAGTA
CTAAGCTTTACTAGGGACAGGATTGGTGACAGAAAAGCCCCATCCTTAGGCCTCCTCC
TTCCTAGTCTCCTGATATTGGGTCTAACCCCCACCTCCTGTTAGGCAGATTCCTTATCT
GGTGACACACCCCCATTTCCTGGAGCCATCTCTCTCCTTGCCAGAACCTCTAAGGTTTG
CTTACGATGGAGCCAGAGAGGATCCTGGGAGGGAGAGCTTGGCAGGGGGTGGGAGG
GAAGGGGGGGATGCGTGACCTGCCCGGTTCTCAGTGGCCACCCTGCGCTACCCTCTCC
CAGAACCTGAGCTGCTCTGACGCGGCTGTCTGGTGCGTTTCACTGATCCTGGTGCTGC
AGCTTCCTTACACTTCCCAAGAGGAGAAGCAGTTTGGAAAAACAAAATCAGAATAAG
TTGGTCCTGAGTTCTAACTTTGGCTCTTCACCTTTCTAGTCCCCAATTTATATTGTTCCT
CCGTGCGTCAGTTTTACCTGTGAGATAAGGCCAGTAGCCAGCCCCGTCCTGGCAGGGC
TGTGGTGAGGAGGGGGGTGTCCGTGTGGAAAACTCCCTTTGTGAGAATGGTGCGTCCT
AGGTGTTCACCAGGTCGTGGCCGCCTCTACTCCCTTTCTCTTTCTCCATCCTTCTTTCCT
TAAAGAGTCCCCAGTGCTATCTGGGACATATTCCTCCGCCCAGAGCAGGGTCCCGCTT
CCCTAAGGCCCTGCTCTGGGCTTCTGGGTTTGAGTCCTTGGCAAGCCCAGGAGAGGCG
CTCAGGCTTCCCTGTCCCCCTTCCTCGTCCACCATCTCATGCCCCTGGCTCTCCTGCCC
CTTCCCTACAGGGGTTCCTGGCTCTGCTCTAAGGGCGAATTCTGCATTAATGAATCGG
CCAACGCGCGGGGAGAGGCGGTTTGCGTATTGGGCGCTCTTCCGCTTCCTCGCTCACT
GACTCGCTGCGCTCGGTCGTTCGGCTGCGGCGAGCGGTATCAGCTCACTCAAAGGCGG
TAATACGGTTATCCACAGAATCAGGGGATAACGCAGGAAAGAACATGTGAGCAAAAG
GCCAGCAAAAGGCCAGGAACCGTAAAAAGGCCGCGTTGCTGGCGTTTTTCCATAGGC
TCCGCCCCCCTGACGAGCATCACAAAAATCGACGCTCAAGTCAGAGGTGGCGAAACC
CGACAGGACTATAAAGATACCAGGCGTTTCCCCCTGGAAGCTCCCTCGTGCGCTCTCC
TGTTCCGACCCTGCCGCTTACCGGATACCTGTCCGCCTTTCTCCCTTCGGGAAGCGTGG
CGCTTTCTCATAGCTCACGCTGTAGGTATCTCAGTTCGGTGTAGGTCGTTCGCTCCAAG
CTGGGCTGTGTGCACGAACCCCCCGTTCAGCCCGACCGCTGCGCCTTATCCGGTAACT
ATCGTCTTGAGTCCAACCCGGTAAGACACGACTTATCGCCACTGGCAGCAGCCACTGG
TAACAGGATTAGCAGAGCGAGGTATGTAGGCGGTGCTACAGAGTTCTTGAAGTGGTG
GCCTAACTACGGCTACACTAGAAGGACAGTATTTGGTATCTGCGCTCTGCTGAAGCCA
GTTACCTTCGGAAAAAGAGTTGGTAGCTCTTGATCCGGCAAACAAACCACCGCTGGTA
GCGGTGGTTTTTTTGTTTGCAAGCAGCAGATTACGCGCAGAAAAAAAGGATCTCAAG
AAGATCCTTTGATCTTTTCTACGGGGTCTGACGCTCAGTGGAACGAAAACTCACGTTA
AGGGATTTTGGTCATGAGATTATCAAAAAGGATCTTCACCTAGATCCTTTTAAATTAA
AAATGAAGTTTTAAATCAATCTAAAGTATATATGAGTAAACTTGGTCTGACAGTTACC
AATGCTTAATCAGTGAGGCACCTATCTCAGCGATCTGTCTATTTCGTTCATCCATAGTT

GCCTGACTCCCCGTCGTGTAGATAACTACGATACGGGAGGGCTTACCATCTGGCCCCA
GTGCTGCAATGATACCGCGAGACCCACGCTCACCGGCTCCAGATTTATCAGCAATAAA
CCAGCCAGCCGGAAGGGCCGAGCGCAGAAGTGGTCCTGCAACTTTATCCGCCTCCAT
CCAGTCTATTAATTGTTGCCGGGAAGCTAGAGTAAGTAGTTCGCCAGTTAATAGTTTG
CGCAACGTTGTTGCCATTGCTACAGGCATCGTGGTGTCACGCTCGTCGTTTGGTATGG
CTTCATTCAGCTCCGGTTCCCAACGATCAAGGCGAGTTACATGATCCCCCATGTTGTG
CAAAAAAGCGGTTAGCTCCTTCGGTCCTCCGATCGTTGTCAGAAGTAAGTTGGCCGCA
GTGTTATCACTCATGGTTATGGCAGCACTGCATAATTCTCTTACTGTCATGCCATCCGT
AAGATGCTTTTCTGTGACTGGTGAGTACTCAACCAAGTCATTCTGAGAATAGTGTATG
CGGCGACCGAGTTGCTCTTGCCCGGCGTCAATACGGGATAATACCGCGCCACATAGC
AGAACTTTAAAAGTGCTCATCATTGGAAAACGTTCTTCGGGGCGAAAACTCTCAAGG
ATCTTACCGCTGTTGAGATCCAGTTCGATGTAACCCACTCGTGCACCCAACTGATCTTC
AGCATCTTTTACTTTCACCAGCGTTTCTGGGTGAGCAAAAACAGGAAGGCAAAATGCC
GCAAAAAAGGGAATAAGGGCGACACGGAAATGTTGAATACTCATACTCTTCCTTTTTC
AATATTATTGAAGCATTTATCAGGGTTATTGTCTCATGAGCGGATACATATTTGAATG
TATTTAGAAAAATAAACAAATAGGGGTTCCGCGCACATTTCCCCGAAAAGTGCCACCT
GACGTCTAAGAAACCATTATTATCATGACATTAACCTATAAAAATAGGCGTATCACGA
GGCCCTTTCGTCTCGCGCGTTTCGGTGATGACGGTGAAAACCTCTGACACATGCAGCT
CCCGGAGACGGTCACAGCTTGTCTGTAAGCGGATGCCGGGAGCAGACAAGCCCGTCA
GGGCGCGTCAGCGGGTGTTGGCGGGTGTCGGGGCTGGCTTAACTATGCGGCATCAGA
GCAGATTGTACTGAGAGTGCACCATATGCGGTGTGAAATACCGCACAGATGCGTAAG
GAGAAAATACCGCATCAGGCGCCATTCGCCATTCAGGCTGCGCAACTGTTGGGAAGG
GCGATCGGTGCGGGCCTCTTCGCTATTACGCCAGAATTCGCCCTTTGCTTTCTCTGACC
AGCATTCTCTCCCCTGGGCCTGTGCCGCTTTCTGTCTGCAGCTTGTGGCCTGGGTCACC
TCTACGGCTGGCCCAGATCCTTCCCTGCCGCCTCCTTCAGGTTCCGTCTTCCTCCACTC
CCTCTTCCCCTTGCTCTCTGCTGTGTTGCTGCCCAAGGATGCTCTTTCCGGAGCACTTC
CTTCTCGGCGCTGCACCACGTGATGTCCTCTGAGCGGATCCTCCCCGTGTCTGGGTCCT
CTCCGGGCATCTCTCCTCCCTCACCCAACCCCATGCCGTCTTCACTCGCTGGGTTCCCT
TTTCCTTCTCCTTCTGGGGCCTGTGCCATCTCTCGTTTCTTAGGATGGCCTTCTCCGACG
GATGTCTCCCTTGCGTCCCGCCTCCCCTTCTTGTAGGCCTGCATCATCACCGTTTTTCT
GGACAACCCCAAAGTACCCCGTCTCCCTGGCTTTAGCCACCTCTCCATCCTCTTGCTTT
CTTTGCCTGGACACCCCGTTCTCCTGTGGATTCGGGTCACCTCTCACTCCTTTCATTTG
GGCAGCTCCCCTACCCCCCTTACCTCTCTAGTCTGTGCTAGCTCTTCCAGCCCCCTGTC
ATGGCATCTTCCAGGGGTCCGAGAGCTCAGCTAGTCTTCTTCCTCCAACCCGGGCCCC
TATGTCCACTTCAGGACAGCATGTTTGCTGCCTCCAGGGATCCTGTGTCCCCGAGCTG
GGACCACCTTATATTCCCAGGGCCGGTTAATGTGGCTCTGGTTCTGGGTACTTTTATCT
GTCCCCTCCACCCCACAGTGGGGCAAGCTTCTGACCTCTTCTCTTCCTCCCACAGGGCC
TCGAGAGATCTGGCGGCGGAGAGGGCAGAGGAAGTCTTCTAACATGCGGTGACGTGG
AGGAGAATCCCGGCCCTAGCACCGAGTACAAGCCCACGGTGCGCCTCGCCACCCGCG
ACGACGTCCCCAGGGCCGTACGCACCCTCGCCGCCGCGTTCGCCGACTACCCCGCCAC
GCGCCACACCGTCGATCCGGACCGCCACATCGAGCGGGTCACCGAGCTGCAAGAACT
CTTCCTCACGCGCGTCGGGCTCGACATCGGCAAGGTGTGGGTCGCGGACGACGGCGC
CGCGGTGGCGGTCTGGACCACGCCGGAGAGCGTCGAAGCGGGGGCGGTGTTCGCCGA
GATCGGCCCGCGCATGGCCGAGTTGAGCGGTTCCCGGCTGGCCGCGCAGCAACAGAT
GGAAGGCCTCCTGGCGCCGCACCGGCCCAAGGAGCCCGCGTGGTTCCTGGCCACCGT
CGGCGTCTCGCCCGACCACCAGGGCAAGGGTCTGGGCAGCGCCGTCGTGCTCCCCGG
AGTGGAGGCGGCCGAGCGCGCCGGGGTGCCCGCCTTCCTGGAGACCTCCGCGCCCCG
CAACCTCCCCTTCTACGAGCGGCTCGGCTTCACCGTCACCGCCGACGTCGAGGTGCCC
GAAGGACCGCGCACCTGGTGCATGACCCGCAAGCCCGGTGCCTGATCTAGACAGACA
TGATAAGATACATTGATGAGTTTGGACAAACCACAACTAGAATGCAGTGAAAAAAAT
GCTTTATTTGTGAAATTTGTGATGCTATTGCTTTATTTGTAACCATTATAAGCTGCAAT
AAACAAGTTAACAACAACAATTGCATTCATTTTATGTTTCAGGTTCAGGGGGAGGTGT
GGGAGGTTTTTTAATGCATCCACGGGGTTGGGGTTGCGCCTTTTCCAAGGCAGCCCTG
GGTTTGCGCAGGGACGCGGCTGCTCTGGGCGTGGTTCCGGGAAACGCAGCGGCGCCG
ACCCTGGGTCTCGCACATTCTTCACGTCCGTTCGCAGCGTCACCCGGATCTTCGCCGCT
ACCCTTGTGGGCCCCCCGGCGACGCTTCCTGCTCCGCCCCTAAGTCGGGAAGGTTCCT
TGCGGTTCGCGGCGTGCCGGACGTGACAAACGGAAGCCGCACGTCTCACTAGTACCC
TCGCAGACGGACAGCGCCAGGGAGCAATGGCAGCGCGCCGACCGCGATGGGCTGTGG
CCAATAGCGGCTGCTCAGCAGGGCGCGCCGAGAGCAGCGGCCGGGAAGGGGCGGTG
CGGGAGGCGGGGTGTGGGGCGGTAGTGTGGGCCCTGTTCCTGCCCGCGCGGTGTTCC
GCATTCTGCAAGCCTCCGGAGCGCACGTCGGCAGTCGGCTCCCTCGTTGACCGAATCA
CCGACCTCTCTCCCCAGGGGTACCCTCAGCC

ATG5-αFR

GCACATAGACTTGCAGGTGTGAGTTAATGGATTATGTATTTTACAAACACTTTTCAAA
TGTCTTCTGATTTTGGTGTGCTTTGTTTCCCTTTTCTAAGTGCATGTATAATCCCAGTTT
ATGCCTCTGTCAGAGATGACATCCTGCCTGTTCACTGAATAGCCCATAATAGGCAAAG
ATATTCTCAATTGTCGTTACTGTTTTTTCTTTTTGTGTCTCAGGTATGCATTCTAGTGTT
TACCTGGAGATGATGTGGAAAAGTAGAAGTGTATTTGTGATGAGGAAATGCTTCTTCT
GTTTCACTTTAATGAAGTCTGCCCTTTGCTTTCCCCCTCATCTCTCTGAGAGGCAGTGC

TGCTCCTCAGCCTGCTCCAGCTACGGAAAGTCAGATTACTGGAGGAAGCTACTTATTA
AGGAGCCCATTCGCTCACTTTTTGGGTATAGGACTGTTTTTTTGTTTTTGTTTTCCTCTG
TGCATCCTCAGCATCTGGCACAGGCTCCTCAAAAGCTTCTGACCTCTTCTCTTCCTCCC
ACAGGGCCTCGAGAGATCTGGCGGCGGAGAGGGCAGAGGAAGTCTTCTAACATGCGG
TGACGTGGAGGAGAATCCCGGCCCTATGGCCTTACCAGTGACCGCCTTGCTCCTGCCG
CTGGCCTTGCTGCTCCACGCCGCCAGGCCGGGATCCCAGCTGGTGGAGTCTGGGGGA
GGCTTGGTACAGCCAGGGCGGTCCCTGAGACTCTCCTGCACAACTTCTGGATTCACTT
TTGGTGATTATGCTATGATCTGGGCCCGCCAGGCTCCAGGGAAGGGGCTGGAGTGGG
TCTCATCCATTAGTAGTAGTAGTAGTTACATATACTACGCAGACTCAGTGAAGGGCCG
ATTCACCATCTCCAGAGACAACGCCAAGAACTCACTGTATCTGCAAATGAACAGCCTG
AGAGCCGAGGACACGGCTGTGTATTACTGTGCGAGAGAACGATACGATTTTTGGAGT
GGAATGGACGTCTGGGGCAAAGGGACCACGGTCACCGTCTCGAGTGGTGGAGGCGGT
TCAGGCGGAGGTGGCTCTGGCGGTAGTGCACAGTCTGCCCTGACTCAGCCTGCCTCCG
TGTCTGGGTCTCCTGGACAGTCGATCACCATCTCCTGCACTGGAACCAGCAGTGATGT
TGGGAGTTATAACCTTGTCTCCTGGTACCAACAGCACCCAGGCAAAGCCCCCAAACTC
ATGATTTATGAGGGCAGTAAGCGGCCCTCAGGGGTTTCTAATCGCTTCTCTGGCTCCA
AGTCTGGCAACGCGGCCTCCCTGACAATCTCTGGGCTCCAGGCTGAGGACGAGGCTG
ATTATTACTGCCAGTCCTATGACAGCAGCCTGAGTGTGGTATTCGGCGGAGGGACCAA
GCTGACCGTCCTAGGTGCTAGCACCACGACGCCAGCGCCGCGACCACCAACACCGGC
GCCCACCATCGCGTCGCAGCCCCTGTCCCTGCGCCCAGAGGCGTGCCGGCCAGCGGC
GGGGGGCGCAGTGCACACGAGGGGGCTGGACTTCGCCTGTGATTTTTGGGTGCTGGT
GGTGGTTGGTGGAGTCCTGGCTTGCTATAGCTTGCTAGTAACAGTGGCCTTTATTATTT
TCTGGGTGAGGAGTAAGAGGAGCAGGCTCCTGCACAGTGACTACATGAACATGACTC
CCCGCCGCCCCGGGCCCACCCGCAAGCATTACCAGCCCTATGCCCCACCACGCGACTT
CGCAGCCTATCGCTCCATCGATAGAGTGAAGTTCAGCAGGAGCGCAGACGCCCCCGC
GTACCAGCAGGGCCAGAACCAGCTCTATAACGAGCTCAATCTAGGACGAAGAGAGGA
GTACGATGTTTTGGACAAGAGACGTGGCCGGGACCCTGAGATGGGGGGAAAGCCGAG
AAGGAAGAACCCTCAGGAAGGCCTGTACAATGAACTGCAGAAAGATAAGATGGCGG
AGGCCTACAGTGAGATTGGGATGAAAGGCGAGCGCCGGAGGGGCAAGGGGCACGAT
GGCCTTTACCAGGGTCTCAGTACAGCCACCAAGGACACCTACGACGCCCTTCACATGC
AGGCCCTGCCCCCTCGCTGATAAGCGGCCGCCTGTGCCTTCTAGTTGCCAGCCATCTG
TTGTTTGCCCCTCCCCCGTGCCTTCCTTGACCCTGGAAGGTGCCACTCCCACTGTCCTT
TCCTAATAAAATGAGGAAATTGCATCGCATTGTCTGAGTAGGTGTCATTCTATTCTGG
GGGGTGGGGTGGGGCAGGACAGCAAGGGGGAGGATTGGGAAGACAATAGCAGGCAT
GCTGGGGATGCGGTGGGCTCTATGGGTCGACGTGGTACTACTCGGTGCATGAATGTTT
CCCCAGGCTCATGTTGGGATTTTGTTTGAAATCATCTTTATGGGTTTTCTTACTAGAAA
TGATAGTTTTAGAGAAGTTCGGCAATCTTGTTACTGGTACTCAAGCTTATATACACGT
GAGTAATCTTAACTTTGGAAATATCAACCGTTTTCTGTCTAGAAAAACATCCACAGTT
AAAAACCAAGTATGGTCATAGTTTTATTTTTAGAAGAATTTCATTTGTTAGAGGTATTT
TTTCTGTTCTTGTTCTGTAATATAGGTTAGGATACCATTTTTTTTTTCCAAACAAGTTTT
TGCTGTTTTAATTACAACTTTTAACCTTCATTGGCTTTGTAATAGTATATAAGAGTATG
TGAGAGTATAAGAGTATATTTGGCCAAATTGACAACAACTG

ATG5-EF1α-αFR

GCACATAGACTTGCAGGTGTGAGTTAATGGATTATGTATTTTACAAACACTTTTCAAA
TGTCTTCTGATTTTGGTGTGCTTTGTTTCCCTTTTCTAAGTGCATGTATAATCCCAGTTT
ATGCCTCTGTCAGAGATGACATCCTGCCTGTTCACTGAATAGCCCATAATAGGCAAAG
ATATTCTCAATTGTCGTTACTGTTTTTTCTTTTTGTGTCTCAGGTATGCATTCTAGTGTT
TACCTGGAGATGATGTGGAAAAGTAGAAGTGTATTTGTGATGAGGAAATGCTTCTTCT
GTTTCACTTTAATGAAGTCTGCCCTTTGCTTTCCCCCTCATCTCTCTGAGAGGCAGTGC
TGCTCCTCAGCCTGCTCCAGCTACGGAAAGTCAGATTACTGGAGGAAGCTACTTATTA
AGGAGCCCATTCGCTCACTTTTTGGGTATAGGACTGTTTTTTTGTTTTTGTTTTCCTCTG
TGCATCCTCAGCATCTGGCACAGGCTCCTCAAAAGCTTCTGCATATGTCTTGAAAGGA
GTGGGAATTGGCTCCGGTGCCCGTCAGTGGGCAGAGCGCACATCGCCCACAGTCCCC
GAGAAGTTGGGGGGAGGGGTCGGCAATTGAACCGGTGCCTAGAGAAGGTGGCGCGG
GGTAAACTGGGAAAGTGATGTCGTGTACTGGCTCCGCCTTTTTCCCGAGGGTGGGGGA
GAACCGTATATAAGTGCAGTAGTCGCCGTGAACGTTCTTTTTCGCAACGGGTTTGCCG
CCAGAACACAGGTAAGTGCCGTGTGTGGTTCCCGCGGGCCTGGCCTCTTTACGGGTTA
TGGCCCTTGCGTGCCTTGAATTACTTCCACCTGGCTGCAGTACGTGATTCTTGATCCCG
AGCTTCGGGTTGGAAGTGGGTGGGAGAGTTCGAGGCCTTGCGCTTAAGGAGCCCCTTC
GCCTCGTGCTTGAGTTGAGGCCTGGCCTGGGCGCTGGGGCCGCCGCGTGCGAATCTGG
TGGCACCTTCGCGCCTGTCTCGCTGCTTTCGATAAGTCTCTAGCCATTTAAAATTTTTG
ATGACCTGCTGCGACGCTTTTTTTCTGGCAAGATAGTCTTGTAAATGCGGGCCAAGAT
CTGCACACTGGTATTTCGGTTTTTGGGGCCGCGGGCGGCGACGGGGCCCGTGCGTCCC
AGCGCACATGTTCGGCGAGGCGGGGCCTGCGAGCGCGGCCACCGAGAATCGGACGGG
GGTAGTCTCAAGCTGGCCGGCCTGCTCTGGTGCCTGGCCTCGCGCCGCCGTGTATCGC
CCCGCCCTGGGCGGCAAGGCTGGCCCGGTCGGCACCAGTTGCGTGAGCGGAAAGATG
GCCGCTTCCCGGCCCTGCTGCAGGGAGCTCAAAATGGAGGACGCGGCGCTCGGGAGA
GCGGGCGGGTGAGTCACCCACACAAAGGAAAAGGGCCTTTCCGTCCTCAGCCGTCGC
TTCATGTGACTCCACGGAGTACCGGGCGCCGTCCAGGCACCTCGATTAGTTCTCGAGC

TTTTGGAGTACGTCGTCTTTAGGTTGGGGGGAGGGGTTTTATGCGATGGAGTTTCCCC
ACACTGAGTGGGTGGAGACTGAAGTTAGGCCAGCTTGGCACTTGATGTAATTCTCCTT
GGAATTTGCCCTTTTTGAGTTTGGATCTTGGTTCATTCTCAAGCCTCAGACAGTGGTTC
AAAGTTTTTTTCTTCCATTTCAGGTGTCGTGACGTACGGGATCCTCTAGAACGCGTGCC
ACCATGGCCTTACCAGTGACCGCCTTGCTCCTGCCGCTGGCCTTGCTGCTCCACGCCG
CCAGGCCGGGATCCCAGCTGGTGGAGTCTGGGGGAGGCTTGGTACAGCCAGGGCGGT
CCCTGAGACTCTCCTGCACAACTTCTGGATTCACTTTTGGTGATTATGCTATGATCTGG
GCCCGCCAGGCTCCAGGGAAGGGGCTGGAGTGGGTCTCATCCATTAGTAGTAGTAGT
AGTTACATATACTACGCAGACTCAGTGAAGGGCCGATTCACCATCTCCAGAGACAACC
GCCAAGAACTCACTGTATCTGCAAATGAACAGCCTGAGAGCCGAGGACACGGCTGTG
TATTACTGTGCGAGAGAACGATACGATTTTTGGAGTGGAATGGACGTCTGGGGCAAA
GGGACCACGGTCACCGTCTCGAGTGGTGGAGGCGGTTCAGGCGGAGGTGGCTCTGGC
GGTAGTGCACAGTCTGCCCTGACTCAGCCTGCCTCCGTGTCTGGGTCTCCTGGACAGT
CGATCACCATCTCCTGCACTGGAACCAGCAGTGATGTTGGGAGTTATAACCTTGTCTC
CTGGTACCAACAGCACCCAGGCAAAGCCCCCAAACTCATGATTTATGAGGGCAGTAA
GCGGCCCTCAGGGGTTTCTAATCGCTTCTCTGGCTCCAAGTCTGGCAACGCGGCCTCC
CTGACAATCTCTGGGCTCCAGGCTGAGGACGAGGCTGATTATTACTGCCAGTCCTATG
ACAGCAGCCTGAGTGTGGTATTCGGCGGAGGGACCAAGCTGACCGTCCTAGGTGCTA
GCACCACGACGCCAGCGCCGCGACCACCAACACCGGCGCCCACCATCGCGTCGCAGC
CCCTGTCCCTGCGCCCAGAGGCGTGCCGGCCAGCGGCGGGGGGCGCAGTGCACACGA
GGGGGCTGGACTTCGCCTGTGATTTTTGGGTGCTGGTGGTGGTTGGTGGAGTCCTGGC
TTGCTATAGCTTGCTAGTAACAGTGGCCTTTATTATTTTCTGGGTGAGGAGTAAGAGG
AGCAGGCTCCTGCACAGTGACTACATGAACATGACTCCCCGCCGCCCCGGGCCCACCC
GCAAGCATTACCAGCCCTATGCCCCACCACGCGACTTCGCAGCCTATCGCTCCATCGA
TAGAGTGAAGTTCAGCAGGAGCGCAGACGCCCCCGCGTACCAGCAGGGCCAGAACCA
GCTCTATAACGAGCTCAATCTAGGACGAAGAGAGGAGTACGATGTTTTGGACAAGAG
ACGTGGCCGGGACCCTGAGATGGGGGGAAAGCCGAGAAGGAAGAACCCTCAGGAAG
GCCTGTACAATGAACTGCAGAAAGATAAGATGGCGGAGGCCTACAGTGAGATTGGGA
TGAAAGGCGAGCGCCGGAGGGGCAAGGGGCACGATGGCCTTTACCAGGGTCTCAGTA
CAGCCACCAAGGACACCTACGACGCCCTTCACATGCAGGCCCTGCCCCCTCGCTGATA
AGCGGCCGCCTGTGCCTTCTAGTTGCCAGCCATCTGTTGTTTGCCCCTCCCCCGTGCCT
TCCTTGACCCTGGAAGGTGCCACTCCCACTGTCCTTTCCTAATAAAATGAGGAAATTG
CATCGCATTGTCTGAGTAGGTGTCATTCTATTCTGGGGGGTGGGGTGGGGCAGGACAG
CAAGGGGGAGGATTGGGAAGACAATAGCAGGCATGCTGGGGATGCGGTGGGCTCTAT
GGGTCGACGTGGTACTACTCGGTGCATGAATGTTTCCCCAGGCTCATGTTGGGATTTT
GTTTGAAATCATCTTTATGGGTTTTCTTACTAGAAATGATAGTTTTAGAGAAGTTCGGC
AATCTTGTTACTGGTACTCAAGCTTATATACACGTGAGTAATCTTAACTTTGGAAATAT
CAACCGTTTTCTGTCTAGAAAAACATCCACAGTTAAAAACCAAGTATGGTCATAGTTT
TATTTTTAGAAGAATTTCATTTGTTAGAGGTATTTTTTCTGTTCTTGTTCTGTAATATAG
GTTAGGATACCATTTTTTTTTTCCAAACAAGTTTTTGCTGTTTTAATTACAACTTTTAAC
CTTCATTGGCTTTGTAATAGTATATAAGAGTATGTGAGAGTATAAGAGTATATTTGGC
CAAATTGACAACAACTG

AAVS1-αFR

TGCTTTCTCTGACCAGCATTCTCTCCCCTGGGCCTGTGCCGCTTTCTGTCTGCAGCTTG
TGGCCTGGGTCACCTCTACGGCTGGCCCAGATCCTTCCCTGCCGCCTCCTTCAGGTTCC
GTCTTCCTCCACTCCCTCTTCCCCTTGCTCTCTGCTGTGTTGCTGCCCAAGGATGCTCTT
TCCGGAGCACTTCCTTCTCGGCGCTGCACCACGTGATGTCCTCTGAGCGGATCCTCCC
CGTGTCTGGGTCCTCTCCGGGCATCTCTCCTCCCTCACCCAACCCCATGCCGTCTTCAC
TCGCTGGGTTCCCTTTTCCTTCTCCTTCTGGGGCCTGTGCCATCTCTCGTTTCTTAGGAT
GGCCTTCTCCGACGGATGTCTCCCTTGCGTCCCGCCTCCCCTTCTTGTAGGCCTGCATC
ATCACCGTTTTTCTGGACAACCCCAAAGTACCCCGTCTCCCTGGCTTTAGCCACCTCTC
CATCCTCTTGCTTTCTTTGCCTGGACACCCCGTTCTCCTGTGGATTCGGGTCACCTCTC
ACTCCTTTCATTTGGGCAGCTCCCCTACCCCCCTTACCTCTCTAGTCTGTGCTAGCTCTT
CCAGCCCCCTGTCATGGCATCTTCCAGGGGTCCGAGAGCTCAGCTAGTCTTCTTCCTCC
AACCCGGGCCCCTATGTCCACTTCAGGACAGCATGTTTGCTGCCTCCAGGGATCCTGT
GTCCCCGAGCTGGGACCACCTTATATTCCCAGGGCCGGTTAATGTGGCTCTGGTTCTG
GGTACTTTTATCTGTCCCCTCCACCCCACAGTGGGGCAAGCTTCTGACCTCTTCTCTTC
CTCCCACAGGGCCTCGAGAGATCTGGCGGCGGAGAGGGCAGAGGAAGTCTTCTAACA
TGCGGTGACGTGGAGGAGAATCCCGGCCCTATGGCCTTACCAGTGACCGCCTTGCTCC
TGCCGCTGGCCTTGCTGCTCCACGCCGCCAGGCCGGGATCCCAGCTGGTGGAGTCTGG
GGGAGGCTTGGTACAGCCAGGGCGGTCCCTGAGACTCTCCTGCACAACTTCTGGATTC
ACTTTTGGTGATTATGCTATGATCTGGGCCCGCCAGGCTCCAGGGAAGGGGCTGGAGT
GGGTCTCATCCATTAGTAGTAGTAGTAGTTACATATACTACGCAGACTCAGTGAAGGG
CCGATTCACCATCTCCAGAGACAACGCCAAGAACTCACTGTATCTGCAAATGAACAG
CCTGAGAGCCGAGGACACGGCTGTGTATTACTGTGCGAGAGAACGATACGATTTTTG
GAGTGGAATGGACGTCTGGGGCAAAGGGACCACGGTCACCGTCTCGAGTGGTGGAGG
CGGTTCAGGCGGAGGTGGCTCTGGCGGTAGTGCACAGTCTGCCCTGACTCAGCCTGCC
TCCGTGTCTGGGTCTCCTGGACAGTCGATCACCATCTCCTGCACTGGAACCAGCAGTG
ATGTTGGGAGTTATAACCTTGTCTCCTGGTACCAACAGCACCCAGGCAAAGCCCCCAA

	ACTCATGATTTATGAGGGCAGTAAGCGGCCCTCAGGGGTTTCTAATCGCTTCTCTGGC TCCAAGTCTGGCAACGCGGCCTCCCTGACAATCTCTGGGCTCCAGGCTGAGGACGAG GCTGATTATTACTGCCAGTCCTATGACAGCAGCCTGAGTGTGGTATTCGGCGGAGGGA CCAAGCTGACCGTCCTAGGTGCTAGCACCACGACGCCAGCGCCGCGACCACCAACAC CGGCGCCCACCATCGCGTCGCAGCCCCTGTCCCTGCGCCCAGAGGCGTGCCGGCCAGC GGCGGGGGGCGCAGTGCACACGAGGGGGCTGGACTTCGCCTGTGATTTTTGGGTGCT GGTGGTGGTTGGTGGAGTCCTGGCTTGCTATAGCTTGCTAGTAACAGTGGCCTTTATT ATTTTCTGGGTGAGGAGTAAGAGGAGCAGGCTCCTGCACAGTGACTACATGAACATG ACTCCCCGCCGCCCCGGGCCCACCCGCAAGCATTACCAGCCCTATGCCCCACCACGCG ACTTCGCAGCCTATCGCTCCATCGATAGAGTGAAGTTCAGCAGGAGCGCAGACGCCC CCGCGTACCAGCAGGGCCAGAACCAGCTCTATAACGAGCTCAATCTAGGACGAAGAG AGGAGTACGATGTTTTGGACAAGAGACGTGGCCGGGACCCTGAGATGGGGGGAAAGC CGAGAAGGAAGAACCCTCAGGAAGGCCTGTACAATGAACTGCAGAAAGATAAGATG GCGGAGGCCTACAGTGAGATTGGGATGAAAGGCGAGCGCCGGAGGGGCAAGGGGCA CGATGGCCTTTACCAGGGTCTCAGTACAGCCACCAAGGACACCTACGACGCCCTTCAC ATGCAGGCCCTGCCCCCTCGCTGATAAGCGGCCGCCTGTGCCTTCTAGTTGCCAGCCA TCTGTTGTTTGCCCCTCCCCCGTGCCTTCCTTGACCCTGGAAGGTGCCACTCCCACTGT CCTTTCCTAATAAAATGAGGAAATTGCATCGCATTGTCTGAGTAGGTGTCATTCTATTC TGGGGGGTGGGGTGGGGCAGGACAGCAAGGGGGAGGATTGGGAAGACAATAGCAGG CATGCTGGGGATGCGGTGGGCTCTATGGGTCGACAGTACTAAGCTTTACTAGGGACA GGATTGGTGACAGAAAAGCCCCATCCTTAGGCCTCCTCCTTCCTAGTCTCCTGATATT GGGTCTAACCCCCACCTCCTGTTAGGCAGATTCCTTATCTGGTGACACACCCCCATTTC CTGGAGCCATCTCTCTCCTTGCCAGAACCTCTAAGGTTTGCTTACGATGGAGCCAGAG AGGATCCTGGGAGGGAGAGCTTGGCAGGGGGTGGGAGGGAAGGGGGGGATGCGTGA CCTGCCCGGTTCTCAGTGGCCACCCTGCGCTACCCTCTCCCAGAACCTGAGCTGCTCT GACGCGGCTGTCTGGTGCGTTTCACTGATCCTGGTGCTGCAGCTTCCTTACACTTCCCA AGAGGAGAAGCAGTTTGGAAAAACAAAATCAGAATAAGTTGGTCCTGAGTTCTAACT TTGGCTCTTCACCTTTCTAGTCCCCAATTTATATTGTTCCTCCGTGCGTCAGTTTTACCT GTGAGATAAGGCCAGTAGCCAGCCCCGTCCTGGCAGGGCTGTGGTGAGGAGGGGGGT GTCCGTGTGGAAAACTCCCTTTGTGAGAATGGTGCGTCCTAGGTGTTCACCAGGTCGT GGCCGCCTCTACTCCCTTTCTCTTTCTCCATCCTTCTTTCCTTAAAGAGTCCCCAGTGCT ATCTGGGACATATTCCTCCGCCCAGAGCAGGGTCCCGCTTCCCTAAGGCCCTGCTCTG GGCTTCTGGGTTTGAGTCCTTGGCAAGCCCAGGAGAGGCGCTCAGGCTTCCCTGTCCC CCTTCCTCGTCCACCATCTCATGCCCCTGGCTCTCCTGCCCCTTCCCTACAGGGGTTCC TGGCTCTGCTCTAAGGG
AAVS1-EF1α-αFR	ATCCTCCCCGTGTCTGGGTCCTCTCCGGGCATCTCTCCTCCCTCACCCAACCCCATGCC GTCTTCACTCGCTGGGTTCCCTTTTCCTTCTCCTTCTGGGGCCTGTGCCATCTCTCGTTT CTTAGGATGGCCTTCTCCGACGGATGTCTCCCTTGCGTCCCGCCTCCCCTTCTTGTAGG CCTGCATCATCACCGTTTTTCTGGACAACCCCAAAGTACCCCGTCTCCCTGGCTTTAGC CACCTCTCCATCCTCTTGCTTTCTTTGCCTGGACACCCCGTTCTCCTGTGGATTCGGGT CACCTCTCACTCCTTTCATTTGGGCAGCTCCCCTACCCCCCTTACCTCTCTAGTCTGTG CTAGCTCTTCCAGCCCCCTGTCATGGCATCTTCCAGGGGTCCGAGAGCTCAGCTAGTC TTCTTCCTCCAACCCGGGCCCCTATGTCCACTTCAGGACAGCATGTTTGCTGCCTCCAG GGATCCTGTGTCCCCGAGCTGGGACCACCTTATATTCCCAGGGCCGGTTAATGTGGCT CTGGTTCTGGGTACTTTTATCTGTCCCCTCCACCCCACAGTGGGGCAAGCTTCTGCATA TGTCTTGAAAGGAGTGGGAATTGGCTCCGGTGCCCGTCAGTGGGCAGAGCGCACATC GCCCACAGTCCCCGAGAAGTTGGGGGGAGGGGTCGGCAATTGAACCGGTGCCTAGAG AAGGTGGCGCGGGGTAAACTGGGAAAGTGATGTCGTGTACTGGCTCCGCCTTTTTCCC GAGGGTGGGGGAGAACCGTATATAAGTGCAGTAGTCGCCGTGAACGTTCTTTTTCGCA ACGGGTTTGCCGCCAGAACACAGGTAAGTGCCGTGTGTGGTTCCCGCGGGCCTGGCCT CTTTACGGGTTATGGCCCTTGCGTGCCTTGAATTACTTCCACCTGGCTGCAGTACGTGA TTCTTGATCCCGAGCTTCGGGTTGGAAGTGGGTGGGAGAGTTCGAGGCCTTGCGCTTA AGGAGCCCCTTCGCCTCGTGCTTGAGTTGAGGCCTGGCCTGGGCGCTGGGGCCGCCGC GTGCGAATCTGGTGGCACCTTCGCGCCTGTCTCGCTGCTTTCGATAAGTCTCTAGCCAT TTAAAATTTTTGATGACCTGCTGCGACGCTTTTTTTCTGGCAAGATAGTCTTGTAAATG CGGGCCAAGATCTGCACACTGGTATTTCGGTTTTTGGGGCCGCGGGCGGCGACGGGG CCCGTGCGTCCCAGCGCACATGTTCGGCGAGGCGGGGCCTGCGAGCGCGGCCACCGA GAATCGGACGGGGGTAGTCTCAAGCTGGCCGGCCTGCTCTGGTGCCTGGCCTCGCGCC GCCGTGTATCGCCCCGCCCTGGGCGGCAAGGCTGGCCCGGTCGGCACCAGTTGCGTG AGCGGAAAGATGGCCGCTTCCCGGCCCTGCTGCAGGGAGCTCAAAATGGAGGACGCG GCGCTCGGGAGAGCGGGCGGGTGAGTCACCCACACAAAGGAAAAGGGCCTTTCCGTC CTCAGCCGTCGCTTCATGTGACTCCACGGAGTACCGGGCGCCGTCCAGGCACCTCGAT TAGTTCTCGAGCTTTTGGAGTACGTCGTCTTTAGGTTGGGGGGAGGGGTTTTATGCGA TGGAGTTTCCCCACACTGAGTGGGTGGAGACTGAAGTTAGGCCAGCTTGGCACTTGAT GTAATTCTCCTTGGAATTTGCCCTTTTTGAGTTTGGATCTTGGTTCATTCTCAAGCCTC AGACAGTGGTTCAAAGTTTTTTTCTTCCATTTCAGGTGTCGTGACGTACGGGATCCTCT AGAACGCGTGCCACCATGGCCTTACCAGTGACCGCCTTGCTCCTGCCGCTGGCCTTGC TGCTCCACGCCGCCAGGCCGGGATCCCAGCTGGTGGAGTCTGGGGGAGGCTTGGTAC

AGCCAGGGCGGTCCCTGAGACTCTCCTGCACAACTTCTGGATTCACTTTTGGTGATTA
TGCTATGATCTGGGCCCGCCAGGCTCCAGGGAAGGGGCTGGAGTGGGTCTCATCCATT
AGTAGTAGTAGTAGTTACATATACTACGCAGACTCAGTGAAGGGCCGATTCACCATCT
CCAGAGACAACGCCAAGAACTCACTGTATCTGCAAATGAACAGCCTGAGAGCCGAGG
ACACGGCTGTGTATTACTGTGCGAGAGAACGATACGATTTTTGGAGTGGAATGGACGT
CTGGGGCAAAGGGACCACGGTCACCGTCTCGAGTGGTGGAGGCGGTTCAGGCGGAGG
TGGCTCTGGCGGTAGTGCACAGTCTGCCCTGACTCAGCCTGCCTCCGTGTCTGGGTCT
CCTGGACAGTCGATCACCATCTCCTGCACTGGAACCAGCAGTGATGTTGGGAGTTATA
ACCTTGTCTCCTGGTACCAACAGCACCCAGGCAAAGCCCCCAAACTCATGATTTATGA
GGGCAGTAAGCGGCCCTCAGGGGTTTCTAATCGCTTCTCTGGCTCCAAGTCTGGCAAC
GCGGCCTCCCTGACAATCTCTGGGCTCCAGGCTGAGGACGAGGCTGATTATTACTGCC
AGTCCTATGACAGCAGCCTGAGTGTGGTATTCGGCGGAGGGACCAAGCTGACCGTCC
TAGGTGCTAGCACCACGACGCCAGCGCCGCGACCACCAACACCGGCGCCCACCATCG
CGTCGCAGCCCCTGTCCCTGCGCCCAGAGGCGTGCCGGCCAGCGGCGGGGGGCGCAG
TGCACACGAGGGGGCTGGACTTCGCCTGTGATTTTTGGGTGCTGGTGGTGGTTGGTGG
AGTCCTGGCTTGCTATAGCTTGCTAGTAACAGTGGCCTTTATTATTTTCTGGGTGAGGA
GTAAGAGGAGCAGGCTCCTGCACAGTGACTACATGAACATGACTCCCCGCCGCCCCG
GGCCCACCCGCAAGCATTACCAGCCCTATGCCCCACCACGCGACTTCGCAGCCTATCG
CTCCATCGATAGAGTGAAGTTCAGCAGGAGCGCAGACGCCCCCGCGTACCAGCAGGG
CCAGAACCAGCTCTATAACGAGCTCAATCTAGGACGAAGAGAGGAGTACGATGTTTT
GGACAAGAGACGTGGCCGGGACCCTGAGATGGGGGGAAAGCCGAGAAGGAAGAACC
CTCAGGAAGGCCTGTACAATGAACTGCAGAAAGATAAGATGGCGGAGGCCTACAGTG
AGATTGGGATGAAAGGCGAGCGCCGGAGGGGCAAGGGGCACGATGGCCTTTACCAG
GGTCTCAGTACAGCCACCAAGGACACCTACGACGCCCTTCACATGCAGGCCCTGCCCC
CTCGCTGATAAGCGGCCGCCTGTGCCTTCTAGTTGCCAGCCATCTGTTGTTTGCCCCTC
CCCCGTGCCTTCCTTGACCCTGGAAGGTGCCACTCCCACTGTCCTTTCCTAATAAAATG
AGGAAATTGCATCGCATTGTCTGAGTAGGTGTCATTCTATTCTGGGGGGTGGGGTGGG
GCAGGACAGCAAGGGGGAGGATTGGGAAGACAATAGCAGGCATGCTGGGGATGCGG
TGGGCTCTATGGGTCGACAGTACTAAGCTTTACTAGGGACAGGATTGGTGACAGAAA
AGCCCCATCCTTAGGCCTCCTCCTTCCTAGTCTCCTGATATTGGGTCTAACCCCCACCT
CCTGTTAGGCAGATTCCTTATCTGGTGACACACCCCCATTTCCTGGAGCCATCTCTCTC
CTTGCCAGAACCTCTAAGGTTTGCTTACGATGGAGCCAGAGAGGATCCTGGGAGGGA
GAGCTTGGCAGGGGGTGGGAGGGAAGGGGGGGATGCGTGACCTGCCCGGTTCTCAGT
GGCCACCCTGCGCTACCCTCTCCCAGAACCTGAGCTGCTCTGACGCGGCTGTCTGGTG
CGTTTCACTGATCCTGGTGCTGCAGCTTCCTTACACTTCCCAAGAGGAGAAGCAGTTT
GGAAAAACAAAATCAGAATAAGTTGGTCCTGAGTTCTAACTTTGGCTCTTCACCTTTC
TAGTCCCCAATTTATATTGTTCCTCCGTGCGTCAGTTTTACCTGTGAGATAAGGCCAGT
AGCCAGCCCCGTCCTGGCAGGGCTGTGGTGAGGAGGGGGGTGTCCGTGTGGAAAACT
CCCTTTGTGAGAATGGTGCGTCCTAGGTGTTCACCAGGTCGTGGCCGCCTCTACTCCCT
TTCTCTTTCTCCATCCTTCTTTCCTTAAAGAGTCCCCAGTGCTATCTGGGACATATTCCT
CCGCCCAGAGCAGGGTCCCGCTTCCCTAAGGCCCTGCTCTGGGCTTCTGGGTTTGAGT
CCTTGGCAAGCCCAGGAGAGGCGCTCAGGCTTCCCTGTCCCCCTTCCTCGTCCACCAT
CTCATGCCCCTGGCTCTCCTGCCCCTTCCCTACAGGGGTTCCTGGCTCTGCTCTAAGGG

TRAC-CD22

cccaacttaatgccaacataccaTAAACCTCCCATTCTGCTAATGCCCAGCCTAAGTTGGGGAGACC
ACTCCAGATTCCAAGATGTACAGTTTGCTTTGCTGGGCCTTTTTCCCATGCCTGCCTTT
ACTCTGCCAGAGTTATATTGCTGGGGTTTTGAAGAAGATCCTATTAAATAAAAGAATA
AGCAGTATTATTAAGTAGCCCTGCATTTCAGGTTTCCTTGAGTGGCAGGCCAGGCCTG
GCCGTGAACGTTCACTGAAATCATGGCCTCTTGGCCAAGATTGATAGCTTGTGCCTGT
CCCTGAGTCCCAGTCCATCACGAGCAGCTGGTTTCTAAGATGCTATTTCCCGTATAAA
GCATGAGACCGTGACTTGCCAGCCCCACAGAGCCCCGCCCTTGTCCATCACTGGCATC
TGGACTCCAGCCTGGGTTGGGGCAAAGAGGGAAATGAGATCATGTCCTAACCCTGAT
CCTCTTGTCCCACAGATATTCAAAACGCCACGAACTTCTCTCTGTTAAAGCAAGCAGG
CGACGTGGAAGAAAACCCCGGTCCCATGCTCCTGTTGGTAACCTCTCTGCTCCTGTGC
GAACTCCCGCATCCGGCGTTTCTGTTGATTCCCCAAGTTCAACTTGTAGAAAGCGGCG
GCGGGCTGGTCCAAGCAGGCGGTTCACTCAGGGTGAGCTGCGAGGCGTCCGGCATTA
CTTTTAGCCGTGCAGCTATGGGTTGGTATAGGCAACGCCCCGGAAAAGAACGTGAGC
GCGTGGCGGTGGTGAACTCTGACTCATCAACTATCTACGCCGATAGTGTCAAAGGAA
GATTTACGATTTCTCGTGATAACGCGAAGAATACCGTATATCTCCAGATGAATTCCCT
CGAGCCCGAAGATACTGCTGTGTACTATTGCTGGTCTCCCGGATTTGGCAGTTATTGG
GGACAAGGTACTCAAGTGACTGTCTCAAGCACAACCACTCCCGCTCCCAGGCCACCC
ACTCCAGCTCCTACGATAGCTAGCCAACCGTTGAGTTTGAGGCCCGAAGCTTGTAGAC
CTGCCGCCGGCGGTGCCGTCCATACTCGAGGCCTCGATTTTGCTTGCGACATATATAT
TTGGGCTCCACTGGCAGGAACATGCGGCGTGCTCTTATTGTCTCTTGTCATTACTCTGT
ATTGTAAGAGAGGTAGGAAGAAGCTGTTGTACATATTTAAGCAGCCCTTCATGAGGC
CCGTGCAGACAACCCAGGAAGAGGACGGGTGCTCTTGTAGGTTCCCCGAGGAAGAAG
AGGGTGGTTGCGAGCTTCGTGTTAAATTTAGTCGATCCGCGGATGCGCCTGCATATCA
ACAAGGACAAAATCAATTATACAATGAACTGAACCTTGGCCGCCGGGAAGAATATGA
CGTCCTCGATAAAAGGCGGGGTAGGGATCCCGAAATGGGCGGGAAACCCCGACGTAA

GAATCCCCAAGAGGGACTTTATAACGAGCTCCAAAAGGACAAAATGGCAGAAGCGTA
TTCCGAAATCGGTATGAAAGGGGAACGTAGGCGCGGTAAAGGACATGACGGTCTGTA
TCAAGGACTGTCAACCGCAACTAAAGATACTTATGATGCGCTCCATATGCAAGCACTT
CCACCCCGGTAACGACTGTGCCTTCTAGTTGCCAGCCATCTGTTGTTTGCCCCTCCCCC
GTGCCTTCCTTGACCCTGGAAGGTGCCACTCCCACTGTCCTTTCCTAATAAAATGAGG
AAATTGCATCGCATTGTCTGAGTAGGTGTCATTCTATTCTGGGGGGTGGGGTGGGGCA
GGACAGCAAGGGGGAGGATTGGGAAGAGAATAGCAGGCATGCTGGGGATAGTTAGT
TAGGGATATTCAAAACCCTGACCCTGCAGTCTACCAGCTGAGAGACTCTAAATCCAGT
GACAAGTCTGTCTGCCTATTCACCGATTTTGATTCTCAAACAAATGTGTCACAAAGTA
AGGATTCTGATGTGTATATCACAGACAAAACTGTGCTAGACATGAGGTCTATGGACTT
CAAGAGCAACAGTGCTGTGGCCTGGAGCAACAAATCTGACTTTGCATGTGCAAACGC
CTTCAACAACAGCATTATTCCAGAAGACACCTTCTTCCCCAGCCCAGGTAAGGGCAGC
TTTGGTGCCTTCGCAGGCTGTTTCCTTGCTTCAGGAATGGCCAGGTTCTGCCCAGAGCT
CTGGTCAATGATGTCTAAAACTCCTCTGATTGGTGGTCTCGGCCTTATCCATTGCCACC
AAAACCCTCTTTTTACTAAGAAACAGTGAGCCTTGTTCTGGCAGTCCAGAGAATGACA
CGGGAAAAAAGCAGAtgaagagaaggtggcaggag

TRAC-CD22-tCTS

agagTCAGCTGGTACACGGCAGGcccaacttaatgccaacataccaTAAACCTCCCATTCTGCTAATG
CCCAGCCTAAGTTGGGGAGACCACTCCAGATTCCAAGATGTACAGTTTGCTTTGCTGG
GCCTTTTTCCCATGCCTGCCTTTACTCTGCCAGAGTTATATTGCTGGGGTTTTGAAGAA
GATCCTATTAAATAAAAGAATAAGCAGTATTATTAAGTAGCCCTGCATTTCAGGTTTC
CTTGAGTGGCAGGCCAGGCCTGGCCGTGAACGTTCACTGAAATCATGGCCTCTTGGCC
AAGATTGATAGCTTGTGCCTGTCCCTGAGTCCCAGTCCATCACGAGCAGCTGGTTTCT
AAGATGCTATTTCCCGTATAAAGCATGAGACCGTGACTTGCCAGCCCCACAGAGCCCC
GCCCTTGTCCATCACTGGCATCTGGACTCCAGCCTGGGTTGGGGCAAAGAGGGAAAT
GAGATCATGTCCTAACCCTGATCCTCTTGTCCCACAGATATTCAAAACGCCACGAACT
TCTCTCTGTTAAAGCAAGCAGGCGACGTGGAAGAAAACCCCGGTCCCATGCTCCTGTT
GGTAACCTCTCTGCTCCTGTGCGAACTCCCGCATCCGGCGTTTCTGTTGATTCCCCAAG
TTCAACTTGTAGAAAGCGGCGGCGGGCTGGTCCAAGCAGGCGGTTCACTCAGGGTGA
GCTGCGAGGCGTCCGGCATTACTTTTAGCCGTGCAGCTATGGGTTGGTATAGGCAACG
CCCCGGAAAAGAACGTGAGCGCGTGGCGGTGGTGAACTCTGACTCATCAACTATCTA
CGCCGATAGTGTCAAAGGAAGATTTACGATTTCTCGTGATAACGCGAAGAATACCGT
ATATCTCCAGATGAATTCCCTCGAGCCCGAAGATACTGCTGTGTACTATTGCTGGTCT
CCCGGATTTGGCAGTTATTGGGGACAAGGTACTCAAGTGACTGTCTCAAGCACAACCA
CTCCCGCTCCCAGGCCACCCACTCCAGCTCCTACGATAGCTAGCCAACCGTTGAGTTT
GAGGCCCGAAGCTTGTAGACCTGCCGCCGGCGGTGCCGTCCATACTCGAGGCCTCGAT
TTTGCTTGCGACATATATATTTGGGCTCCACTGGCAGGAACATGCGGCGTGCTCTTATT
GTCTCTTGTCATTACTCTGTATTGTAAGAGAGGTAGGAAGAAGCTGTTGTACATATTT
AAGCAGCCCTTCATGAGGCCCGTGCAGACAACCCAGGAAGAGGACGGGTGCTCTTGT
AGGTTCCCCGAGGAAGAAGAGGGTGGTTGCGAGCTTCGTGTTAAATTTAGTCGATCCG
CGGATGCGCCTGCATATCAACAAGGACAAAATCAATTATACAATGAACTGAACCTTG
GCCGCCGGGAAGAATATGACGTCCTCGATAAAAGGCGGGGTAGGGATCCCGAAATGG
GCGGGAAACCCCGACGTAAGAATCCCCAAGAGGGACTTTATAACGAGCTCCAAAAGG
ACAAAATGGCAGAAGCGTATTCCGAAATCGGTATGAAAGGGGAACGTAGGCGCGGTA
AAGGACATGACGGTCTGTATCAAGGACTGTCAACCGCAACTAAAGATACTTATGATG
CGCTCCATATGCAAGCACTTCCACCCCGGTAACGACTGTGCCTTCTAGTTGCCAGCCA
TCTGTTGTTTGCCCCTCCCCCGTGCCTTCCTTGACCCTGGAAGGTGCCACTCCCACTGT
CCTTTCCTAATAAAATGAGGAAATTGCATCGCATTGTCTGAGTAGGTGTCATTCTATTC
TGGGGGGTGGGGTGGGGCAGGACAGCAAGGGGGAGGATTGGGAAGAGAATAGCAGG
CATGCTGGGGATAGTTAGTTAGGGATATTCAAAACCCTGACCCTGCAGTCTACCAGCT
GAGAGACTCTAAATCCAGTGACAAGTCTGTCTGCCTATTCACCGATTTTGATTCTCAA
ACAAATGTGTCACAAAGTAAGGATTCTGATGTGTATATCACAGACAAAACTGTGCTA
GACATGAGGTCTATGGACTTCAAGAGCAACAGTGCTGTGGCCTGGAGCAACAAATCT
GACTTTGCATGTGCAAACGCCTTCAACAACAGCATTATTCCAGAAGACACCTTCTTCC
CCAGCCCAGGTAAGGGCAGCTTTGGTGCCTTCGCAGGCTGTTTCCTTGCTTCAGGAAT
GGCCAGGTTCTGCCCAGAGCTCTGGTCAATGATGTCTAAAACTCCTCTGATTGGTGGT
CTCGGCCTTATCCATTGCCACCAAAACCCTCTTTTTACTAAGAAACAGTGAGCCTTGTT
CTGGCAGTCCAGAGAATGACACGGGAAAAAAGCAGAtgaagagaaggtggcaggagCCTGCCG
TGTACCAGCTGActct

Supplementary Table 8. Primer sequences.

Primer name	Sequence	Product size (bp)
ATG5-Out-F ATG5-Out-R	CATCAGCTATGGTGCCTTCTTG CAACTTACGCTCTAGTGCTCAC	695 bp (WT) or 758 bp (KI)
ATG5-I2A-824-TIDE-F ATG5-I2A-824-TIDE-R	GACTTGCAGGTGTGAGTTAATGG GAGTACCAGTAACAAGATTGCCG	624 bp
ATG5-E4-56-TIDE-F ATG5-E4-56-TIDE-R	GCCTAGGCACGTAACTGTAGAATG GCAACTAAAACAGTGTCAGGGG	352 bp
AAVS1-I1-TIDE-F AAVS1-I1-TIDE-R	TTCGGGTCACCTCTCACTCC GGCTCCATCGTAAGCAAACC	469 bp
ATG5-I2A-824-OT1-F ATG5-I2A-824-OT1-R	AAAATCCTTCCCCGTTCCTCGAG CACATTAATAGTGCACGTGACCCTC	773 bp
ATG5-I2A-NGS-F	ACACTCTTTCCCTACACGACGCTCTTCCGATCTTGAAGTCTGCCCTTTG CTTTCC	392 bp with extension 461 bp after indexing
ATG5-I2A-NGS-R	GTGACTGGAGTTCAGACGTGTGCTCTTCCGATCTGAGTACCAGTAACA AGATTGCCG	
ATG5-824-OT1-NGS-F	ACACTCTTTCCCTACACGACGCTCTTCCGATCTTTTCAAGGCAAGTGAC CGGAATG	437 bp with extension 506 bp after indexing
ATG5-824-OT1-NGS-R	GTGACTGGAGTTCAGACGTGTGCTCTTCCGATCTCACATTAATAGTGC ACGTGACCCTC	
αFR_CAR-qPCR-F αFR_CAR-qPCR-R	CTGTGCGAGAGAACGATACG GTTCCAGTGCAGGAGATGGT	192 bp
ACTB-qPCR-F ACTB-qPCR-R	CACCATTGGCAATGAGCGGTTC AGGTCTTTGCGGATGTCCACGT	135 bp
TRAC-HDRT-F TRAC-HDRT-R	CCCAACTTAATGCCAACATACCA CTCCTGCCACCTTCTCTTCA	2355 bp
TRAC-HDRT-tCTS-F TRAC-HDRT-tCTS-R	AGAGTCAGCTGGTACACGGCAGGCCCAACTTAATGCCAACATACCA AGAGTCAGCTGGTACACGGCAGGCTCCTGCCACCTTCTCTTCA	2395 bp

Supplementary Table 9. Antibodies for flow cytometry analysis.

Fluorochrome	Marker	Expression	Clone	Company	Cat. Number
-	Glucose-Cy5	Glucose uptake	-	Sigma	SML3233
AF647	G4S linker	αFR-CAR-T cells	-	Cell Signaling	69782S
AF647	V_HH	CD22-CAR-T cells	-	In-house	-
PerCP	CD8	Effector T cells	RPA-T8	Biolegend	301030
PE-Cy7	CD45RO	Phenotype	UCHL1	Invitrogen	25-0457-42
AF700	CD4	Helper T cells	RPA-T4	Biolegend	300526
APC/Fire750	CCR7	Phenotype	G043H7	Biolegend	353246
eFluor506	Viability	Live/dead cells	-	Invitrogen	65-0866-14
BV605	CD137	Activation	4B4-1	Biolegend	309822
BV421	CD279	Exhaustion	EH12.2H7	Biolegend	329920
BV750	CD3	T cells	SK7	Biolegend	344845
BV421	IFN-γ	Cytokine	4S.B3	Biolegend	502508

Supplementary Table 10. Sequences for GUIDE-Seq adapters and primers.

Phosphorothioate linkages are illustrated with a star (*).

Primer or adapter name	Sequence
dsODN_Fwd	/5Phos/GTTTAATTGAGTTGTCATATGTTAATAACGGT*A*T
dsODN_Rev	/5Phos/ATACCGTTATTAACATATGACAACTCAATTAA*A*C
GUIDE-Seq_Adapter_Top	ACACTCTTTCCCTACACGACGCTCTTCCGATCTNNWNNWNNCCATCTCATCCCTGC*T
GUIDE-Seq_Adapter_Bot	/5Phos/GCAGGGATGAGAT*G*G
GUIDE-Seq_PCR1_Common	ACACTCTTTCCCTACACGACGCTCTTCCGATCT
GUIDE-Seq_PCR1_Plus	GTGACTGGAGTTCAGACGTGTGCTCTTCCGATCTCGTTATTAACATATGACAACTCAATTAAAC
GUIDE-Seq_PCR1_Minus	GTGACTGGAGTTCAGACGTGTGCTCTTCCGATCTTTGAGTTGTCATATGTTAATAACGGTA